UNIVERSITA' DEGLI STUDI DI PADOVA

Dipartimento di Ingegneria Industriale

Facolta' di Ingegneria

Corso di Laurea Magistrale in Ingegneria Energetica

Tesi di Laurea

Experimental analysis of a novel Savonius based spline geometry with flexible blades for VAWT

Relatore: Prof. Andrea Lazzaretto

Correlatore: Prof. Asfaw Beyene

Laureando: Piero Danieli

Anno Accademico 2015/2016

ABSTRACT

During the last few decades renewable energies have increased their diffusion due to the constant growing concern about the climate change caused by greenhouse gases emissions and the pollution generated by the use of oil-derived substances for energy production. Wind power is one of the fastest energy sources in terms of growing percentage because of its reliability and its abundance all around the world. Currently, the wind-power market is governed by the Horizontal Axis Wind Turbines (HAWT) thanks to their high efficiency and Vertical Axis Wind Turbines (VAWT) are for now in a neglected position. However, there are many drawbacks such as high cost, high noise output and the need for large areas and specific wind conditions. There are also safety concerns with the high level of risk that maintenance personnel experience during normal operations because of the high positions of all the power producing equipment. The combination of all of these disadvantages for a HAWT could allow the VAWT to be competitive thanks to the absence of these issues. Therefore, an improvement in the efficiency of Vertical rotors could close the existing gap and even make them the more attractive technology for wind energy conversion.

The first aim of this thesis is to prove the effectiveness of some performance improvements achieved on computational 2D simulations with the CFD software Fluent on a new blade spline concept of Savonius rotor by experimental tests. The new concept was proposed by Dr. Beyene. The simulations were conducted on two novel spline blade shaped rotors; one rotor being rigid and another with the blade tips capable of flexing. Important improvements were found in the flexible rotor compared to the same but rigid rotor, especially at part-load conditions.

For the experimental analysis two Savonius rotors were built: the first was built rigid with the spline blade's shape and the second one with the same blade's shape but with a morphing section located on the blade's tips. A target deformation range was set for the flexible rotor to be manufactured according to the results of previous studies on flexible blade VAWT. To find the correct deformation the flexible rotor's manufacture was conducted by trial and error and after a first failed attempt the correct deformation was achieved. A high-speed camera was utilized to verify the deformation of the blade.

The two rotors were then tested and compared to prove the performance improvements at 3, 5, 7, 8, 9, 9.5 m/s wind speed. The low speed wind tunnel at SDSU was utilized for this purpose. Moreover, a combined analysis of the performance and flexibility was done to find the deformation associated with the best performance for this kind of rotor. Finally, a comparison was made on the energy production of the rotors at low wind speed for a possible urban application. Data show a 50% power coefficient improvement of the flexible rotor compared with the standard rotor, around the main working conditions. A 30% increase of the energy produced by the flexible rotor during one year in the city of San Diego was calculated. Eventually the most productive wind speed for the flexible rotor was found at 9m/s so the deformation obtained at that value (22°-32°) was considered as the best deformation for this kind of rotor. As an additional result, the flexible rotor's energy production in urban application will be much higher if the optimal deformation (22°-32°) is obtained at the average San Diego's annual wind speed (3.5m/s).

SOMMARIO

Negli ultimi decenni le energie rinnovabili hanno aumentato la loro diffusione a causa della crescente preoccupazione relativamente ai cambiamenti climatici provocati da inquinanti come i gas serra. L'energia eolica è una delle fonti rinnovabili che ha avuto la più veloce crescita in termini di percentuale di nuove installazioni grazie alla sua affidabilità e abbondanza in tutto il mondo. Al momento, i rotori eolici ad asse orizzontale (HAWT) mantengono un ruolo principale nel mercato eolico grazi alla loro elevata efficienza lasciando, per il momento in disparte, i rotori eolici ad asse verticale (VAWT). In realtà, sussistono molti aspetti negativi relativamente ai HAWT come: costo elevato, rumore, necessità di vaste aree e di specifiche condizioni di vento. Inoltre, l'elevata posizione dell'apparato di conversione comporta problematiche dal punto di vista della sicurezza durante gli interventi di manutenzione. L'assenza dei sopraelencati svantaggi per i rotori ad asse verticale potrebbe permettere agli stessi di diventare competitivi nel mercato. Un incremento dell'efficienza potrebbe chiudere il divario esistente tra le due tipologie di rotore.

Il principale obiettivo di questa tesi è di provare sperimentalmente i miglioramenti di rendimento ottenuti da simulazioni CFD condotte su un nuovo concetto di rotore Savonius con pale flessibili a forma non semicircolare. La nuova tipologia di rotore è stata proposta dal Dr. Beyene. Le simulazioni sono state condotte su due rotori pale a forma non semicircolare ma Spline; uno con le pale rigide e uno con le pale flessibili. Dai risultati sono scaturiti dati sorprendenti relativamente l'efficienza del rotore flessibile confronto con quello rigido specialmente in condizioni di carico parziale.

Per l'analisi sperimentale sono stati costruiti due rotori identici: uno completamente rigido e uno con una sezione flessibile in corrispondenza della parte terminale di ciascuna pala. Un certo range di deformazione (in gradi rispetto alla tangente all'estremità della pala) è stato fissato grazie studi precedenti condotti alla San Diego State University (SDSU). La corretta deformazione e' stata trovata procedendo per tentativi nella costruzione del rotore verificando ogni volta tramite una telecamera ad alta velocità installata all'interno della galleria del vento. Sono stati necessari due tentativi per raggiungere tale deformazione.

I due rotori sono stati successivamente testati per verificare l'incremento di rendimento del rotore flessibile su quello rigido. I test sono stati condotti alle seguenti velocità del vento: 3, 5, 7, 8, 9, 9.5 m/s. La galleria del vento a bassa velocità presente alla SDSU è stata usata per tutti gli esperimenti. Con i dati relativi a deformazione ed efficienza è stata calcolata la deformazione corrispondente alla massima efficienza per questo tipo di rotore. Infine è stato fatto un confronto basato sull'energia producibile dai rotori in un'applicazione urbana. I risultati hanno mostrato un incremento di rendimento del 50% del rotore flessibile rispetto a quello rigido, nell'intorno delle condizioni di lavoro di massima efficienza. Per quanto riguarda l'energia prodotta annualmente nel caso di applicazione urbana a San Diego è stato calcolato un incremento del 30% di energia prodotta dal rotore flessibile confrontato con quello rigido. Infine dai dati è scaturito che il rotore flessibile mostra il miglior incremento di efficienza alla velocità del vento di 9m/s. Per questo motivo la deformazione ottenuta a quella velocità (22°-32°) può essere considerata la deformazione che il rotore dovrebbe avere alla velocità del vento di design. Ne consegue che lo studio effettuato sull'applicazione urbana del rotore potrebbe avere dei risultati ben migliori se quel range di deformazione ottimale fosse stato ottenuto per la velocità media del vento presente a San Diego (3.5m/s).

LIST OF CONTENTS

LIST OF TABLES

LIST OF FIGURES

ACKNOWLEDGEMENTS

INTRODUCTION

Due to the increasing energy consumption around the world, greenhouse gas emissions are becoming a serious problem for all countries. For this reason, governments are moving to promote alternative, environmentally friendly energy sources. One of the most abundant and well-established power sources is wind power. Is it important to underline that the technologic level reached during the last few decades has made wind power economically competitive with other renewable energy sources. Wind power derives from solar power which heats the air and the ground on the earth's surface causing differences in the pressure of air which are responsible for the air movements and therefore the wind flow creation. The total solar energy that impacts the earth every year is about $5 * 10^6$ $[EJ]$ and the percentage of this energy which is converted into wind power is estimated to be about 1% which is about $5 * 10^4$ $[EJ]$ [1]. Considering the global consumption of energy in 2010, which is $5.3 * 10^2 [EJ]$ [2], a simple comparison could be made between energy use and potential wind power output. Proper utilization of wind power could supply about 100 times the current global energy consumption. In the 2000-2015 inclusive, the global annual installed wind capacity has constantly increased except in 2012. In particular, in 2000 the new installation was about 3'760 $[MW]$ and 2015 was 63'467 $[MW]$ [3]. China is the country which has the highest new installation and is followed by USA [3]. Looking at these records it is clear that the wind power is and will be a fundamental energy source for covering the current and future consumption. Nevertheless, the most widespread technology for the wind power conversion is the Horizontal Axis Wind Turbine which rules because of its high efficiency. Although it is a renewable energy source, the HAWT utilization has some problems linked with the need of wide fields and the dangerous and expensive maintenances operations. It has been estimated that a wind farm needs of about 4047 $\left[\frac{m^2}{MW}\right]$ which is a huge permanently disturbed area [4]. Without a field characterized by high quality wind HAWTs cannot reach high efficiency because of wind speed and direction fluctuations or strong turbulence. Even though HAWT's large scale wind farms produce renewable energy various authors such as Wang et al. [5], Keith et al. [6], Fiedler et al. [7] demonstrate that they are not completely sustainable. Therefore, small scale wind turbines installed in urban environment is the actual best options. Thanks to their suitability to work with low quality wind [8] and to their feasibility in decentralized small grid systems [9], VAWTs might be the best choice in wind power

production. However, because of the VAWT's lower efficiency, researches should be focused on their improvement to make them more competitive. In particular, VAWT Savonius rotors show some positive features such as low noise, no wind direction sensitivity, cheap manufacture, high torque production, easy maintenance, no gearbox need [10]. Since Savonius rotors have typically lower efficiency than others VAWT such as Darrieus and Cycloturbine [11], this kind of rotors is mainly adopted to produce electricity when cost and reliability are more important than efficiency. With a reasonable efficiency improvement Savonius rotors could became extremely competitive in wind turbine's market. Savonius rotor is mostly a drag-driven device which produces also some lift. Decrease of drag force on the convex side or increase of lift force are the only two ways to obtain a higher efficiency on these rotors. Several experimental studies were conducted with the aim to improve the power coefficient of a Savonius rotor. Jeom et al. [12] experimentally studied the effects of endplates with various shapes and sizes and they found a power coefficient's improvement of 36% compared to the same rotor with no endplates. Kamoji et al. [13] studied the influence of the central shaft on power coefficient. They found a power coefficient improvement by using a rotor with no central shaft. Mahmoud et al. [14] studied different geometries of Savonius wind turbine and they found that the two blades rotor is the most efficient configuration compared to three and four blades rotors. Besides, they found that endplates and double stage rotors have higher performance compare to no endplates and single stage rotors respectively. Another study conducted by Wenehenubum et al. [15] showed that three blades Savonius rotor is more efficient than two and four blades rotors, only at high value of the TSR though. Other improvements were achieved using helical blades, flapping blades and curtaining systems. Kamoji et al. [16] tested helical Savonius rotors and they found that at each rotational angle the torque resulted to be positive. At some angles, a standard Savonius rotor, shows negative values of the torque. With the aim to prevent the negative torque that occur on the convex blade of a Savonius rotor, Altan et al. [17] tested rotors with and without a curtain, experimentally and numerically. They found a 38.5% power coefficient improvement using an optimized curtain compared to the standard configuration. Tartuferi et al [18] studied the effect of airfoil blades shape and curtain on Savonius rotors. They found a slight improvement either numerically or experimentally using airfoil shape blades and noticeable improvement with the curtain configuration. Yang et al. [19] even though only numerically, they found improvements of power coefficient utilizing Savonius derived rotor with flapping blades. Probably the most

2

used and tested configuration to improve the efficiency of Savonius rotor is the presence of a gap located at rotor's center area. Moving the bucket sideways, the drag force decreases and the lift force increases thanks to the flow which passes side to side. This is commonly called overlap. Kacprzak et al. [20] studied with CFD simulations the optimal overlap ratio finding best results for values close to 0. The thesis on which this work is based, was initially focused in presenting a novel blade's shape Savonius rotor. Inspired by aforementioned works, three arc-type blades rotors and slotted blades rotors were simulated similarly to Tian et al. [21] and Alaimo et al. [22] respectively. A more recent improvement was initially tested on HAWT. An HAWT needs an expensive control system to adapt the angle of attack to variable external conditions. A passive control obtained thanks to a flexible wind turbine rotor has been investigated in various studies conducted by Hoogedoorn et al. [23], Krawczyk et al. [24], Mc Phee et al. [25]. All these studies were conducted by SDSU's mechanical engineering department in collaboration with other institutes. The idea proposed in those studies has been applied to HAWT and to a Darrieus rotor VAWT. The two studies were conducted by Mc Phee et al. [26] and Butbul et al. [27] respectively. Since this new idea had never been studied on Savonius rotors a numerical study was conducted on the previous thesis work. Positive improvements were achieved by utilizing morphing blades. Since the work was conducted only numerically an experimental proof is provided by this thesis work.

1 HAWT AND VAWT OVERVIEW

1.1 Origin of Wind Power Usage

The first utilization of wind power can be recognized around 5000 B.C. [28] when it was used as a propeller for boats on the Nile River. Subsequently the next development was about using the wind for mechanical power. There are no records to prove which civilization was the first to build a working mill for that functional target but researchers affirm that it happened between 500 and 900 B.C. [28] by the introduction of the first few pumps for irrigation purposes and the first few mills for grinding grain. The first documented wind mill design is a vertical axis machine dated 200 B.C. and it was a Persian wind mill with the aim of grinding grain. The principle of operation is shown in **Figure1.1**. Someone argues that this technology was born 2000 year before the Persian mill in China but the first documented Chinese windmill dates back to 1219 A.D. by the Chinese statesman Yehlu Chhu-Tshai. [29]
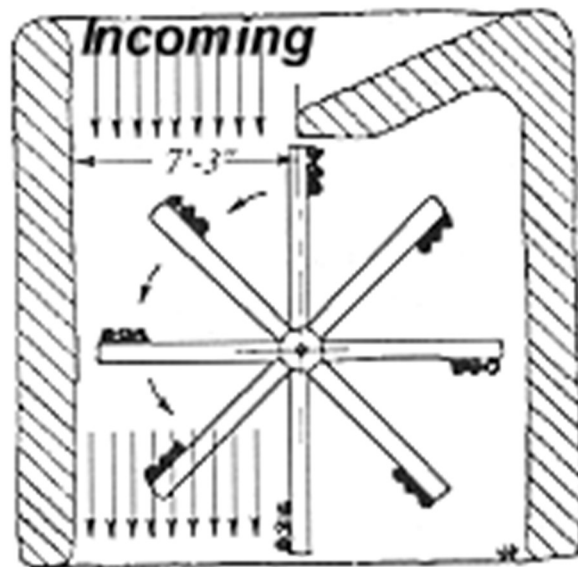
Figure 1.1 - First documented device for the mehanical use of wind power as a mill by Persians (Source: [29])

Starting in Persia the use of windmills spread across the Middle East and they were extensively used in food production. There is also proof that French and English people started to use this technology around 1105 A.D. and 1191 A.D. respectively [30]. Nevertheless, there was a

fundamental difference between the Persian and the European mill which can be found on the rotational axis. Sure enough the Persian was a vertical axis rotor and the European had horizontal axis. The explanation under this dissimilarity is unknown but the reason might be attributed to older water wheels which had had the same horizontal configuration. Furthermore, it is possible that the higher efficiency achieved by the horizontal-axis design approach may have encouraged European people to use it [29]. The structure of these mills was composed mainly of a fixed supporting tower and a rotatable cap which was mounted on the rotor allowing it to follow the prevailing wind direction thanks to the cap rotation. In some configuration, to obtain the rotor movement there was a tail extending out the cap and down to ground level where there were posts to which the rotor could be tied by the miller once the main wind direction was found. The best of this new type of rotor was designed by Jan Adriaenszoon, from Holland. It is important to underline that these rotors were twisted and tapered in the same way as modern rotors reaching a very high level of efficiency. It is likely that the optimization process, which is at the base of this design, took a long time to be accomplished and indicates that really high quality aerodynamic engineering was reached at this time in Holland [31].

Figure 1.2 - Typical Holland mill (Source: [31])

The mills in Holland (**Figure1.2**) were very useful not only to grind the grain but also because Dutch people were able to drain miry lands with their help and the water pumping mill is still

6

considered one of the best applications of wind power. The first wind mills appeared in America around the second half of 1700, imported by the Dutch. During the late 1800s the world famous American multi bladed wind turbine started its prolific diffusion all around the country with over six million installations just in US [29]. These rotors were designed as water pumps to be applied mainly for agricultural usage and their huge success has to be attributed to the good performance that they could offer. For the first mill designed specifically for electrical power we have to wait till 1900 and to be precisely it was built in 1890 in Denmark and during the same period other wind generators were built in US. Starting from 1925 the American market launched commercial electric generators based on wind power and the main brands were Wincharger and Jacobs which sold generators between 200 to 3000 W of power [32]. Nevertheless, wind power had a secondary role on electric production during this period in fact it was used only for battery charging due to their low power barely comparable to the electricity grid one. One of the first remarkable development in large-scale systems was a 53m diameter rotor designed by Smith-Putnam company on 1948 which represented the technical feasibility of this technology for large-scale electrical generation[33] (**Figure1.3**).
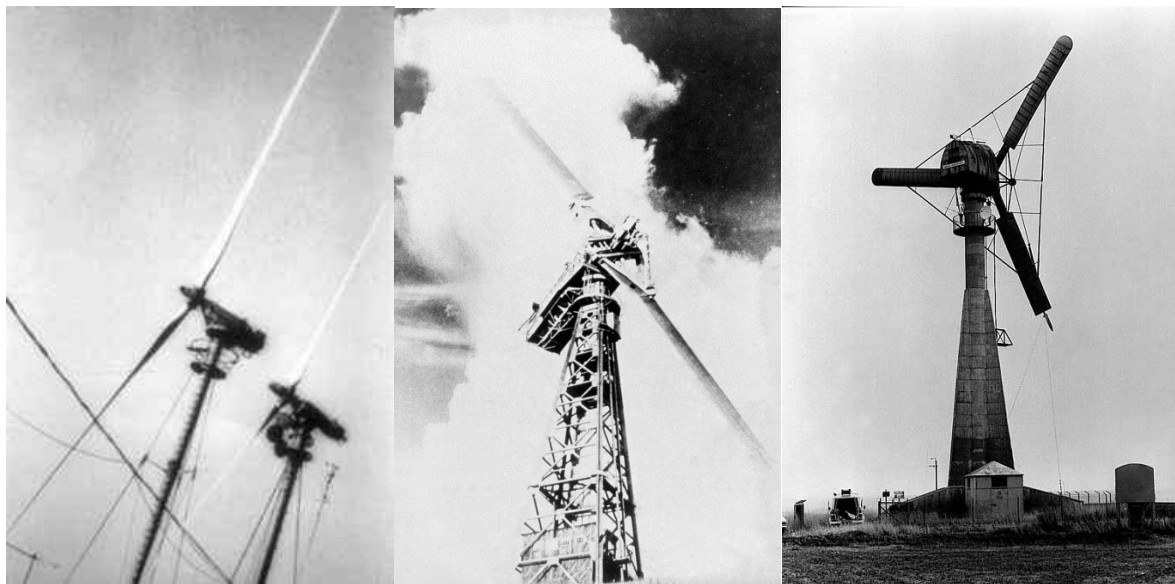
Figure 1.3 - From left to right: Wincharger (Source: [32]), Smith-Putnam (Source: [33]) and Gedser rotors (Source: [34])

Despite the success of horizontal axis turbines, other new concepts were designed starting in the 1920s with the French Darrieus G.J.M. [35] who presented a narrow curved rotor with a vertical

rotational axis. Just ten years later another interesting vertical axis rotor was designed by a Finnish engineer S.J. Savonius in 1931 [36] which was composed by two halves of cylinder split longitudinally and arranged radially on a vertical shaft. Just due to the intensive research activities conducted during the 50's there were new developments on wind turbines with the introduction of the tip speed ratio and solidity concept. During the next few decades a lot of new wind turbines were developed mainly in Germany, USSR, UK, France and Denmark. Some important examples are the Gedser machine (1956) which was built in Denmark with a remarkable power of 200KW and the 1.1MW 35m turbine tested by Electricite' de France [37]. After this positive period the electrical power became available from fossil fuel with a price that in 1970 was only 3 cents/Kwh. Moreover, the new interest on nuclear energy which at that time was thought to be an almost unlimited energy source, added to the easier and cheaper fossil power, caused a decline on wind energy interest. Although the positive aspects of these energy sources in the following years were realized. Fossil fuels were not unlimited after all and there were many safety concerns with nuclear power; numerous countries didn't want to develop the technology due to the highly dangerous nuclear waste and the possibility of destructive accidents. For the previous reasons and for the gaining oil price, Governments were stimulated in increasing the funding for programs involved in the research of renewable energy and in particular, wind power.

1.2 HAWT and VAWT

Generally, modern wind turbines are classified based on the position of the rotational axis and in that way are divided in Horizontal-axis wind turbine and Vertical-axis wind turbine but the first type, for now, is the most common commercial configuration by far. Considering the capacity, they are also classified in micro, small, medium, large and ultra-large turbines. The micro size is suitable for isolated installations, where grid is not available and their capacity is commonly set to be less than several kilowatts. In that way the turbine can provide electrical energy for light and household electrical appliances and even heat for domestic heating if it is used as an electrical based heating plant. Moreover, the micro turbine can be used only for mechanical purposes such as water pumping. Small turbines usually have less than 100KW [38] of capacity and are used mainly in residential areas with the aim of increase the available power where it is

difficult to obtain from the grid. Medium size turbines are definitely the most common because of their adaptability to a several uses such as on-grid, off-grid, hybrid systems, distributed power and wind farms. Their capacity goes from 100KW to 1 MW [38]. Large rotors with a power up to 10MW [38] are employed in large modern wind farms either in onshore or offshore installations. Eventually, ultra large turbines have a power greater than 10MW and are still under development. The physical size that is needed to reach these power levels makes them suitable principally for offshore employments.

1.2.1 HAWT rotors

The majority of large wind turbine are today HAWT. These machines can have one, two, three or multiple blades and their typical configuration is shown in **Figure1.4**.
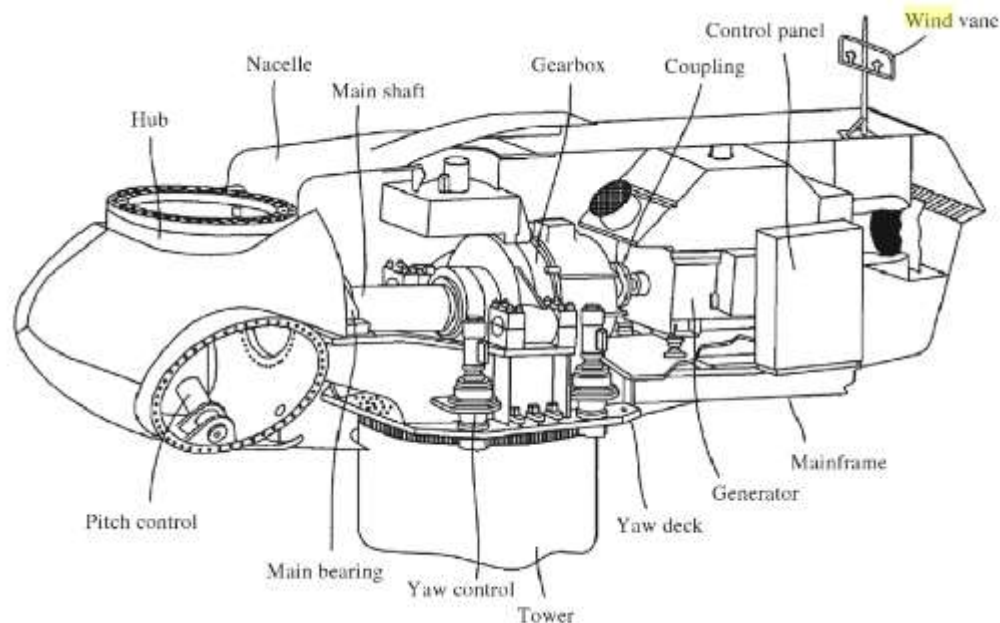
Figure 1.4 - Typical HAWT configuration (Source: [38])

The main components are the nacelle, the tower and the hub. Inside the first, all the tools needed to convert the mechanical power, obtained by the rotor movement, to electrical power are stored. The second component, the tower, is needed to keep the structure at a high altitude in order to avoid the turbulent flow conditions at ground level. These rotors are really sensitive to wind flow

conditions that, in case of turbulence, can affect the efficiency and power production. Finally, the hub is the moving element on which the blades are mounted. To allow the most efficient working conditions, the nacelle and the hub are moved by a mechanism at the front to face the main wind direction at all times. That involves two possible orientations for the nacelle: one with the nacelle facing the wind called downwind and the second with the hub impacting wind flow called upwind. Is it simple to notice that in the downwind configuration the flow that hits the rotor is previously disturbed by the presence of the nacelle so the upwind turbines are almost always the favorite. On the figure is shown a typical three blade wind turbine but other configurations are shown in the next **Figure1.5**.

Figure 1.5 - 2,3,4,5 blades HAWT (left) (Source: [39]), American Multi-blades rotor (right) (Source: [40])

These rotors are preferred because have the following advantages upon the Vertical axis turbine on the current state of art:

- Higher turbine efficiency
- Higher power density
- Lower cut-in speed
- Lower cost per unit power output

The standard configuration previously shown is only the most common but others using the HAWT design were proposed over the years with the principle aim of increasing the amount of

energy produced. Early attempts employed the use of multiple rotors or other strategies. The first example is the energy tower. It is composed of a big tower inside which is sprayed with water. When the water evaporates, it cools the air that becomes denser and falls to the base of the tower where the wind turbines are set [41]. The biggest advantage of this technology is that it doesn't need wind flow but it can only work as long as very dry and hot air conditions are maintained outside the structure. The difficulties in finding a good spot, the constant need for large amounts of water and the wide dimensions of the structure make this technology suitable for only a few places around the world. A scheme of the energy tower working system is shown in **Figure1.6**.
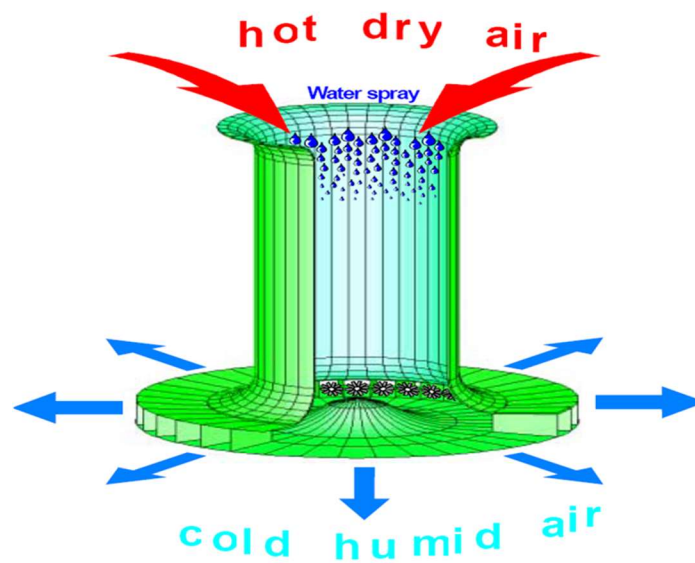
Figure 1.6 - Energy tower working scheme (Source: [41])

Another family of non-standard wind turbines is multirotor wind turbine or MRWTs which are simply several turbines mounted on the same support [42]. They were initially designed because it was virtually impossible to build very big rotors before the arrival of fiberglass and composite materials. Yet, there are still some advantages mainly linked with lower cost of production, maintenance and transport. There is also the possibility of increasing the average power due to the independent rotational speed of each rotor and the reduced impact of centrifugal forces. Nevertheless, some drawbacks such as the increased complexity of the system, the increased mass of steel needed to build the structure and the difficulties in the prediction of the interaction

between the rotor and the wind flow make this technology hard to use on a large scale (**Figure 1.7**).

Figure 1.7 - Example of MRWT (Source: [42])

Airborne wind turbine is another unconventional design founded on the concept of a wind rotor kept in the air without a physical tower [43]. That involves obvious improvements such as the minor cost for the absence of the tower, the utilization of stronger and more constant wind flows at high altitudes. However, several issues such as the safe suspension of the rotor in the air, the energy transfer and the possible interference with aviation remain unsolved. These rotors are generally made of two components which are connected by tethers (ropes). They can be classified as in Ground-gen systems when the conversion from mechanical energy to electrical is made on the ground and in Fly-gen systems when that process takes place on the rotor. The altitude reached by these systems can vary between 70m and 500m but there are studies that show a possible altitude of 12km. In **Figure1.8** is described the operating principle of a Fly-gen system.
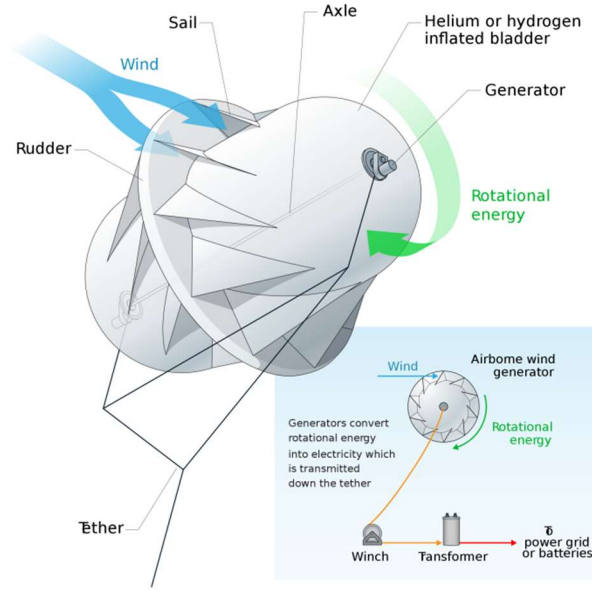
Figure 1.8 - Operational principle of a Fly-gen airborne wind generator (Source: [44])

Finally, it is worth touching on Ducted and Dual rotor HAWT [45]. The first is a very simple configuration which can achieve higher energy conversion by the use of a converging shroud that avoids the formation of vortices behind the rotor and furthermore it produces a high speed wind flow. Nonetheless the high cost of the shroud's manufacturing outweighs the performance enhancements. The Dual rotor HAWT design is composed by two rotors with one of them facing the wind stream and the other one in the opposite direction [46]. There are some theoretical studies that claim improvements in efficiency but have still to be verified by experimental testing. In **Figure1.9** the Ducted and Dual rotor designs.
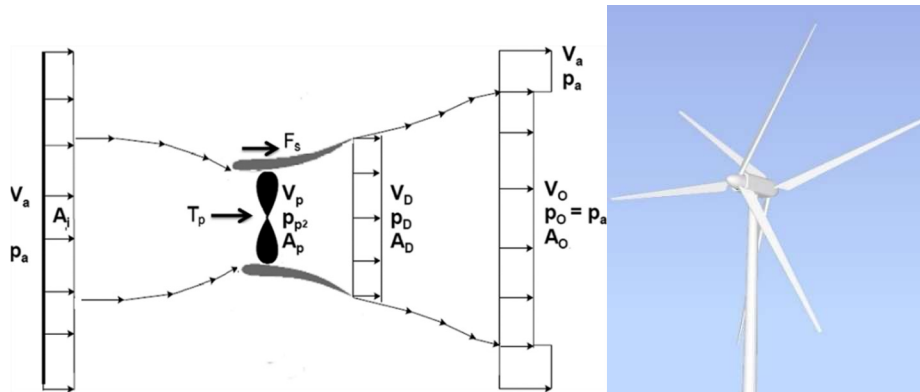
Figure 1.9 - Ducted (left) (Source: [47]) and Dual rotor (right) scheme

1.2.2 VAWT rotors

This section will provide a brief review of the vertical axis wind turbine. A more specific description mainly focused on Savonius rotor will be given in further sections of this work. The VAWT are turbines that differ from the HAWT because they have a rotational axis that is transverse to the wind so they do not need to be pointed towards the main direction of the wind. It involves an orientation mechanism and the wind direction sensors are no longer needed which causes a reduction in cost. All the main components including the generator and gears are located at the base of the turbine facilitating service and maintenance operations. This reduces cost and increases safety. At the current state of art only three different designs of these rotors exist. The first is the Darrieus rotor which is composed of two blades with airfoil shape that use mainly lift force generated by the wind hitting the blades creating rotation. One of the main features of the Darrieus VAWT is the high rotational speed that it can achieve. In fact, it can be many times higher than the wind speed. However, the torque generated is very low and it makes them much more suitable for electrical purposes than for mechanical such as water pumping or similar activities. The first downside that is important to consider is that the high rotational speed involves heavy centrifugal forces acting on the blade while rotating which implies very high strength blades with an obviously higher cost. The principal issue of this technology concerns the possibility to self-start which is not possible for Darrieus rotors. There are two commonly recommended ways for solving this: a powered motor or a coupling with another vertical axis rotor able to start by itself. It is clear that the second choice is the simplest because of the maintenance issues that a powered motor could bring. [48]. In **Figure1.10** a classic Darrieus turbine is shown.

Figure 1.10 - Classic Darrieus rotor (Source: [49])

The second VAWT type that is going to be described is the Giromill rotor which is a Darrieus-derived concept that uses lift forces to generate mechanical movement from wind power. The main difference with the Darrieus VAWT is the position of the blades which are air foiled but strictly vertical, without the tips linked to the shaft. There are typically two or three blades that are attached to the shaft by horizontal supports. By the fact that they are derived from the standard Darrieus turbines, they bring with them the same issues such as the difficulties in self-start and the high speed rotation. In addition, they have some problems in maintaining a constant rate of rotation but with the advantage of an excellent aptness to turbulent wind conditions which are prohibitive for the HAWT. A really interesting variant of these turbines is the Cycloturbine which includes a mechanical orientation system to change the position of the pitch in order to obtain the maximum efficiency. Furthermore, the main achievement is related to the possibility of rotating the pitch in order to adapt the attack angle to the wind speed. In that way the self-start ability is noticeably increased and when a good rotational speed is reached, the airfoils are kept in a good orientation to use the lift forces to accelerate their speed [48]. Following a picture of a Cycloturbine in **Figure1.11**.

Figure 1.11 - An installed Cycloturbine (Source: [50])

With a different design from the previously described turbine, the Savonius rotor is a drag-type VAWT and has a really simple geometry. It is made up of two halves of a pipe connected along one edge, to the shaft. The operating principle has its base on the fact that the drag force in inner side of the pipes is bigger than in the outside and this disequilibrium allows the rotor to rotate. To be more precise, starting from the position shown in **Figure1.12**, and considering a wind flow coming from the left side, the drag force in the upper cup is higher than in the lower so the rotor starts to rotate and when it reaches one third of a revolution the two cups have inverted their position and now the previous lower cup becomes the upper cup and thanks to the higher drag force, it allows a continue spin as long as the wind is blowing. These rotors are very suitable for turbulent wind conditions but they have a low efficiency if compared with the Darrieus [48] however a higher torque is generated by the Savonius. The last feature makes the Savonius turbine more suitable for mechanical purposes instead of electricity generation because a high rotational speed is needed to generate high currents and voltages. Nonetheless a gear transmission box could solve the problem but involving higher weight and cost. Savonius rotor is able to self-start with a pretty low wind speed but in case of gear transmission box usage it would be increased a lot. Even if the low rotational speed of the Savonius turbine doesn't make it really

16

suitable for electric purposes, its silent working conditions, relatively easy manufacturing and the possibility of working in really turbulent wind conditions are aspects that give these rotors the chance to be the best option within all the other configurations. In **Figure1.12** is presented a scheme of a Savonius turbine.
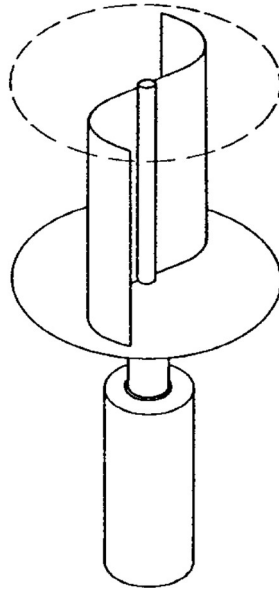
Figure 1.12 - Savonius rotor scheme (Source: [48])

To increase the performance of VAWT there were proposed several configurations which are mainly based on the coupling of different vertical rotor such as Savonius and Darrieus in order to take advantage from the positive aspects of each of them. Other achievements were reached by the use of new different blade shapes.

2 WIND POWER EVALUATION PARAMETERS AND POWER CONVERSION LIMITS

2.1 Wind Power and Betz's Law

[51] A wind turbine produces mechanical power converting the wind power acting on its blades to torque. The amount of energy transferred from the wind to the rotor depends on air density, rotor sectional area, wind speed and therefore on the kinetic energy which the rotor can subtract from the wind flow. The kinetic energy of a flow is proportional to its mass so to its density. To quantify the available energy which the wind can provide for a rotor, an air cylinder is taken into consideration with the same radius of the wind rotor and a thickness of 1 meter. Remembering the kinetic energy equation, and considering the air cylinder previously mentioned, the available power at the rotor surface is:

$$P_0 = \dot{m}\frac{1}{2}v_1^2 = A\rho v_1 \frac{1}{2}v_1^2 = 0.5 A\rho v_1^3 \qquad (2.1.1)$$

With:

- $\dot{m}$ = air mass flow rate
- A = rotor area
- ρ = air density
- v_1 = free wind flow speed

The air density depends on its humidity and can be calculated as follows:

$$\rho = \frac{1+x}{R_a + xR_v}\frac{p}{T} \qquad (2.1.2)$$

With:

- x = title

- R_a = dry air constant ($287.0 \ J \ Kg^{-1}K^{-1}$)
- R_v = water steam constant ($461.5 \ J \ Kg^{-1}K^{-1}$)
- p = air pressure
- T = air temperature

It is easy to confirm that a higher kinetic energy taken from the flow by the turbine results in a higher speed reduction of the wind. Therefore, the flow speed behind the rotor has to be included between 0 and the free wind speed v_1 available without the presence of the turbine. The first case is clearly impossible to obtain but it has calculated the maximum convertible power from an ideal rotor, thanks to the Betz theory. According to this theory only the 59% of the entire power available from wind flow is convertible to mechanical energy. Betz considered as the ideal rotor an actuator disk which is an air permeable circular surface. In addition, there are some hypotheses on which the theory is based:

1. An air tube passing through the actuator disk is considered and it doesn't interact with the surrounding air.
2. In every infinitesimal cylindrical section of the stream, the speed is uniform with a parallel direction to the wind tube axis. The slowing down through the actuator disk is uniform across the disk surface.
3. In the sections, infinitely far from the disk either in front of it or behind it the fluid conditions are the same as the free stream.
4. There are no obstacles upwind and downwind the actuator disk.
5. The wind has to be steady state with a constant intensity with the altitude.
6. The actuator disk has no rotational effect on the wind flow.
7. The air density is considered constant so the air is incompressible.
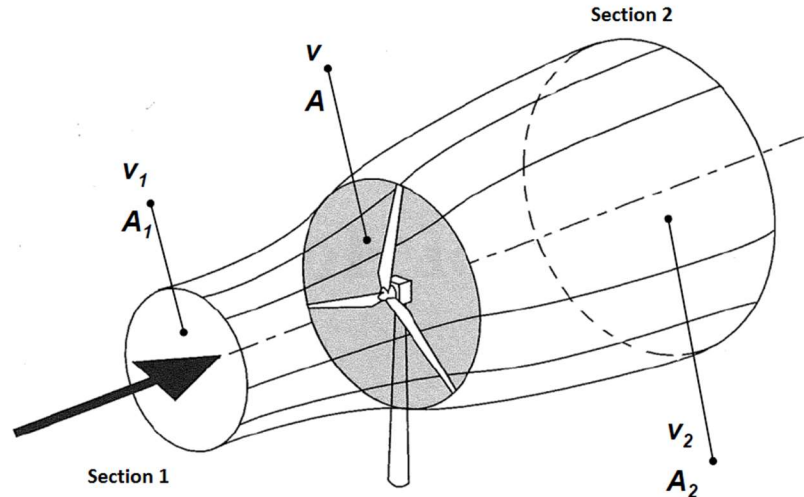
Figure 2.1 - Actuator disk scheme (Source: [51])

As it is shown in **Figure2.1** the free stream has a speed of v_1 and has been slowed until section 2 through which the speed reaches the value v_2. Thanks to the chosen hypothesis it is possible to write the continuity equation:

$$\rho v_1 A_1 = \rho v_2 A_2 = \dot{m} \tag{2.1.3}$$

The horizontal force applied to the rotor is:

$$T = \dot{m}(v_1 - v_2) \tag{2.1.4}$$

Therefore, the power can be written as follows:

$$P = T * v = T * \dot{m}(v_1 - v_2) \tag{2.1.5}$$

Another way to write the power is by a balance between the kinetic energy of the air stream before and after the actuator disk:

$$P = \dot{m} * \frac{v_1^2 - v_2^2}{2} \qquad (2.1.6)$$

Combining the two expressions (2.1.5) and (2.1.6), it is easy to find the wind speed on the disk surface:

$$v = \frac{(v_1 + v_2)}{2} \qquad (2.1.7)$$

The last equation shows that the breaking down takes place up wind for one half and downwind for the other half. Betz defines axial disturbance factor which is a measure of how much the flow is broken down through the actuator disk:

$$a = 1 - \frac{v}{v_1} = \frac{(v_1 - v)}{v_1} \qquad (2.1.8)$$

$$v = v_1(1 - a) \qquad (2.1.9)$$

and combining it with the previous equation:

$$v_2 = v_1(1 - 2a) \qquad (2.1.10)$$

Therefore, substituting the expressions (2.1.9) and (2.1.10) in the (2.1.6) the extractable power equation for the Betz theory is obtained:

$$P = \frac{1}{2}A\rho v_1^3 4a(1 - a)^2 \qquad (2.1.11)$$

So by setting the derivative to zero of (2.1.11) the value of a is found which maximizes the extracted power. Values 1 and $\frac{1}{3}$ are found but because the first one has no relevant purpose, the

22

second one is chosen as optimal. Is now possible to define the power coefficient C_p as the ratio between P and P_0 where P_0 is the total theoretical power that the wind flow makes available.

$$P_0 = \frac{1}{2} A \rho v_1^3 \qquad (2.1.12)$$

$$C_p = \frac{P}{P_0} = \frac{\frac{1}{2} A \rho v_1^3 \, 4a(1-a)^2}{\frac{1}{2} A \rho v_1^3} = 4a(1-a)^2 \qquad (2.1.13)$$

The value of C_p for the optimal a is $C_{p\,max} = \frac{16}{27} \cong 0.59$ so a maximum extractable power of 59%. This theory is only suitable to describe an ideal rotor performance but in order to calculate the real efficiency of a wind rotor a force analysis has to be done. The real efficiency is calculated considering the torque that the rotor can produce or in other words the mechanical power transferred to the gears. There are two forces acting on a rotor which produce the torque: lift and drag. The lift force is produced by the pressure difference between the two sides of the blade. The drag force is simply produced by the friction between the blade and the air flow. The efficiency of a real rotor is then defined as the ratio between the mechanical power produced by the torque and the available wind power:

$$C_p = \frac{mechanical\ power}{available\ power} = \frac{P_m}{P_0} = \frac{Torque * \omega}{\frac{1}{2} \rho A v_1^3} \qquad (2.1.14)$$

2.1.1   Force analysis on a HAWT airfoil blade

[51] It is necessary to define the lift and drag forces acting on an airfoil blade to present the concept of relative speed v_r which is defined as the composition of wind speed vector and the opposite of rotational rotor speed vector as shown in **Figure2.2**.
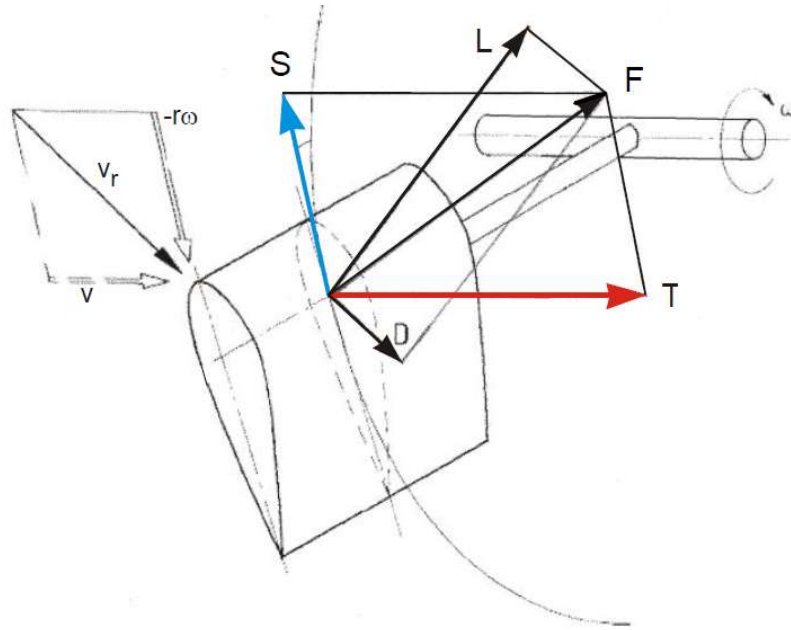
Figure 2.2 - Relative speed on a wind rotor's blade (Source: [51])

The lift force (L) is perpendicular to the relative speed direction and the drag force (D) is parallel to it. The composition of the two vectors produces the vector of the total force acting on the blade. Considering the rotational plane of the rotor, it is possible to split the total acting force F in one component (S) parallel to that plane which pushes the rotor in the direction of its rotational movement and another component (T) perpendicular to it, which does not add to the rotation but is rather a wasted force and therefore wasted energy. The lift force is the most important to increase because it contributes to the S component magnitude. Drag and lift coefficients are defined as follows:

$$C_D = \frac{D}{\frac{1}{2} A_P \rho v_r^2} \tag{2.1.1.1}$$

$$C_L = \frac{L}{\frac{1}{2} A_P \rho v_r^2} \tag{2.1.1.2}$$

Therefore, the responsible force to obtain the torque is the S vector which is positively affected by the lift force. To define mathematically the force S the angle between the relative speed and the rotational direction of the blade (defined as ϕ) must be considered. This angle affects the direction of the forces L and D which in turn affect the intensity of S and T. The last two forces and the respective coefficients can then be defined as follow:

$$S = L * sin\phi - D * cos\phi \qquad (2.1.1.3)$$
$$T = L * cos\phi + D * sin\phi \qquad (2.1.1.4)$$
$$C_S = C_L * sin\phi - C_D * cos\phi \qquad (2.1.1.5)$$
$$C_T = C_L * sin\phi + C_D * sin\phi \qquad (2.1.1.6)$$

The torque can be defined as:

$$Torque = S * R = \frac{1}{2} C_s \rho A v_r^2 R \qquad (2.1.1.7)$$

And the mechanical power:

$$P_m = Torque * \omega \qquad (2.1.1.8)$$

By adjusting the angle ϕ with a dynamic control system, the highest producible lift force can be constantly used. Theoretically a rotor which works with only lift forces and with no other losses could reach the Betz limit of efficiency.

2.1.2 Force analysis on a Savonius rotor

[51] When the maximum performance of a Savonius rotor is investigated, the drag component is usually examined, mainly because it's a drag based rotor. A really limited lift component acts on this kind of rotor and it can be demonstrated by analyzing the interaction between the rotor and the air flow as shown in the **Figure2.3**. In fact on the upper bucket the wind flow produces high pressure on the concave side which is responsible for a pressure gradient between the two

bucket's sides which in turn produce lift. The same phenomenon takes place on the lower bucket but with less intensity so a total positive contribution to the torque is given by the lift force.
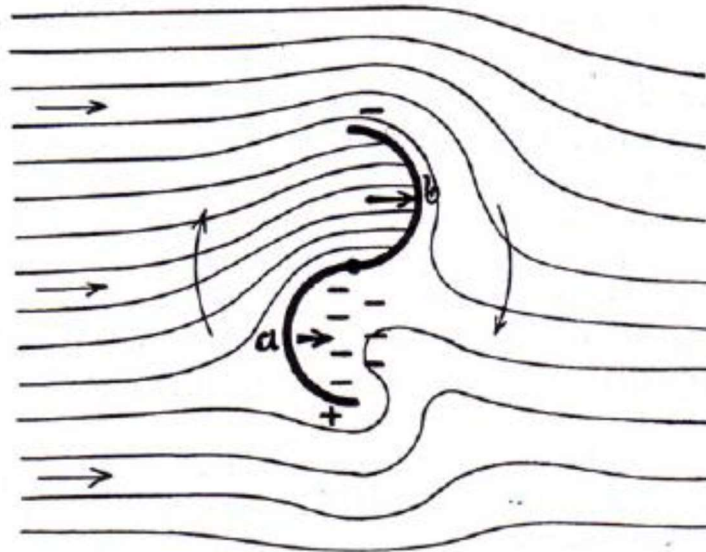
Figure 2.3 - Interaction between Savonius rotor and air flow (Source: [52])

Since this component is really small, in order to give a qualitative maximum value of efficiency, a drag-based model is used. The rotor scheme considered is shown in Fig and in order to simplify the calculations an average radius length is used. Moreover, the rotational movement of the blade is simplified in a translational movement as shown in **Figure2.4** and the wind impacting the blade has the free speed value v_1.
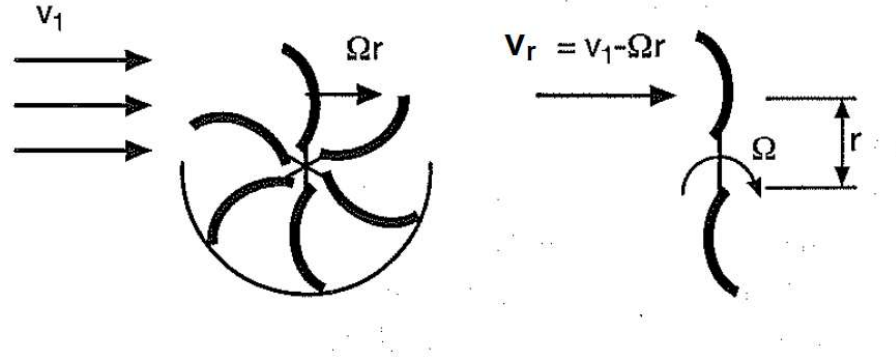
Figure 2.4 - Wind flow direction and speed (left), translational blade movement and radius considered (right), (Source: [51])

The wind hits the blade which has an area A with the absolute speed v_1 and the blade has a relative speed:

$$v_r = v_1 - \Omega r \qquad (2.1.2.1)$$

where Ω is the angular speed of the blade. The drag force acting on the blade is therefore:

$$D = \frac{1}{2} C_D A \rho v_r^2 = \frac{1}{2} C_D A \rho (v_1 - \Omega r)^2 \qquad (2.1.2.2)$$

And the rotor mechanical power:

$$P_m = D * \Omega r = \frac{1}{2} C_D A \rho (v_1 - \Omega r)^2 \Omega r \qquad (2.1.2.3)$$

Remembering and substituting the expression for the Tip Speed Ratio ($TSR = \frac{\Omega r}{v_1}$) in the previous formula:

$$P_m = [C_D * TSR * (1 - TSR)^2] \frac{1}{2} A \rho v_1^3 \qquad (2.1.2.4)$$

27

This produces a power coefficient, C_p which is:

$$C_P = C_D * TSR * (1 - TSR)^2 \qquad (2.1.2.5)$$

Deriving the previous equation with respect to TSR and maximizing the value by setting it to zero the best value of TSR is found (TSR=1/3) and thus the maximum power coefficient is $(C_P)_{max} = \frac{4}{27} C_D$. The drag coefficient is chosen at a value 1.2 because it is the corresponding highest value for a half pipe shape such as the one considered. As a result, the maximum power coefficient is 0.18 or 18% of the total available wind energy which is far smaller than the lift based rotor. Nevertheless, as previously anticipated the little lift force acting on the rotor can improve the maximum rotational speed and efficiency reaching values higher than 1 and 18% for the TSR and efficiency respectively.

Considering the last two paragraphs the reasons for the high difference in efficiency between a Savonius rotor and an airfoil blade HAWT can be found. Firstly, the most important aspect is the value of the relative speed. The relative speed is an important parameter to evaluate the power production (it is in fact present in the equation of C_s and C_D, which are necessary to calculate P_m and for a lift based HAWT is calculated as follow:

$$v_r = \sqrt{v^2 + (\Omega r)^2} \qquad (2.1.2.6)$$

While for a Savonius rotor:

$$v_r = v_1 - \Omega r \qquad (2.1.2.7)$$

The relative speed is much higher for a HAWT. Secondly the drag force acting against the positive torque on a Savonius rotor is really high and the effects of the same force on a lift based rotor are far lower.

The power coefficient trend of different types of rotors can be plotted vs the TSR coefficient defined as:

$$TSR = \frac{\omega R}{v_1} \tag{2.1.2.8}$$

Where:

- ω = angular speed of the rotor $[\frac{rad}{s}]$
- R = rotor radius $[m]$
- v_1 = free speed of the wind $[\frac{m}{s}]$

The TSR is an important coefficient because it allows a comparison of rotors with different geometries on the same graph (**Figure2.5**). It is easily noticeable that because of a slow rotational wind speed, the TSR range of a Savonius rotor is really low and it can barely pass a value of 1 thanks to the action of the lift force.
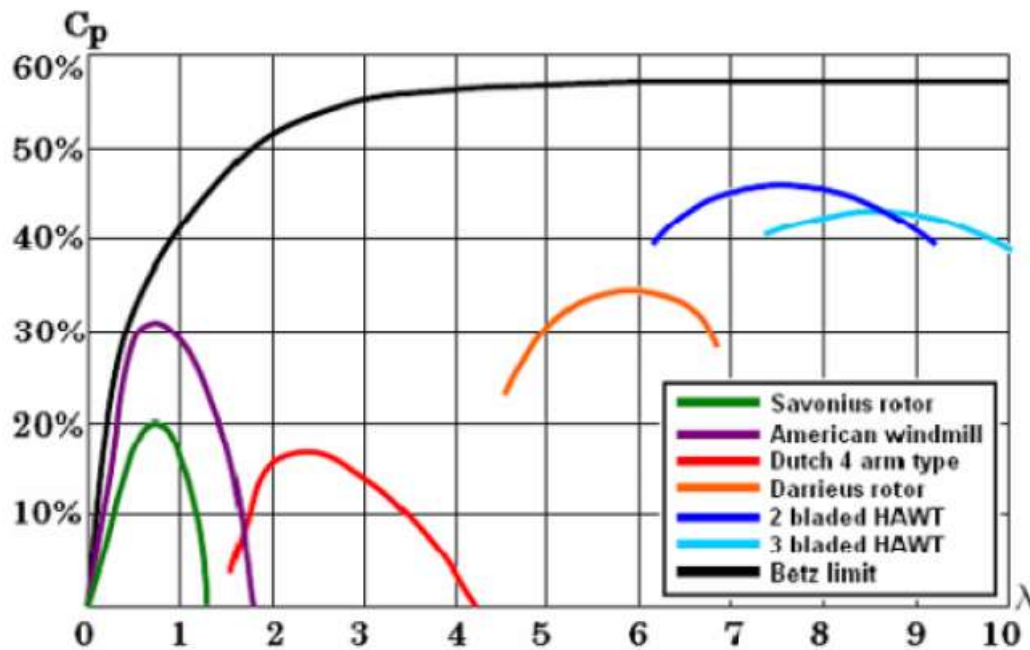
Figure 2.5 – TSR vs Efficiency chart (Source: [52])

3 PREVIOUS WORK ACHIEVEMENTS

3.1 Previous Work

It was anticipated that this thesis would validate the results achieved by Michele Mari from Ferrara University who also worked on his Master's thesis at SDSU [52]. On that work, two methods were investigated to improve the efficiency of the Savonius wind rotor. This rotor type was chosen because of certain technological advantages: it doesn't require a gearbox thanks to a simple direct drive design, it is not expensive to produce, it produces a high torque even at low wind speeds, it has no wind direction sensitivity, it produces a very low noise and it is easy and inexpensive to maintain because the generator is located at the ground level contrary to the HAWT, where the generator is located inside the nacelle on the top of the structure. Therefore, with an efficiency improvement, this type of rotor has the potential to become, in the near future, one of the most common devices for the small scale electrical production.

The first improvement is related to the shape of the blades with the aim of increasing lift force which is a good way to obtain an increased rotational speed, efficiency and power production. Classically the Savonius' blades have a semicircular shape and on this previous work a novel Spline-shape was investigated by the use of 2D CFD simulations. The reason behind this choice came from the simulations of a semicircular blade profile which showed a bubble separation point on the concave blade which is the one that provides the positive torque (**Figure3.1**).
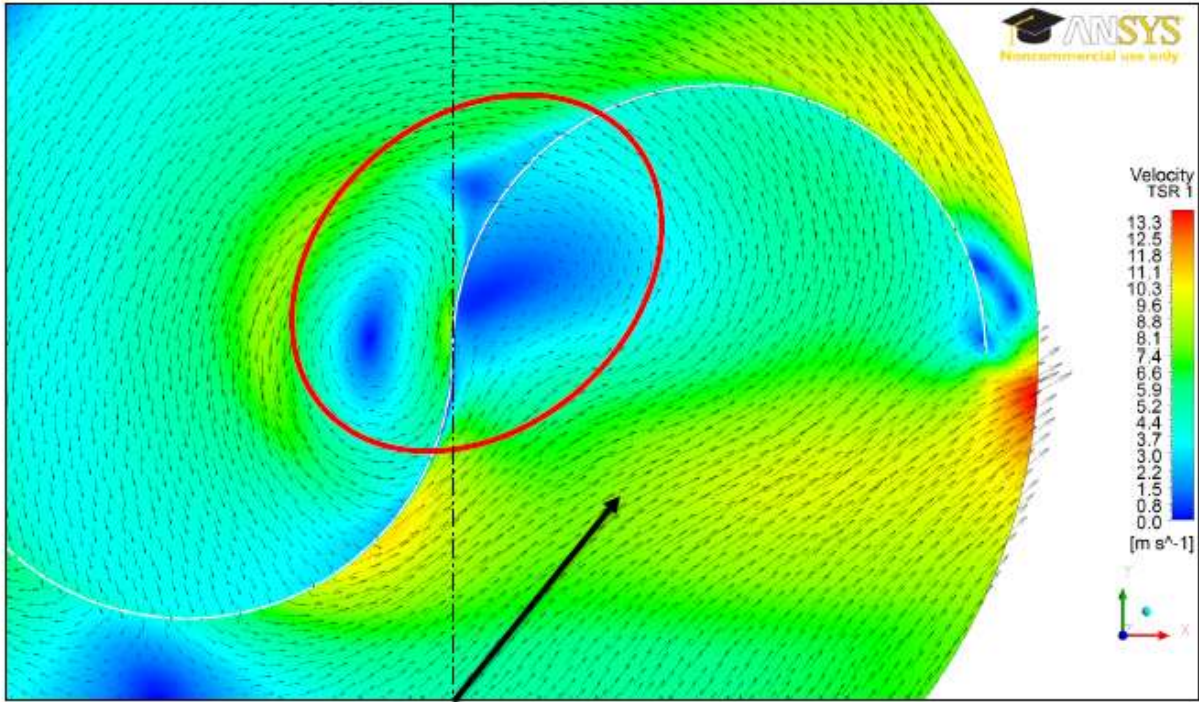
Figure 3.1 - Velocity vector of the flow on a circular blade rotor with TSR 1 (Source: [52])

Thus, the blade was redesigned with a three-point Spline keeping the same two tip points and varying the third one at different angle values measured by keeping a line perpendicular to the connection between the bucket's tip and the shaft as a reference point. The three angles 20°, 30° and 40° were investigated and it was found that the 40° Spline shape had the best torque coefficient C_T, power coefficient C_P at each TSR value on the circular, 20 degree and 30 degree Spline, bucket shape. The following **Figure3.2** show the shape and the plots obtained by the CFD simulations.
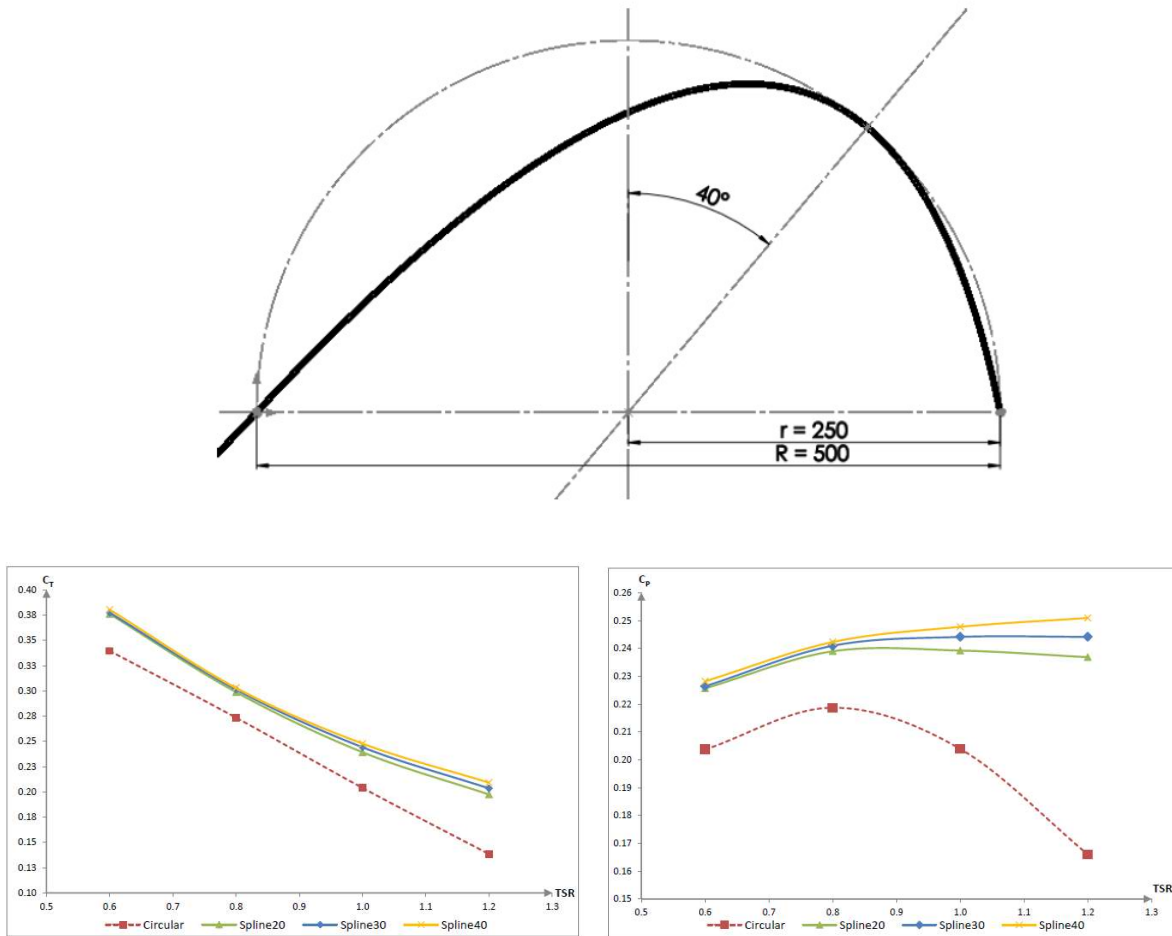
Figure 3.2 – Spline blade shape (upper), torque coefficient vs TSR and power coefficient vs TSR charts (down) obtained in CFD simulations (Source: [52])

The second improvement was achieved by using a flexible Savonius rotor which is a novel development that has never been studied before on this type of rotor. The idea to morph the final section of the Savonius spline-type blade previously shown came from the necessity to adapt the angle of attack of airfoil shape blades to variable external conditions in order to maintain a high efficiency also in off-design working conditions. The classic HAWTs usually adopt an expensive pitch control system which involves several electronic components. Therefore, a passive system using a flexible turbine might be an effective and inexpensive option. This strategy has already been studied for HAWTs [23-25] and for Darrieus rotors [30] and it has been introduced by observing fish locomotion [23-25]. Considering an airfoil profile at part load working conditions, which means at a lower wind speed than the design value, the morphing process is expected to

enhance lift thanks to the increased angle of attack. On the contrary when the wind speed overtakes the design point the angle of attack should be decreased preventing flow separation and thus efficiency losses. A qualitative tail bending is shown for the previously described conditions in the next **Figure3.3** where a horizontal wind direction from the left side is considered. The colored lines show the attack angle variation provided by bending the profile.
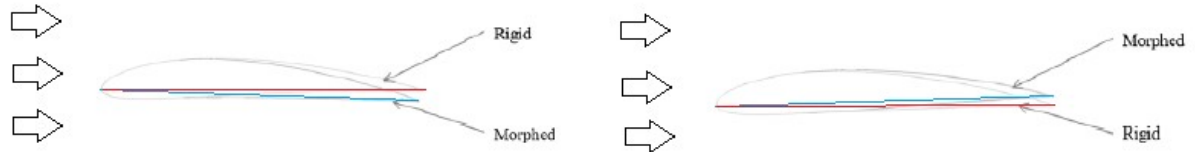
Figure 3.3 - Airfoil deformation at off-design conditions. Under design speed (left), over design speed (right) (Source: [52])

A Savonius rotor has no airfoil profiles so the attack angle concept is not applied but the morphing process is useful to increase the positive torque and at the same time reduce the negative one. This is possible thanks to the rising area of the retreating blade (positive torque) and the decreasing area of the advancing one (negative torque) **Figure3.5**. The power extracted by the wind flow is in fact dependent on the area that the rotor put against it as shown on the previous chapter. The power is then directly related to the power coefficient which gives a measure of the efficiency.
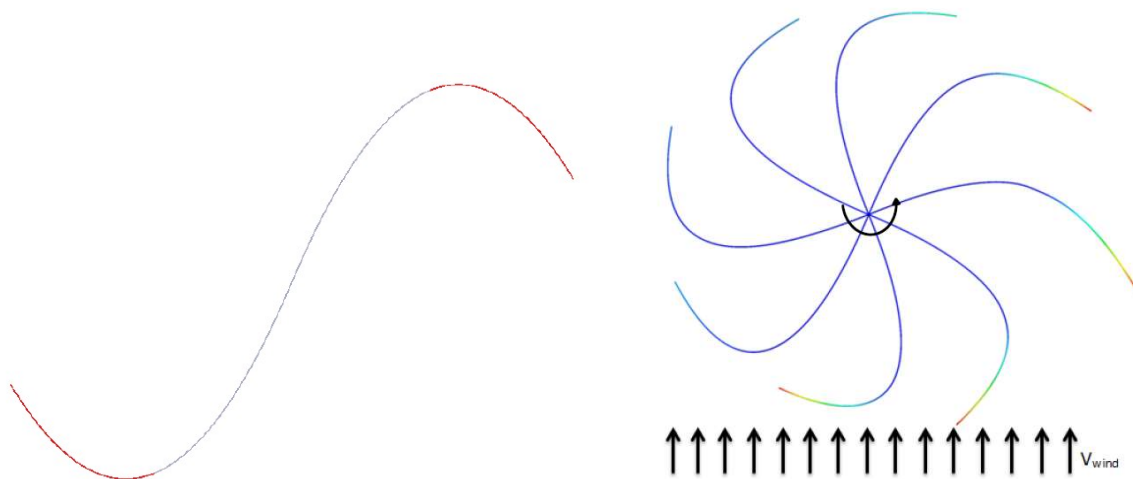
Figure 3.4 - Bending section (left), deformation during rotation with wind direction (right) (Source: [52])

34

The CFD simulations were conducted varying the TSR between 0.6 and 1.2 and for two different materials to evaluate the impact of Young's modulus variation on morphing process. The two chosen materials had the following characteristics:

- $E_1 = 4.2 \, GPa, \nu = 0.4$
- $E_2 = 3.5 \, GPa, \nu = 0.4$

So, a low Young's modulus is not usual for a Savonius rotor which is typically built with a 70-200 GPa range of materials. The first set of simulations was conducted with the inertia being completely neglected and improvements for torque and power coefficient were found at low rotational speeds. Considering that a Savonius rotor is slow and presents a high starting torque the morphing technology can push these rotors to a wider market. The following two graphs (**Figure3.5**) show the improvements on the torque and power coefficient of morphing blade rotors compared to the classic stiff rotor.
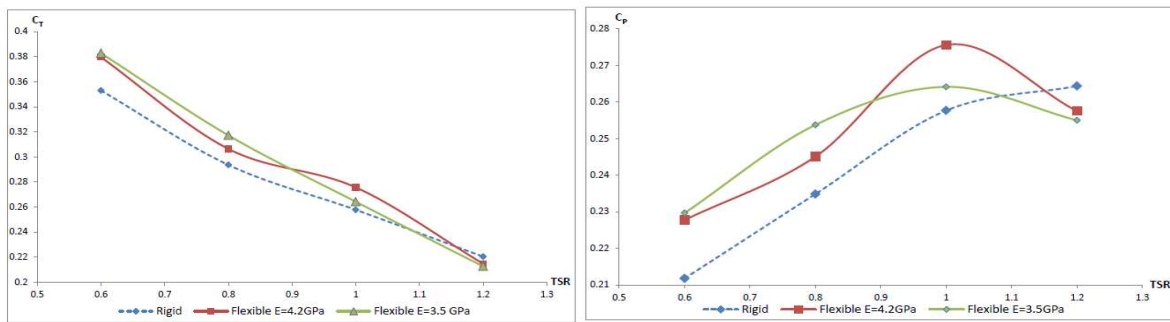
Figure 3.5 - Torque improvement on the left and power coefficient improvement on the right (Source: [52])

Nevertheless, the hypothesis of no inertial forces was no longer acceptable after the centrifugal displacement was investigated. In fact, it was found (**Figure3.6**) that even for low TSR values the inertial forces overwhelmed the adaptive locomotion of the blades and a solution had to be found.
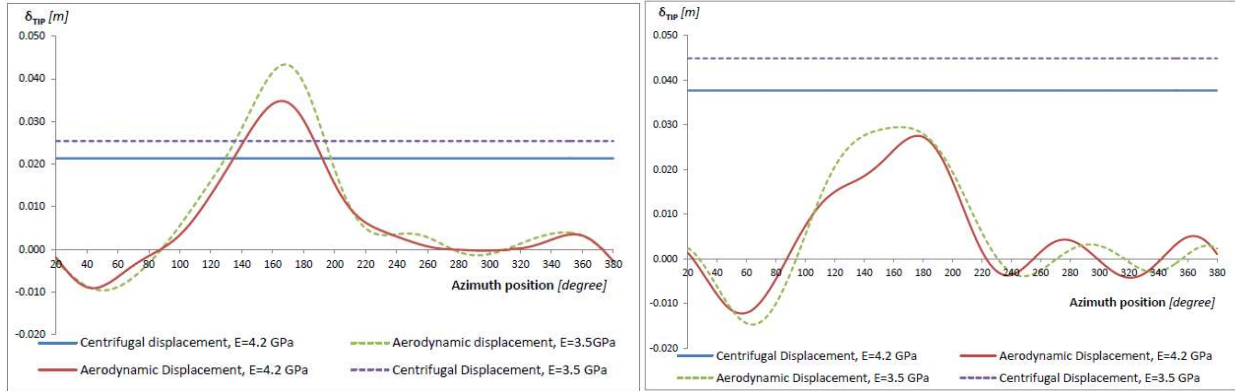
Figure 3.6 - Tip displacement from aerodynamic and inertial forces for a TSR=0.6 (left) and TSR=0.8 (right) (Source: [52])

The idea to solve this problem came from Dr. Beyene who suggested connecting the two tips in order to negate the centrifugal forces and therefore the annexed deformations. Since the blades were connected at that point, their deformation was no longer the same because they were forced to the same displacement. In that way a rotor whose blades can adapt to the incoming flow was obtained with no influence from centrifugal forces. On the next **Figure3.7** the link method and the expected aerodynamic displacement for both the blade linked by the beam with a TSR=1.
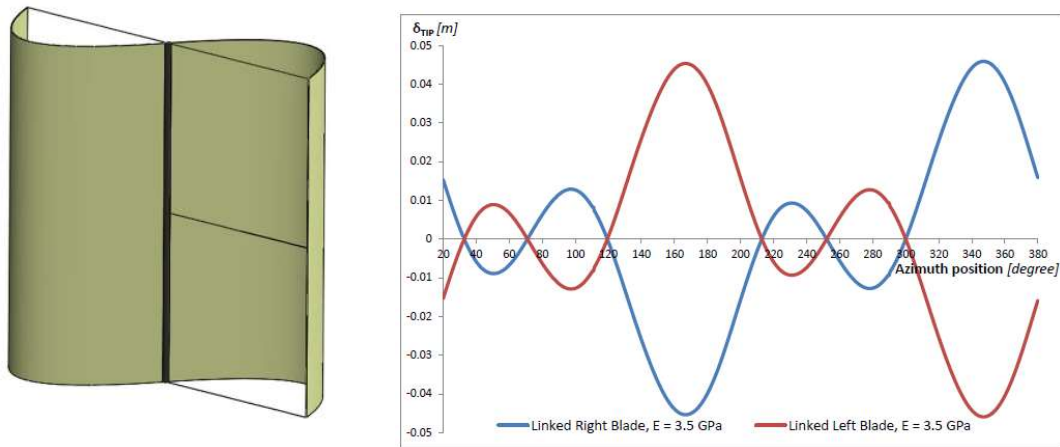
Figure 3.7 - Tips linking system (left) and expected tips' displacement (right) (Source: [52])

36

The final step of that work would have been to study, more specifically, the influence of Young's modulus on the tip displacement with the aim of obtaining a rotor that works with the same tip displacement shown on the previous figure but without the linking beam.

Since the outcomes are accomplished by computational simulations, they cannot be considered to have substantial value without experimental supporting results. Therefore, the aim of this thesis is to provide real proof of these achievements through experimentation.

4 FACILITY DESCRIPTION, DESIGN AND MANUFACTURING PROCESS

4.1 Facility Description

The design process started from the choice of the sectional area occupied by the rotor which was obviously influenced by the dimension of the wind tunnel utilized for the experiments. Therefore, a brief overview of the wind tunnel facility is going to be given. The main structure is an open portion of plastic pipe which terminates on its outlet with a tube axial fan. On the inlet, there is a cluster of hexagonally packed PVC pipes needed to keep the flow as straight as possible inside the tunnel (visible in **Figure4.3**). Concerning the dimensions, the entire tunnel including the flow straightener section is 6.1m, the test section is 1.83m long and it starts and ends at 1.83m and 3.66m from the straightener respectively. The diameter measures about 1.52m and the chosen fan has a diameter of about 1.22m which is not ideal because it doesn't match the tunnel size but at the time of assembly there was no room left in the budget for a larger one. A wind tunnel scheme is provided as follows in **Figure4.1**.
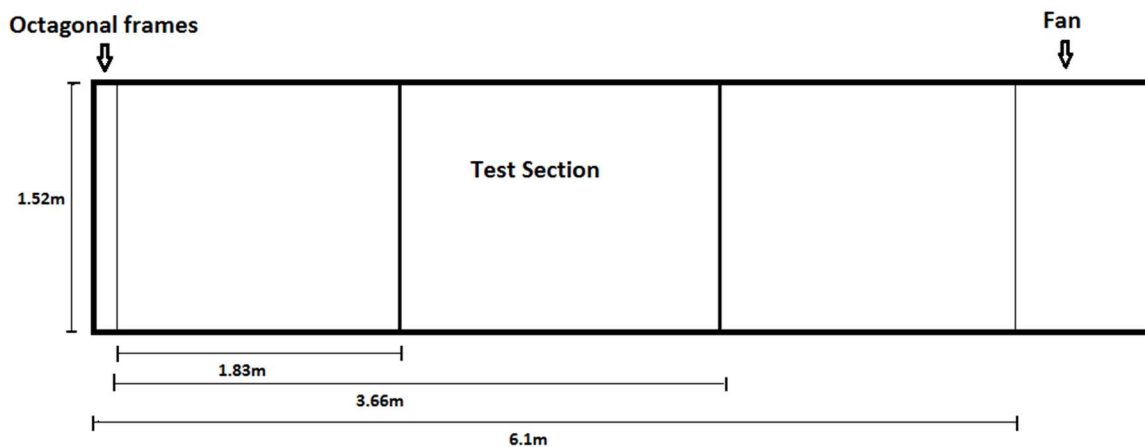
Figure 4.1 - Wind tunnel scheme

The fan system is composed of the fan, the support frame and a variable frequency drive (VFD) which controls the rotational speed with great precision; responsible for creating the flow in the wind tunnel. A metal fan guard and a shroud were manufactured in San Diego State University's engineering department fabrication facility for safety reasons and to adapt the different sizes of the tunnel and the fan (both visible in **Figure4.2**). The fan is supported by a frame equipped with casters so it is easy to move and it allows quick access to the interior of the tunnel. Finally, the support frame for the tunnel is composed of 8 octagonal frames which are tangent to the tunnel in 8 points preventing deformations and to support the weight of a person without compromising the shape of the structure (visible in **Figure4.2**). The inner part of the tunnel is illuminated by three lines of LEDs (visible in **Figure4.3**) and a wireless webcam provides images of the tunnel during the tests.

Figure 4.2 – Wind tunnel's structure and fan
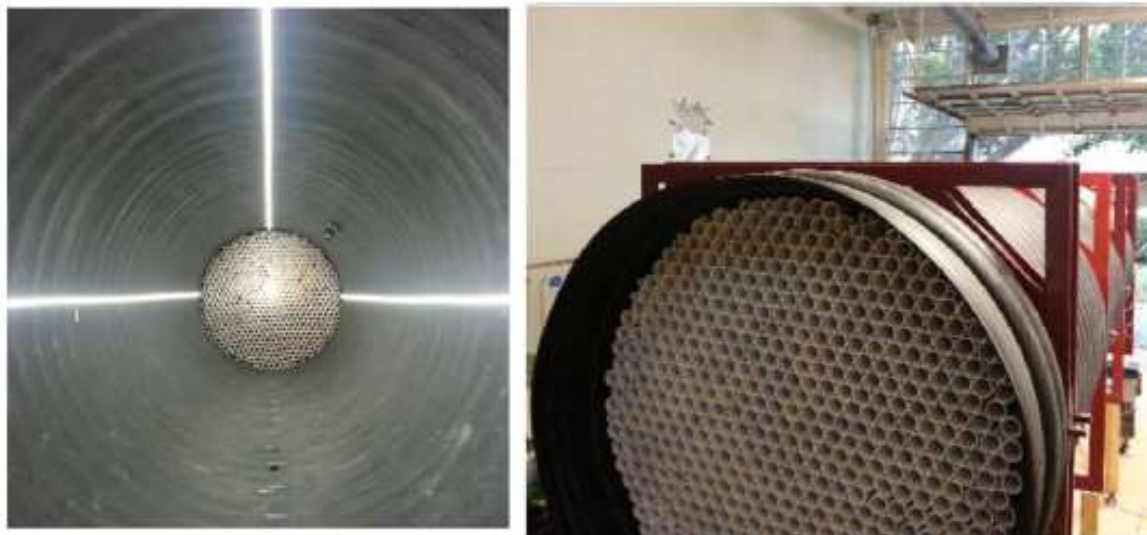
Figure 4.3 – Wind tunnel's inner side with LEDs (left), flow straighteners disposition (right) (Source: [53])

The LED drivers were unfortunately lost during a facility transfer so for that reason three new drivers were bought and installed to make the three LED lines working again. Some electrical connections were repaired (**Figure4.4**). The rotor shaft was replaced for the same reason.
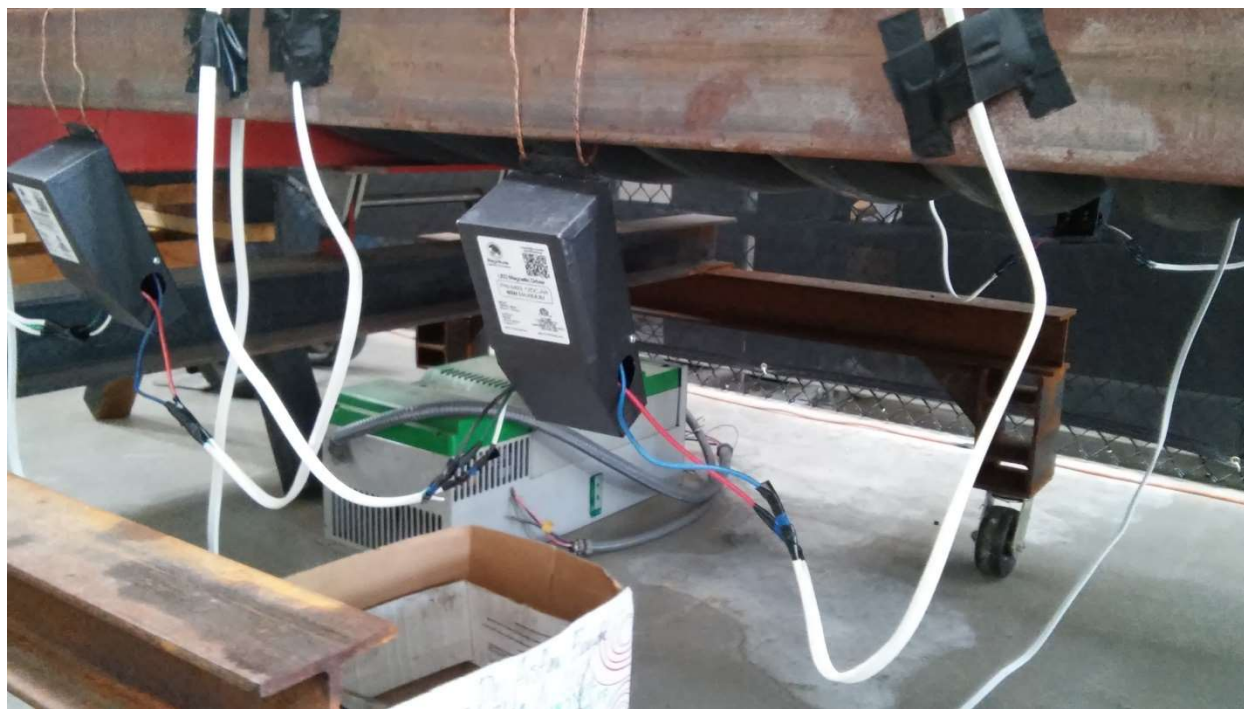
Figure 4.4 – LED's driver installation

A supporting structure was needed to keep the rotor in position, either VAWT or HAWT, and all the accompanying sensors during the tests. This structure is referred to as "test stand" and is shown in the next **Figure4.5**.
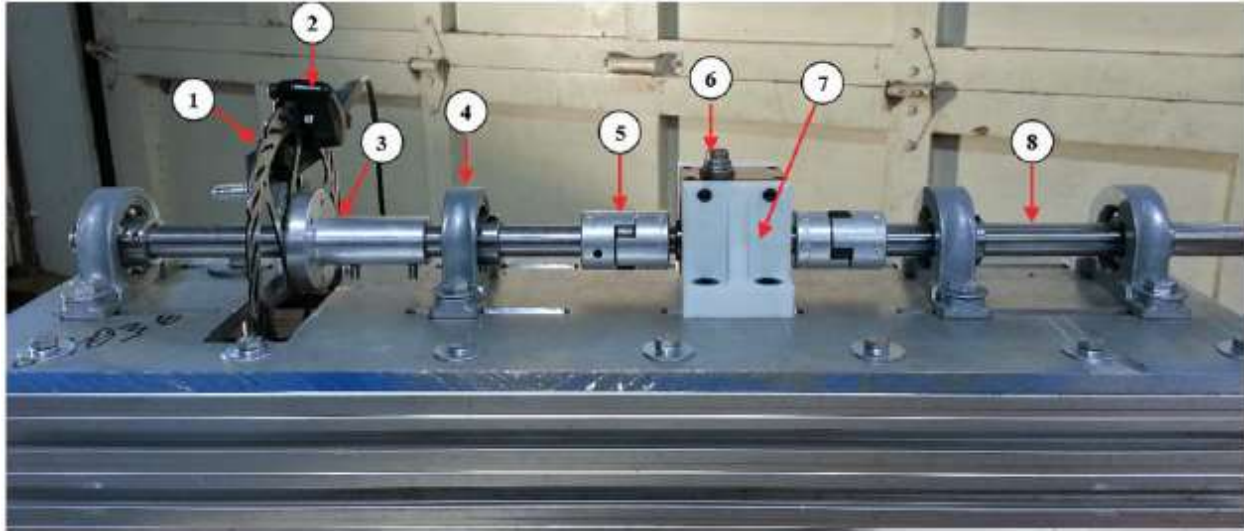
Figure 4.5 - The working components of the test stand: (1) brake disk, (2) brake caliper, (3) brake disk mount, (4) pillow block ball bearing, (5) spider shaft coupling, (6) rotary torque sensor, (7) 3-d printed torque sensor housing, (8) test rig shaft (Source: [53])

The performance evaluation was done by measuring turbine torque and rotational speed through a Futek rotary torque sensor Model TRS-605 with a capacity of 50N.m. This was done in a similar way as the tests carried out by Sandia national labs measuring the performance of Darrieus and Savonius rotors [54]. A National Instruments DAQ chassis connected to a desktop computer running LabVIEW was used to transform and collect the voltage output coming from the sensor. The torque sensor is coupled on one end with the rotor shaft and on the other end with a variable load device that, in this case is a disk brake. The structure that supports the disk brake was built again (**Figure4.6**) because it was lost during the facility transfer.

Figure 4.6 – Brake support (left), brake mounted on the test stand (right)

Nevertheless, the disk brake didn't provide a sufficiently sensible control of the rotational speed. Without precise control of speed, it was difficult to check the blade deformation during the preliminary experiments. Sure enough it was difficult to maintain constant rotational speed at the desired values so a crude solution was adopted using a "hand brake" made of a cloth sheet and the operator's hand (**Figure4.7**). By removing the disk brake support it was possible to grab the entire portion of shaft responsible for the load on the torque sensor. In that way was easier to maintain a constant speed and furthermore to reach really low speed, which was important for evaluating the final performance of the turbine more precisely.

Figure 4.7 – Hand brake

During the first test in the wind tunnel the shaft shook strongly even at low rpm. A decision was made to build an additional support for the shaft (**Figure4.8**), located on the top of the wind tunnel. Therefore, sufficient stability was maintained at every rotational speed tested.
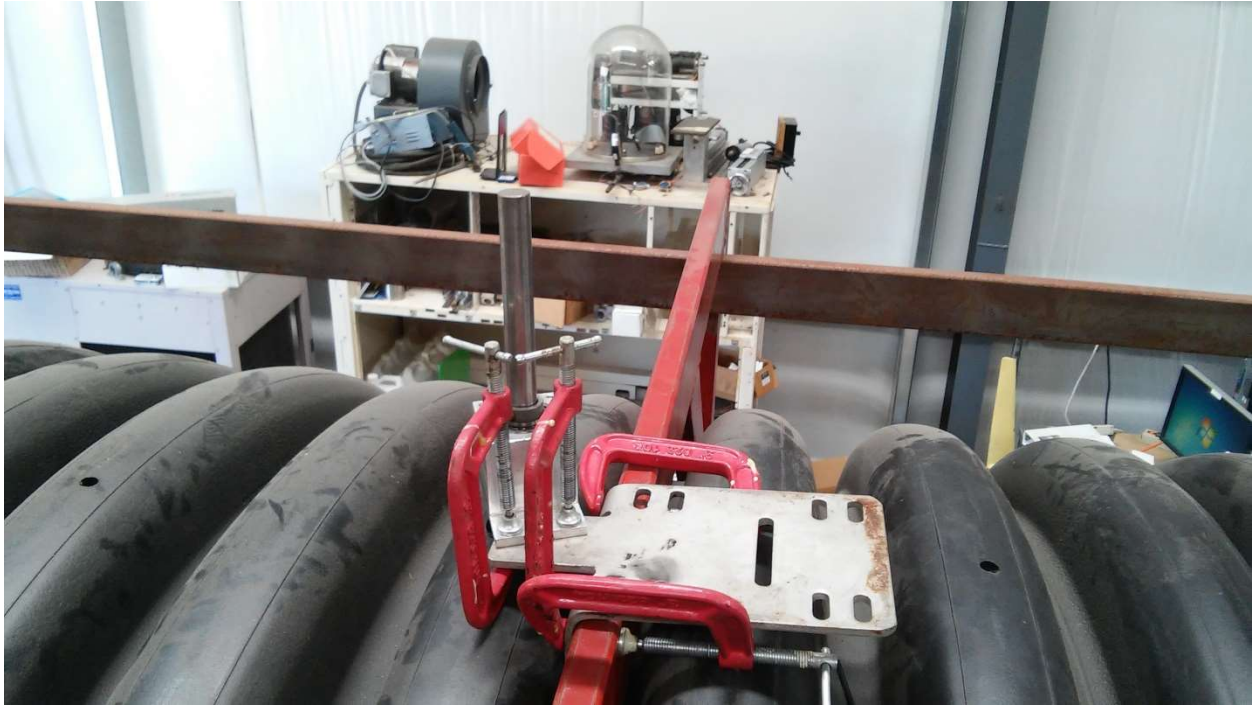
Figure 4.8 – Shaft support at the wind tunnel's top

4.2 Design

This rotor obstructs the wind flow with a large area so a relatively small rotor with a square sectional area of 0.50m side length was chosen. High speed fluctuation would have been recorded in the case of a bigger rotor and since the target of the wind tunnel is to simulate the most realistic conditions possible, this size was chosen. The shape of the rotor was a Spline with a 40° inclination simulated on the previous numerical work and to obtain a square section of 0.50m edge every blade was designed to start and terminate along a 0.25m line. Moreover, the rotor was designed to be as light as possible so a free structure without the use of classical endplates was preferred. As a result, the two blades were directly connected to the shaft with no central gap, usually implemented in this kind of rotor (**Figure4.9**). Starting from a 2D model of one blade designed in Solidworks, two 3D models were built, (**Figure4.10**) the first showing the entire rotor and the second only one of the two blades. It is important to observe that this rotor has a specular structure so the model of one blade is identical to the second one which is just rolled over.
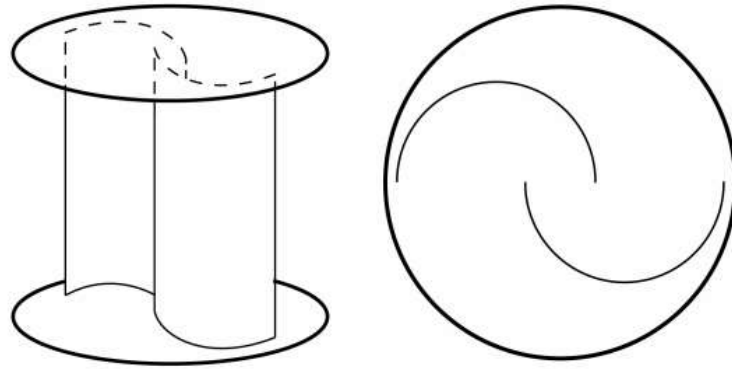
Figure 4.9 - Classic Savonius concept with endplates and central gap
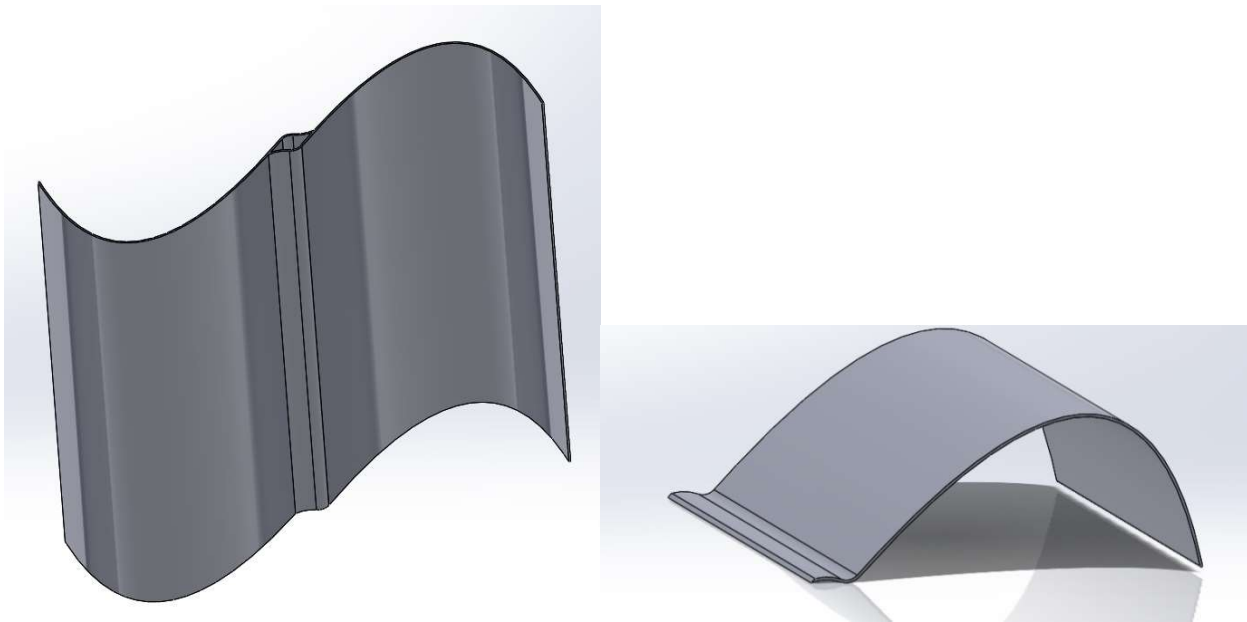
Figure 4.10 - 3D model of the rotor (right), 3D model of one blade (left)

For that phase the thickness was chosen to be 2mm but it is a parameter that will be regulated in next phase of the manufacturing process.

4.3 Manufacturing Process

In order to choose how to manufacture the rotor, a specific material must be selected. Since it was necessary to control the flexibility, a composite material was a good choice because of its ability to be constructed in layers. This feature allows effective control of the thickness and therefore the flexibility could be modulated. Even if carbon fiber and Kevlar fabric were the highest quality materials, fiber glass was chosen because it is less expensive than the others yet it has similar properties. Fiber glass is a material composed of a fabric and a resin. The process with which an object is built is basically an overlap of fabric layers soaked with resin spread on a mold which keeps the desired shape until the resin is dried and therefore rigid. This would lead to the first step of the manufacturing process which was to build a mold.

4.3.1 Mold building

The mold was built with the aim of shaping only one blade, as explained before, the second blade is just the first one rolled over so it was easier to build a mold suitable to shape each blade individually. A mold shaped to build the entire rotor would have been really difficult to build, because of the dimensions and especially because the central shaft location which would present some hollow areas. MDF sheets were chosen as a material for the mold and by measuring the size of the blade from the Solidworks' model, about eight wooden layers were cut from the MDF sheet and overlapped to obtain a volume with the right dimensions. All the layers were stuck to each other using glue and then put under a press (**Figure4.11**) for 24 hours to avoid any air bubbles between the layers.

Figure 4.11 - Press used to help to stick the mold's wood layers

After the glue was completely dry, the 3D model of the blade was transferred to a milling machine which conducted the cutting process of the mold in two phases. In the first, the bulk of the material was roughly removed. Then the milling machine was equipped with a round bit to obtain a smooth shape. Subsequently, to prevent unwanted grooves on the rotor's blade, the entire surface of the mold was sanded achieving perfectly smooth superficies. The last three steps are shown in **Figure4.12** and **Figure4.13**.

Figure 4.12 - Preliminary rough removal of material from the mold (left) and real precise shape cut (right)

Figure 4.13 - Mold after sanding process

After the mold was sanded it was completely covered with four layers of sealer which were needed to avoid absorption of resin during the shaping process of the fiberglass. Furthermore, the sealer was useful to reduce the porosity of the wood and obtain a smoother surface.

4.3.2   Stiff rotor building

Although it was previously stated that the fiberglass is composed of two components, the resin and the fabric, the resin is actually composed of two substances which are resin and a hardener. When mixed in the right proportion these substances are able to solidify. Aeromarine Epoxy Resin 300/21 was the chosen resin for the project. The two substances have to be mixed in a perfect proportion because even a minor error could compromise the features of the fiberglass. The mass proportions of resin were chosen depending on the amount required to reach the desired effect. The mix then consisted of resin with an added mass of hardener which was 48.8% of the total resin mass. The weight of the fabric was 10oz for each square foot. For the building process of the first stiff rotor 8 layers were utilized so 8 fabric sheets of the right dimensions were cut and spread on the mold with the resin (**Figure4.14**). Finally, to maintain a regular shape in the shaft location a pole of the same size of the real shaft was squeezed into this position and left there for 24h.

Figure 4.14 - First fiber layer spread on the mold (left) and the blade after 6 layer of fiberglass with a sample of the real shaft pressed on its location to preserve a good semicircular shape (right)

After the two blades were dried they were cut using a band saw to obtain the same size as the model built with Solidworks software. They were then sanded on all edges. In order to avoid movements of the shaft in its location, a sort of shaft location was built by the use of a mixture of resin (epoxy resin+hardener) and a plastic powder. That mixture was adopted because in case of the use of just resin, the location would have been too rigid producing some issues once the rotor

was attached to the shaft for testing. Therefore, the shaft was placed in the correct position on the first blade and the mixture was spread in three points. Subsequently a plastic sheet was put over the shaft then the mixture was spread again in the same three spots. Finally, the second blade was squeezed in the correct position against the shaft to give the right shape to the mixture. The plastic sheet was necessary to avoid sticking the two blades together because of the mixture. Once the resin was dry the upper blade was detached and then so was the plastic sheet and finally the shaft was removed from its location. In the next **Figure4.15** the two blades stuck to form the shaft location and the final result.

Figure 4.15 - Squeezed blades to mold the shaft location (left), the shaft location obtained and drilled (right)

Thanks to the elasticity of the dried mixture it was relatively easy to place the rotor onto the real shaft. Is easy to notice that with this method it is simple to install different rotors onto the shaft without dismantling any part of the supporting structure. Finally, to connect the blades, six holes were drilled on the two rotor's blades along the position of the shaft to allow the use of screws.

4.3.3   Flexible rotor building

The concept at the base of the flexible rotor development was the simple control of flexibility done by managing the number and the position of layers, mainly on the terminal part of each bucket which was the necessary flexible section. The goal was to obtain a deformation between 10 and 15 degrees around the main operational working range. The 10-15 range was chosen as a result of previous researches conducted at SDSU [55]. Since it was practically impossible to

predict the deformation of each different disposition of fiberglass layers, the only way to proceed was through successive attempts. Therefore, a first rotor with the layer disposition shown in the next **Figure4.16** was built and to check the deformation it was tested in the wind tunnel with the use of a high-speed camera able to collect clean images of the spinning rotor.
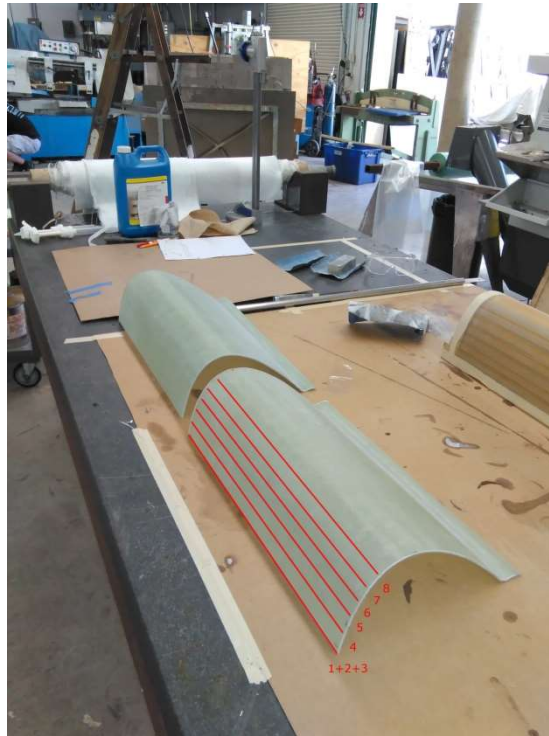
Figure 4.16 - First flexible rotor attempt. Scheme of layer's disposition

Unfortunately, no noticeable deformation arose from the pictures so it was decided to proceed to build another rotor with less layers in the proximity of the tip as shown in the next **Figure4.17**.
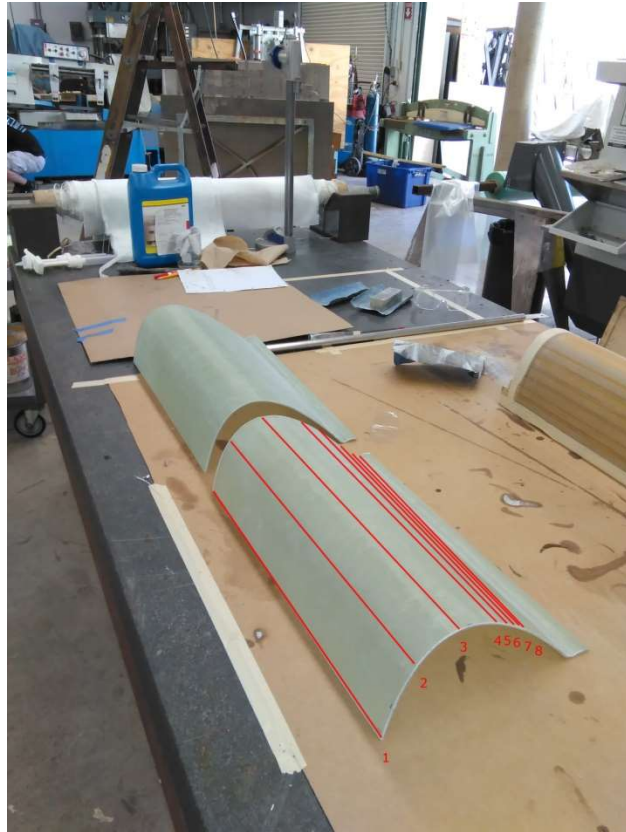
Figure 4.17 - Second flexible rotor attempt. Scheme of layer's disposition

The rotor was then tested and a deformation included in the range 30-35° was found. It is necessary to remember that this type of rotor shows really high inertial forces thus a large part of the checked deformation has to be attributed to the centrifugal forces. For a qualitative evaluation of the inertial deformation the rotor was spun without wind flow. A highly sensitive drill able to spin at low rpm was utilized to reach that target. The supporting bearings were partially taken off to leave room for the drill and an aluminum adapter was built to be able to link the drill to the shaft. A lathe was utilized to build the adapter. In the following **Figure4.18** the new component and the drill placed in its working position.
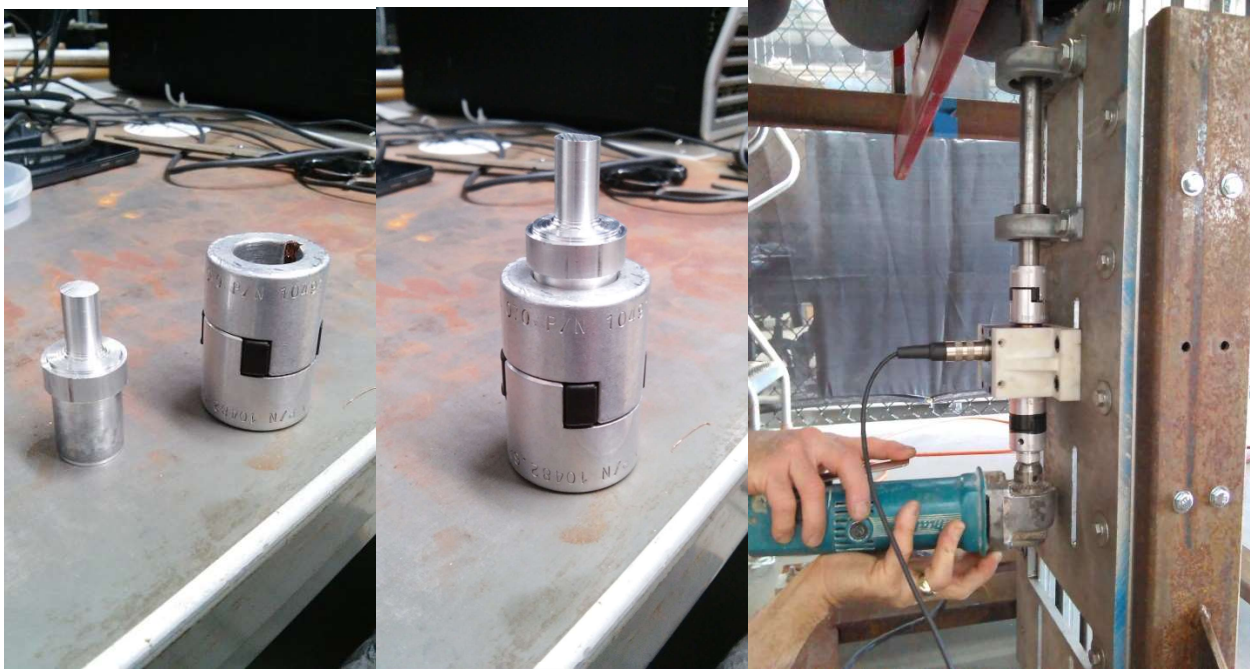
Figure 4.18 - From the left in order: 1) Connection between drill and Shaft-torque sensor adapter. 2) Two connected parts. 3) Connected parts linked to the torque sensor and to the drill

A 15-25° deformation of centrifugal forces was found and a qualitative evaluation of the aerodynamic deformation could be done by a subtraction between the two values found with and without wind flow respectively. In that case an interval between 10-20° degrees is reached. It is clear that the next step of the building process was to connect the two tips because of excessively high inertial forces found either on CFD simulations or the experimental tests. Once the two tips are connected the deformation process radically changes because the two tips are forced to deform within the same range but in the opposite direction. The deformation test conducted with and without the wind flow in the wind tunnel boded well so the two tips were connected in four points by a fishing line as shown in the next **Figure4.19**.
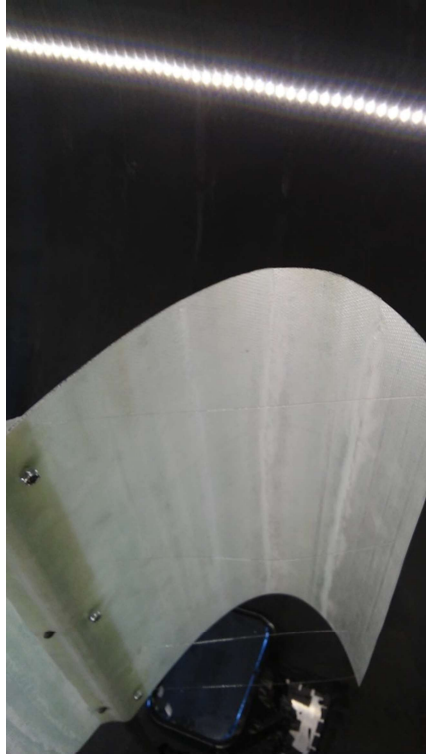
Figure 4.19 - Fishing chord used to link the two tips on the flexible rotor

Other tests were done to check the deformation of this rotor and the required deformation was found. However, the two rotors were not ready for the final tests because of the difference in weight that they had in order to obtain a fair comparison, the same weight had to be reached for each rotor. As a result, more material was added to the flexible rotor to manage its weight. The images from the high-speed camera show some bumps in the portion of the blade between two connection points so it was decided to reinforce the tips by two narrow fiber bands, one for each side, spread all long the two extremities of the blades. The material used to increase the weight was added as close as possible to the shaft location in order to avoid unwanted changes in the tip's flexibility. The material was weighed and spread on the two side of the blades (**Figure4.20**).

Figure 4.20 - Additional spread material for the increase of the weight and to reinforce the tips

5   HIGH SPEED CAMERA DATA

5.1   Introduction

The method utilized to check the deformation of the rotor was the analysis of images taken during different turbine working conditions. Therefore, a high-speed camera was installed inside the wind tunnel (**Figure5.1**) to capture images for analysis. Unfortunately, the camera was not suitable to take shots of the rotor from underneath because of a lack of space in the wind tunnel. A different strategy was used involving a mirror attached to the wind tunnel surface, underneath the bottom of the rotor. This method allowed clear images to be captured.

Figure 5.1 - High speed camera placed in the tunnel focusing the reflected image on the mirror

5.2   Stiff Rotor Deformation Check

It was important to perform an initial check for the absence of any deformation on the stiff rotor. To do this, some images at different rotational speed were taken while maintaining a constant wind speed. Three tests were done with a 7m/s wind speed as listed below (**Table5.1**, **Figure5.2**) and subsequently an additional test at 8.5m/s was conducted to confirm the hypothesis of complete stiffness. In order to obtain these results, the images were analyzed checking the angle between two lines used as reference points. The two lines were drawn using the image

manipulating software "Gimp" and the images were collected by Photron Fast Cam Viewer software.

IMAGE COMPARISON STIFF ROTOR		
REFERENCE ANGLE [°]		60.14
RPM	ANGLE [°]	DISPLACEMENT [°]
260 (8.5m/s)	61.29	-1.15
200 (7m/s)	59.32	0.82
160 (7m/s)	61.54	-1.4
100 (7m/s)	59.81	0.33

Table 5.1 – Stiff rotor blade's displacement data
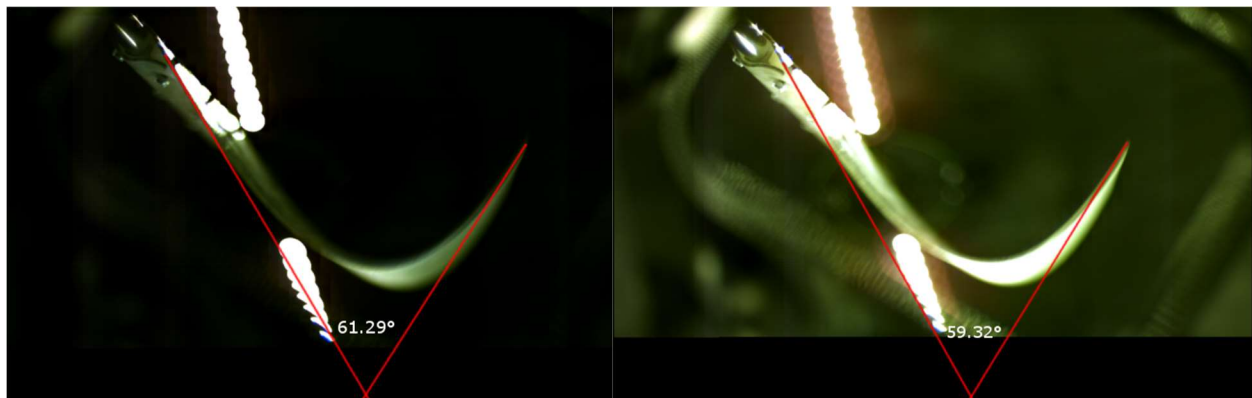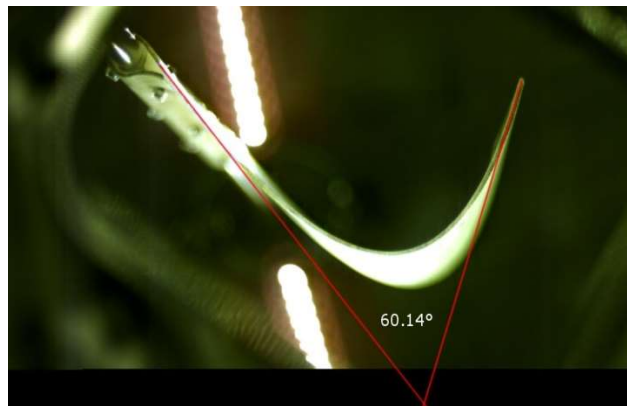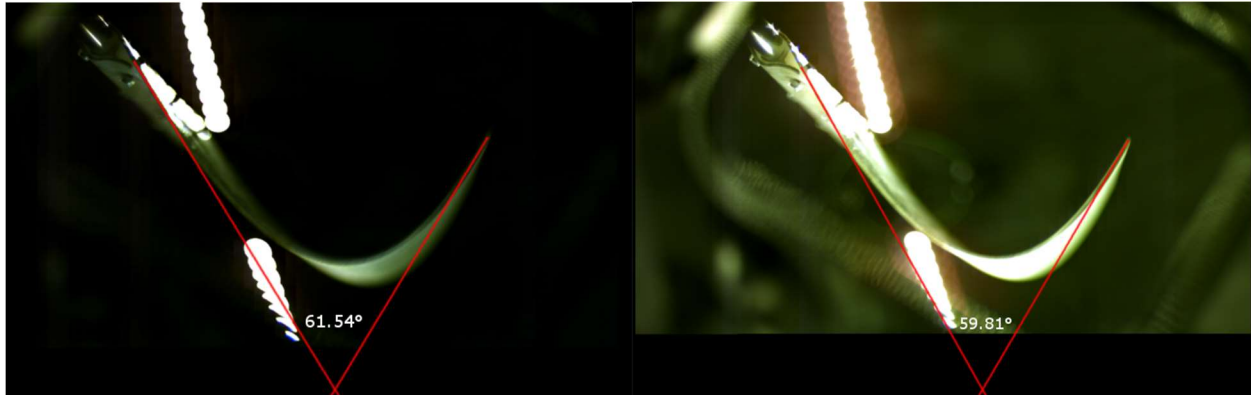
Figure 5.2 – Stiff rotor: standing blade image (top), moving blade images at each rotational speed (other four)

It was chosen to mark two lines, one along the tangent of the blade's tip and the other one along the first few centimeters of the blade, starting from the axis. The second line was considered to be stationary because the wind force acting against that part of the blade was really weak and because of this the centrifugal force only acted along a linear path towards the outer ends of the rotor blades. The variation of angle between the two lines was only attributable to the tip displacement (second tracked line) which was the section that needed to be checked. The reference point angle was the angle between the two lines found in the picture of the rotor when completely stationary and no forces acting on it. By angle subtraction, the tip displacement was found on each tested working condition. The rotor was considered completely rigid even if the differences between the reference point angle and the others were not exactly zero. There are two reasons which explain this choice, firstly the difference between the various angles is never over 1°. Secondly thanks to the additional experiment at 8.5m/s of wind speed, it was found that the angle differences had no physical validation. In fact, it was expected that there would be increased deformation for low and high rpm because of the aerodynamic and inertial forces respectively. At low rpms (using the braking system), the forces from the wind should cause deformation and at high rpms, the inertial forces should cause deformation. As the recordings showed that trend was not followed. For those reasons the little displacement found was attributed not to the forces acting on the blade but rather a lack of precision in measurement. The negative deformation values have no relevance and the rotor will be assumed to have maintained its rigid structure.

5.3 First Flexible Attempt Deformation Check

Subsequently the first flexible rotor was built and the deformation was checked using the same procedure. Almost the same results as the previous rotor were found and a deformation of 2° degrees was shown (**Table5.2**, **Figure5.3).** This time though, the rotor deformation followed the physical expectations. In fact, the higher deformation was found for the highest wind speed and it was simply attributable to the high centrifugal forces. It was also noticed that the displacement started to increase again at very low rotational speeds which is ascribable to the prevalent aerodynamic forces acting at that working condition. However, the deformation was minimal so the rotor was considered too stiff and therefore still unsuitable to provide the desired results.

IMAGE COMPARISON FIRST FLEXIBLE ROTOR		
REFERENCE ANGLE [°]		60.57
RPM	ANGLE [°]	DISPLACEMENT [°]
250 (8.5m/s)	63.66	3.09
203 (7m/s)	63.46	2.89
160 (7m/s)	61.33	0.76
100 (7m/s)	61.96	1.39

Table 5.2 – First flexible rotor attempt blade displacement data
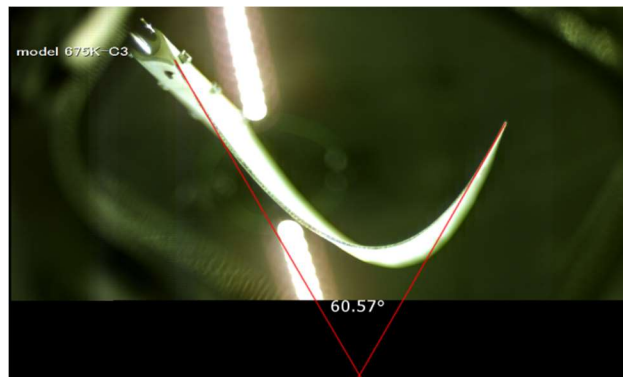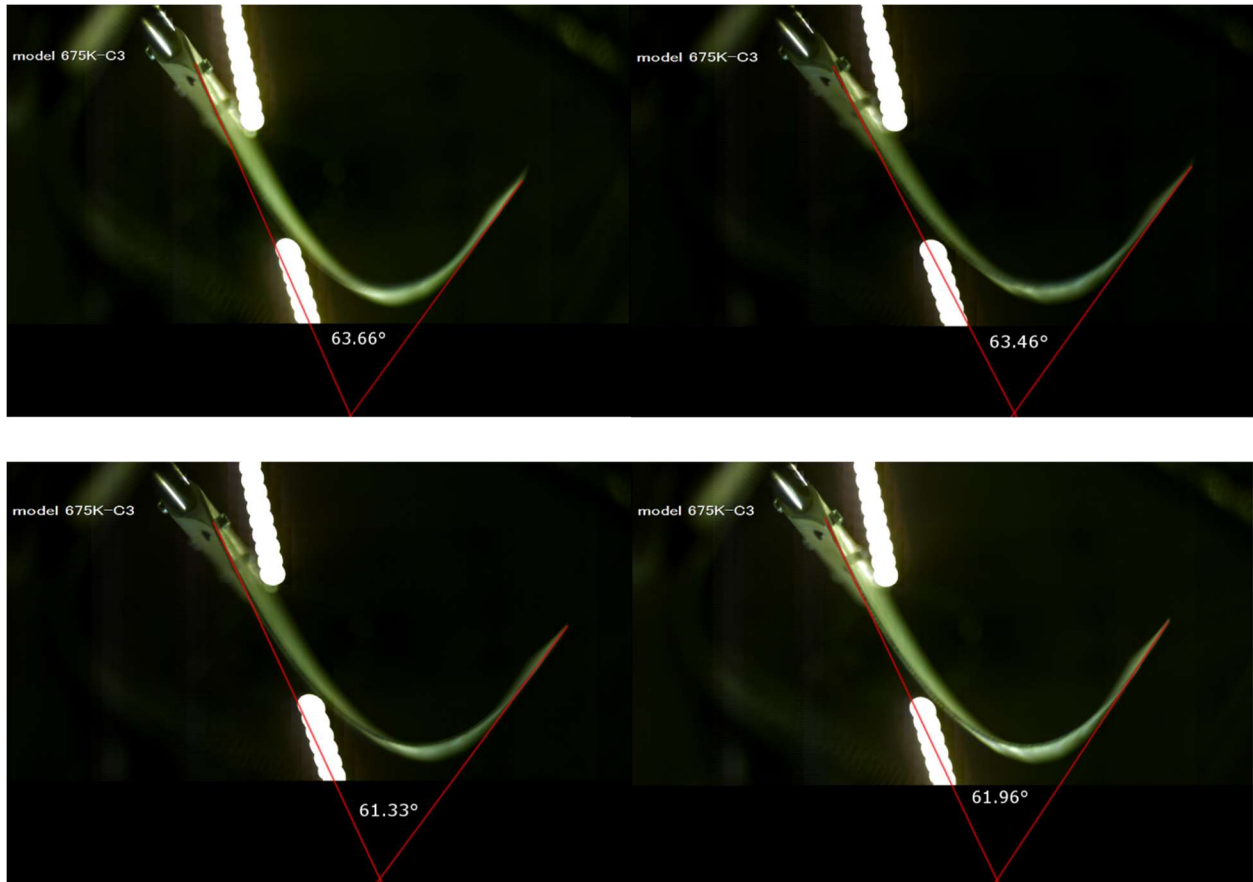
Figure 5.3 – First flexible rotor attempt: standing blade image (top), moving blade images at each rotational speed (other four)

5.4 Second Flexible Rotor Attempt Deformation Check

The same wind flow speed conditions were used but completely different results were achieved with the third built rotor (**Table5.3**, **Figure5.4**). In that case a large deformation was checked in particular between 30° and 38° degrees. According to previous research [mcphee research] the target aerodynamic displacement was a value between 10° and 15° degrees obtained at the maximum efficiency rotational speed. Even if the found displacement looks much higher than the target, it is important to consider that the simulations conducted on this type of rotor showed a high displacement caused by inertial forces since the two tips were not linked in this first test. The result has to be considered only indicative of the desired results. In order to evaluate qualitatively the centrifugal deformation another test was conducted using a drill to spin the rotor without a wind flow and a 5°-21° deformation was found, leaving a good range attributable to

aerodynamic displacement (**Table5.4**, **Figure5.5**). Starting from these results a decision was made to link the two tips in order to negate the centrifugal deformation and 8°-18° degrees of deformation were found (**Table5.5**, **Figure5.6**). In the last case, the experiments were conducted at only one wind speed (7m/s) because the additional test would provide no additional data as the deformation was already found at the lower wind speed. An 8° deformation corresponding to a rotational speed of 230rpm with the rotor spinning without any brake and an 18° deformation corresponding to 100rpm were found. The 230-100rpm range included almost all the operational range because 100rpm was really close to the minimum maintainable rotational speed and 230rpm corresponded to the free rotational speed of the rotor. Since the maximum efficient working condition had to be included in the maximum/minimum speed interval, the rotor was considered suitable for the comparison tests. All the results for the three different tests are shown below.

IMAGE COMPARISON 2ND FLEXIBLE ROTOR (NO TIPS LINKED AND NO ADDITIONAL WEIGHT)		
REFERENCE ANGLE [°]		59.03
RPM	ANGLE [°]	DISPLACEMENT [°]
190 (8.5m/s)	96.95	37.92
150 (7m/s)	95.2	36.17
100 (7m/s)	95	35.97
85 (7m/s)	89.84	30.81

Table 5.3 - Second flexible rotor attempt blade displacement data
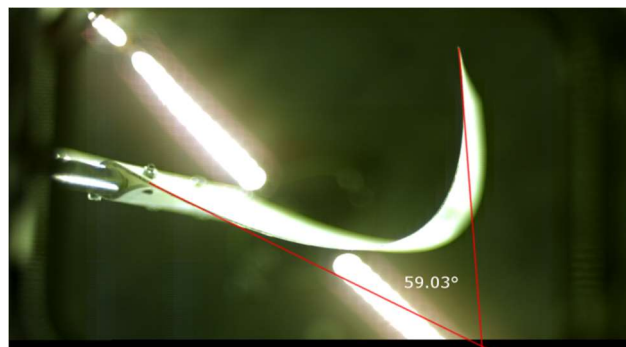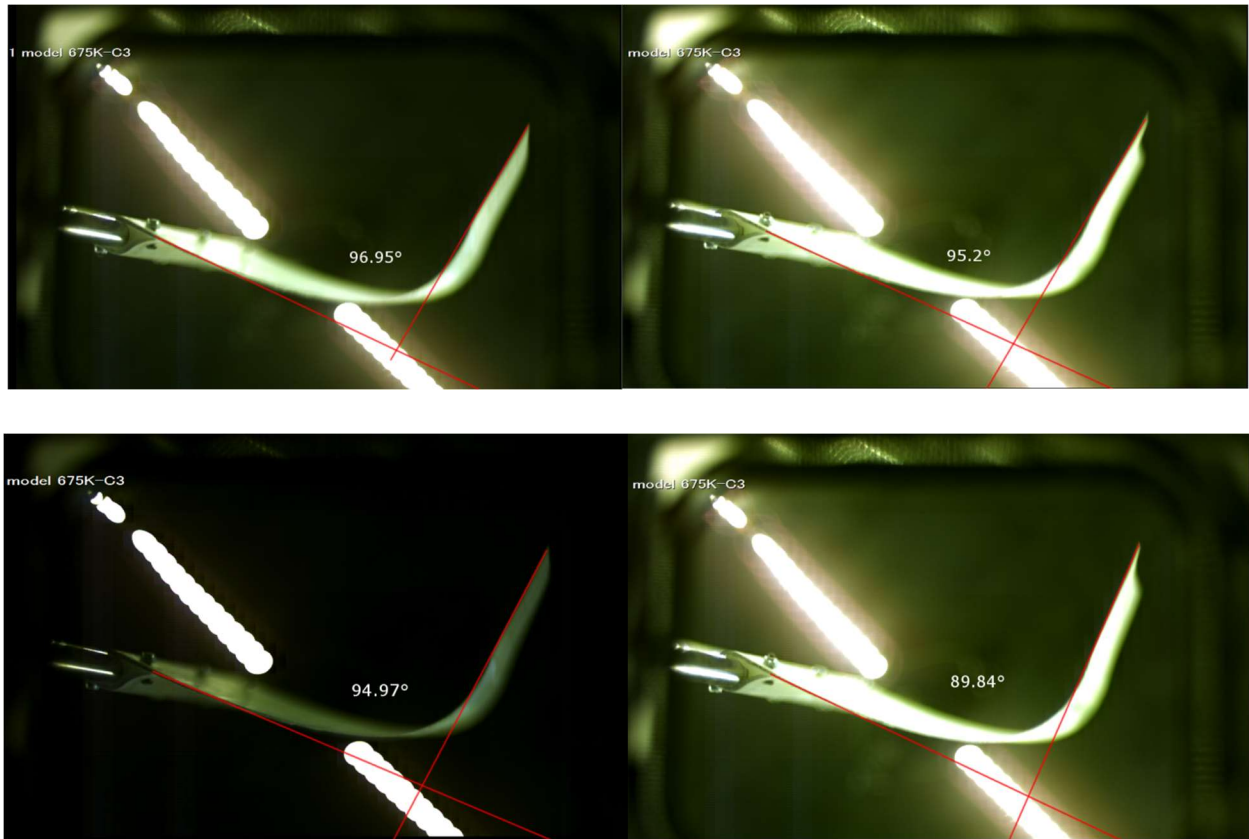
Figure 5.4 – Second flexible rotor attempt: standing blade image (top), moving blade images at each rotational speed (other four)

IMAGE COMPARISON 2ND FLEXIBLE ROTOR (CENTRIFUGAL FORCES)		
REFERENCE ANGLE [°]		62.96
RPM	ANGLE [°]	DISPLACEMENT [°]
300	84.11	21.15
200	75.31	12.35
150	74.43	11.47
100	68.81	5.85

Table 5.4 - Second flexible rotor attempt blade centrifugal displacement data
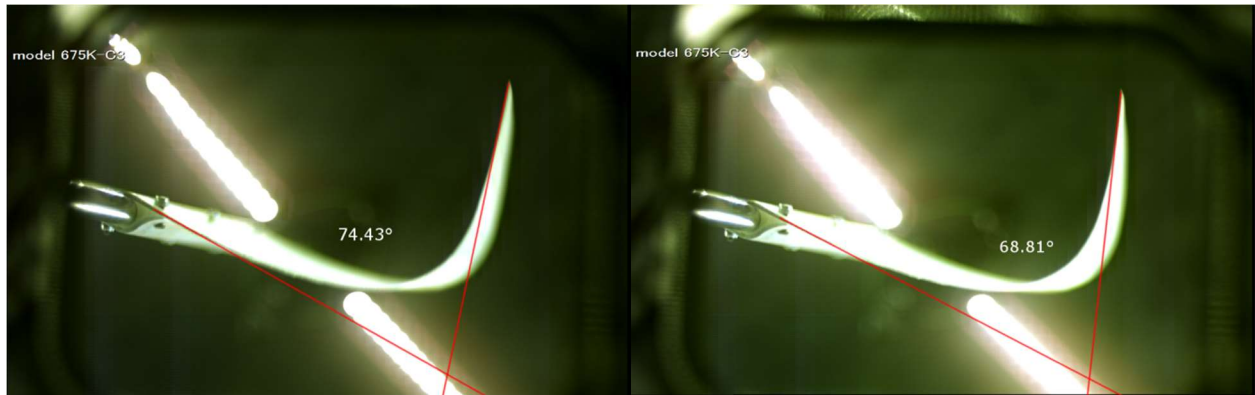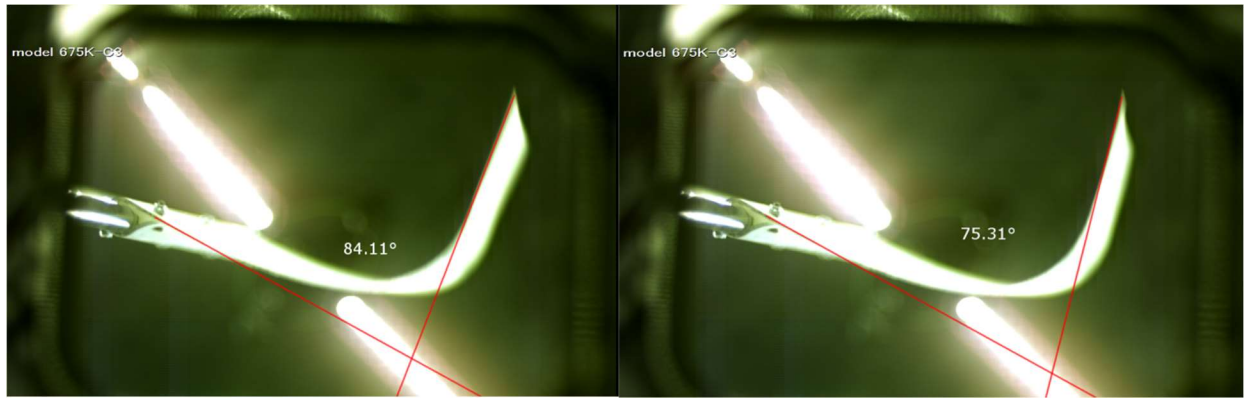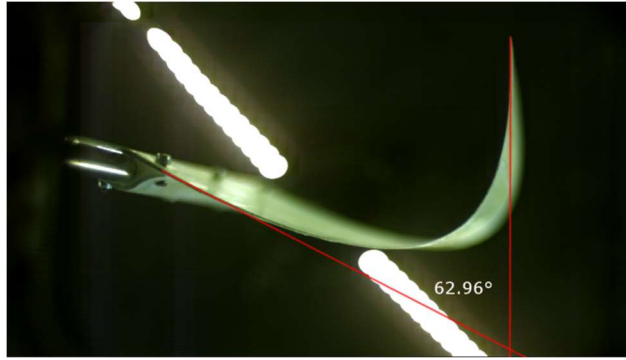
Figure 5.5 – Second flexible rotor attempt (centrifugal forces): standing blade image (top), moving blade images at each rotational speed (other four)

IMAGE COMPARISON 2ND FLEXIBLE ROTOR (TIPS LINKED AND NOT INCREASED WEIGHT)		
WIND SPEED [m/s]		7
REFERENCE ANGLE [°]		53.41
RPM	ANGLE [°]	DISPLACEMENT [°]
230	60.56	8.87
150	66.98	15.29
100	69.73	18.04

Table 5.5 - Second flexible rotor attempt blade displacement data with linked tips
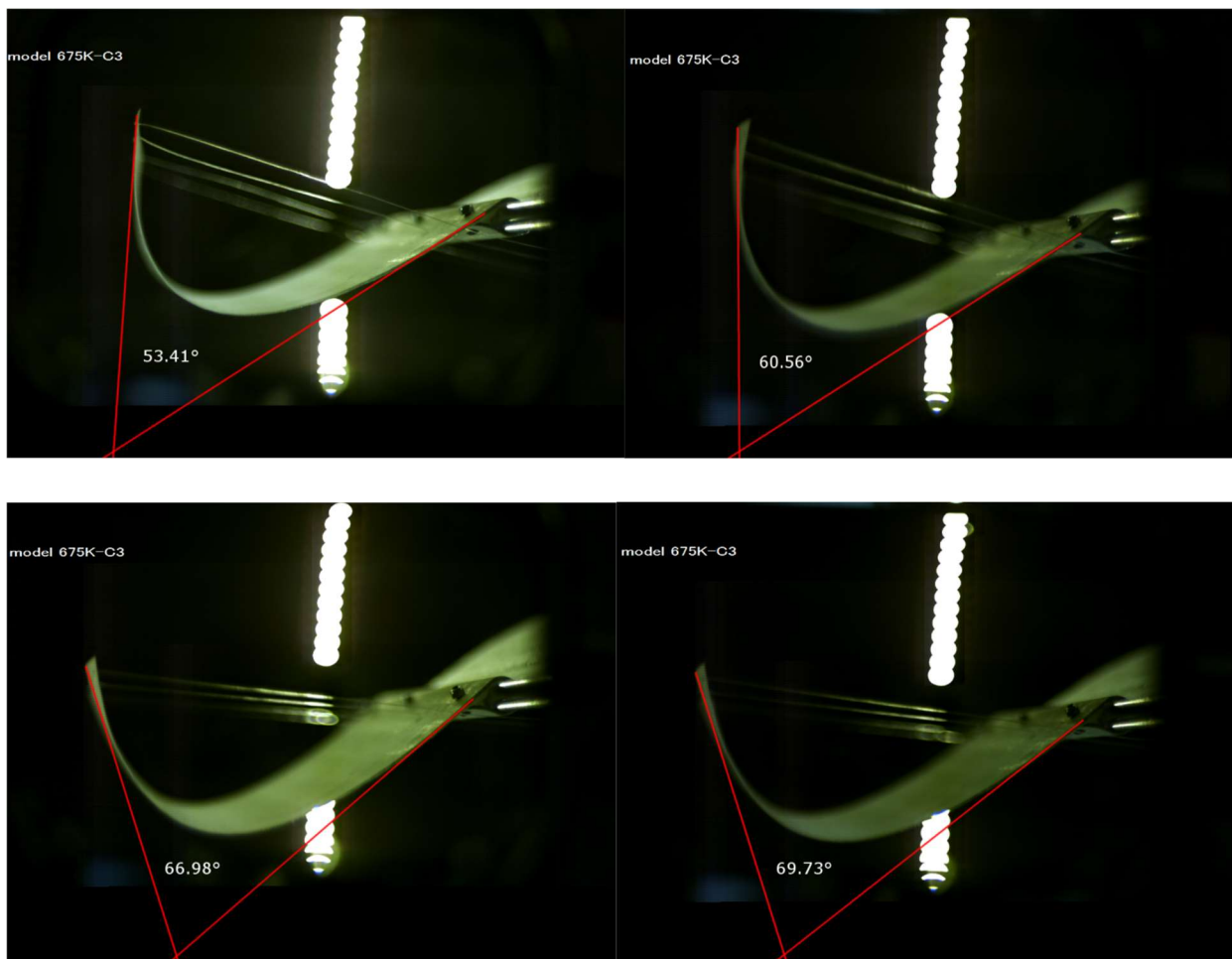
Figure 5.6 – Second flexible rotor attempt with linked tips: standing blade image (upper-left), moving blade images at each rotational speed (other three)

5.5 Second Flexible Attempt Deformation Check After Material Addition

Since the rotor weight was increased, a little variation in the flexibility could have occurred so another deformation check was conducted. Even if the wind speed utilized in the previous thesis work was 7m/s, other tests at 9.5m/s, 8m/s, 5m/s and 3m/s were done in order to evaluate the deformation of the rotors for low wind speed conditions which is the objective of the performance analysis (**Table5.6**, **Table5.7, Table5.8**, **Table5.9**, **Table5.10**, **Table5.11**, **Figure5.7**, **Figure5.8**, **Figure5.9**, **Figure5.10**, **Figure5.11**, **Table5.12**). A defined deformation, for every testing condition was found for three different values of rpm. All the results are listed on the following tabs and images.

IMAGE COMPARISON 2ND FLEXIBLE ROTOR (TIPS LINKED AND INCREASED WEIGHT)		
WIND SPEED [m/s]		7
REFERENCE ANGLE [°]		51.69
RPM	ANGLE [°]	DISPLACEMENT [°]
230	59.95	8.26
165	67.01	15.32
100	69.04	17.35

Table 5.6 - Second flexible rotor attempt blade displacement data with linked tips and increased weight at 7m/s wind speed
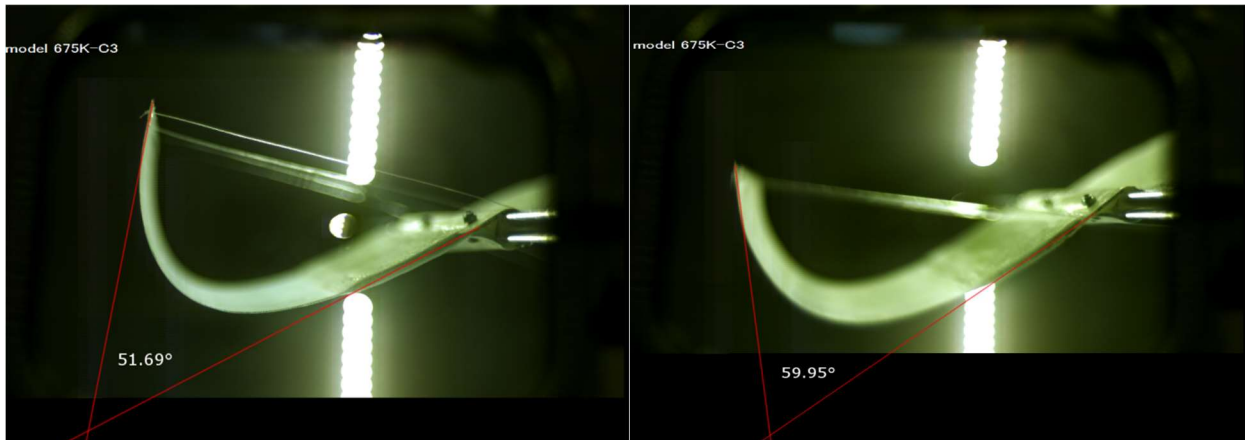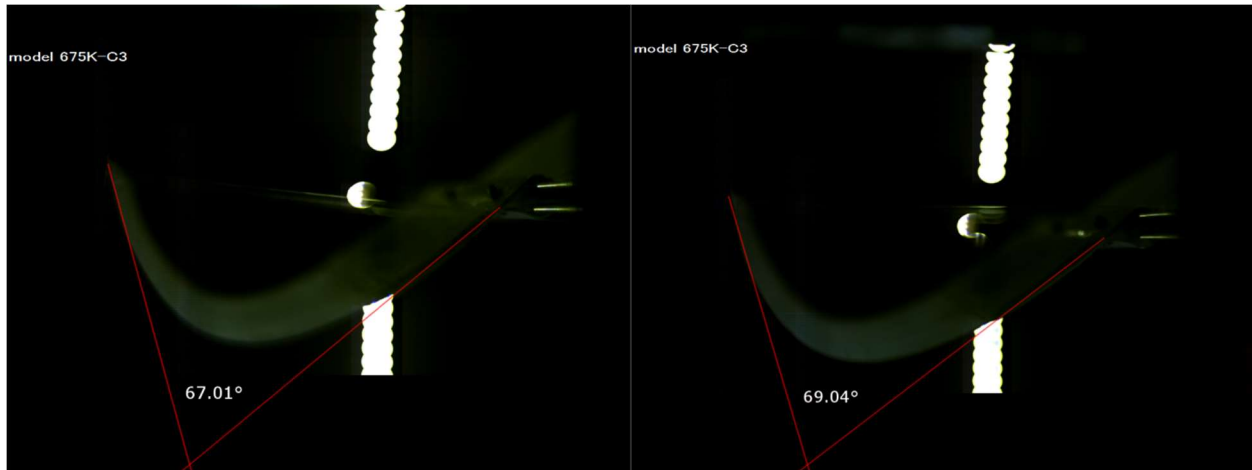
Figure 5.7 – Second flexible rotor attempt with linked tips and increased weight at 7m/s wind speed: standing blade image (upper-left), moving blade images at each rotational speed (other three)

IMAGE COMPARISON 2ND FLEXIBLE ROTOR (TIPS LINKED AND INCREASED WEIGHT)		
WIND SPEED [m/s]		8
REFERENCE ANGLE [°]		51.69
RPM	ANGLE [°]	DISPLACEMENT [°]
260	60.88	9.19
190	67.9	16.21
115	84.72	33.03

Table 5.7 - Second flexible rotor attempt blade displacement data with linked tips and increased weight at 8m/s wind speed
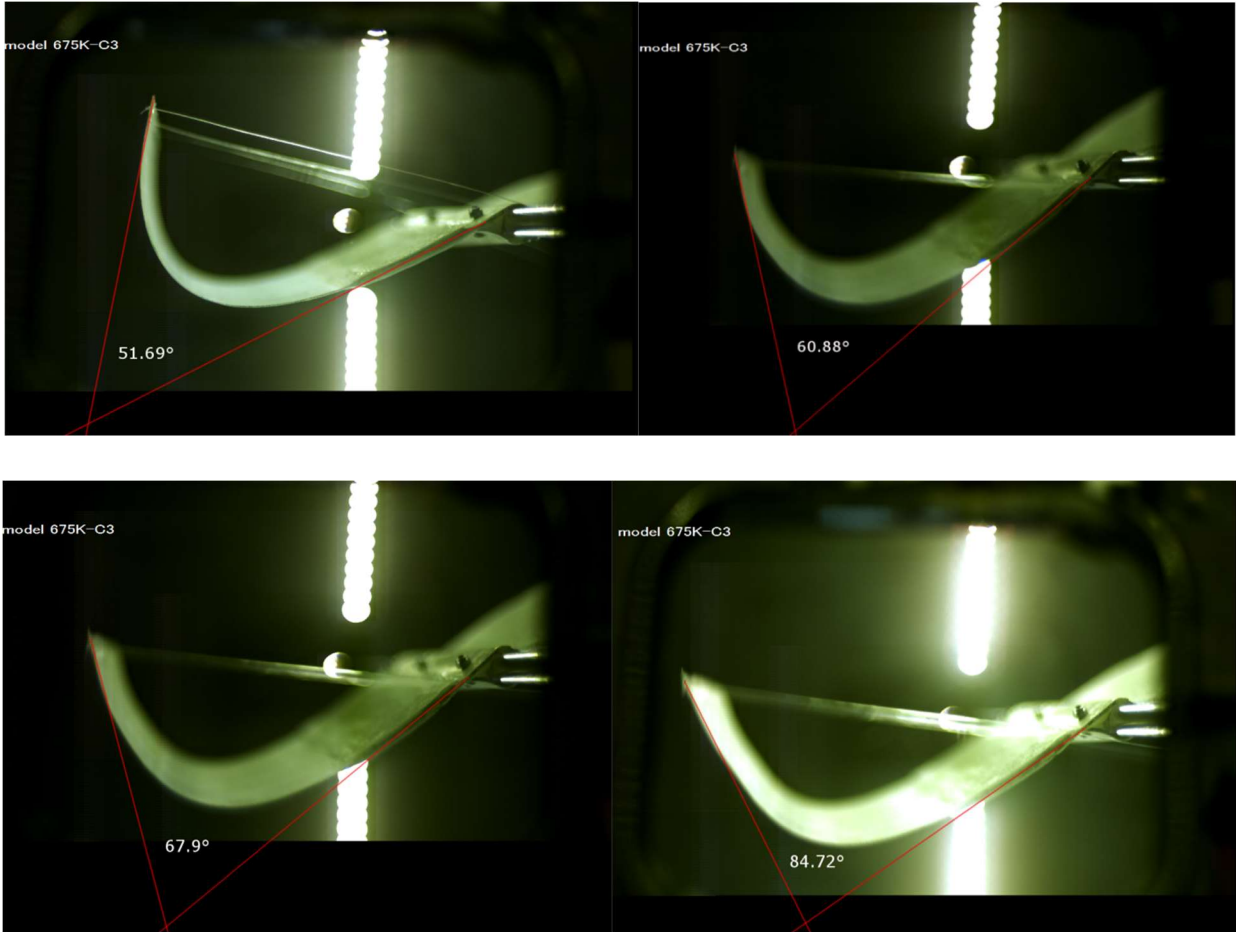
Figure 5.8 – Second flexible rotor attempt with linked tips and increased weight at 8m/s wind speed: standing blade image (upper-left), moving blade images at each rotational speed (other three)

IMAGE COMPARISON 2ND FLEXIBLE ROTOR (TIPS LINKED AND INCREASED WEIGHT)		
WIND SPEED [m/s]		9
REFERENCE ANGLE [°]		51.69
RPM	ANGLE [°]	DISPLACEMENT [°]
295	66.7	15.01
215	71.57	19.88
130	85.64	33.95

Table 5.8 - Second flexible rotor attempt blade displacement data with linked tips and increased weight at 9m/s wind speed
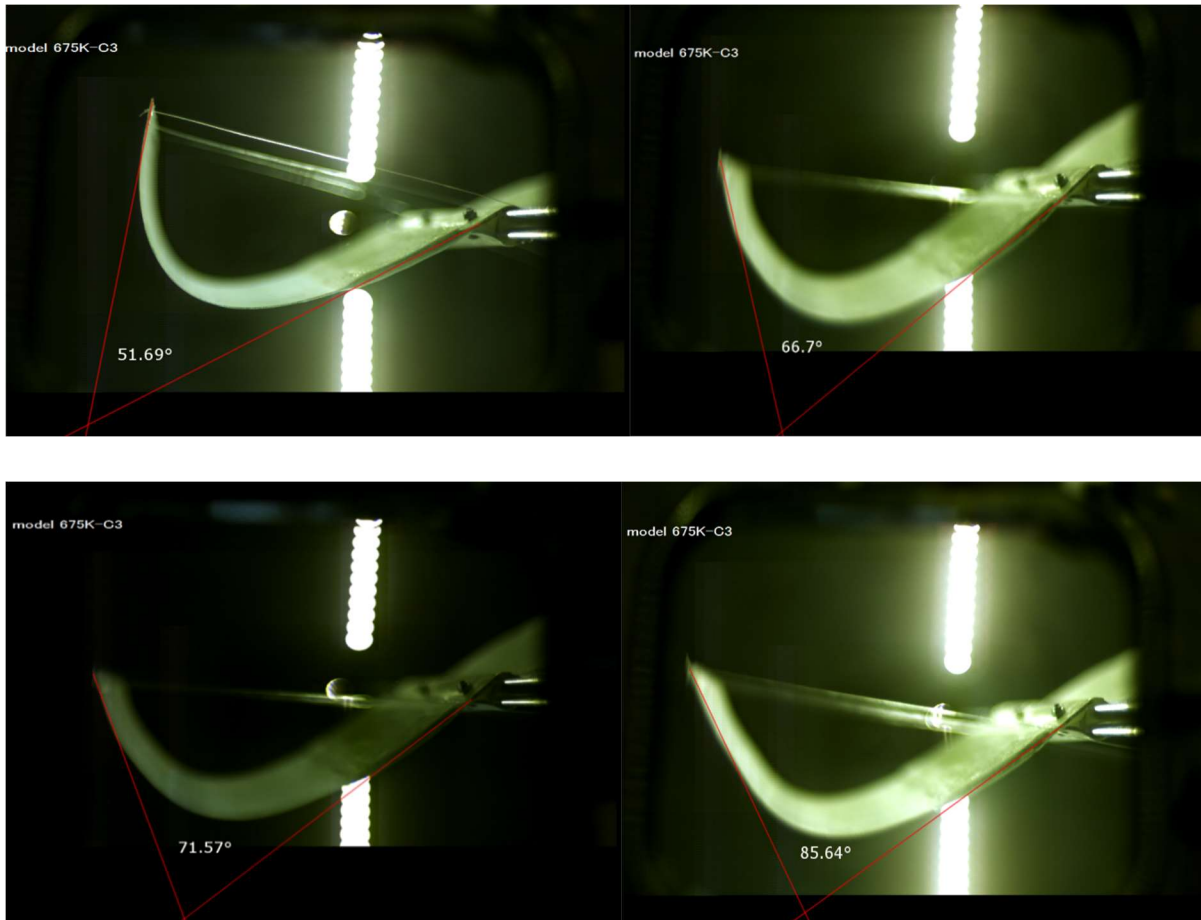
Figure 5.9 – Second flexible rotor attempt with linked tips and increased weight at 9m/s wind speed: standing blade image (upper-left), moving blade images at each rotational speed (other three)

IMAGE COMPARISON 2ND FLEXIBLE ROTOR (TIPS LINKED AND INCREASED WEIGHT)		
WIND SPEED [m/s]		9.5
REFERENCE ANGLE [°]		55.52
RPM	ANGLE [°]	DISPLACEMENT [°]
305	70.86	15.34
230	78.64	23.12
140	90.31	34.79

Table 5.9 - Second flexible rotor attempt blade displacement data with linked tips and increased weight at 9.5m/s wind speed
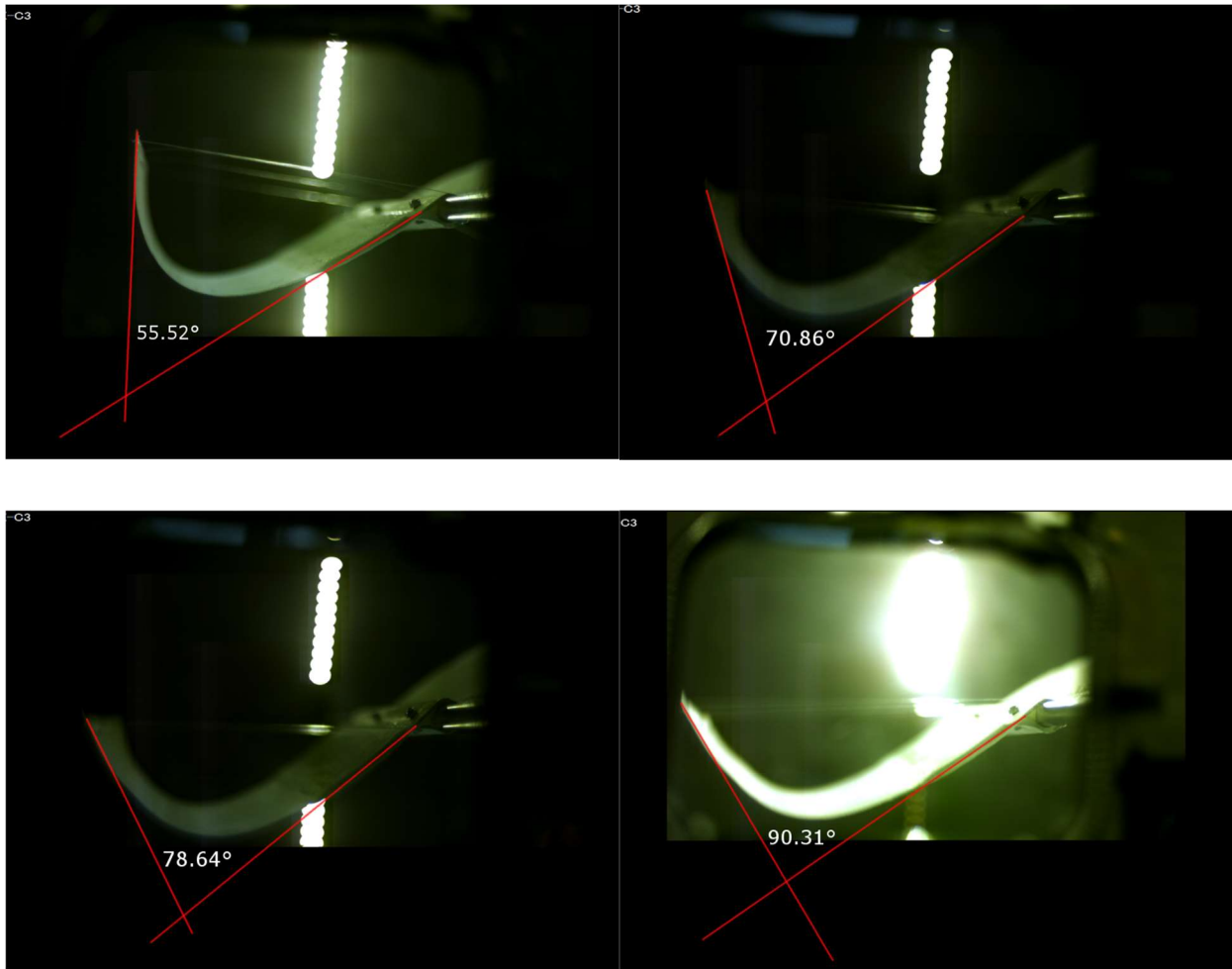
Figure 5.10 – Second flexible rotor attempt with linked tips and increased weight at 9.5m/s wind speed: standing blade image (upper-left), moving blade images at each rotational speed (other three)

IMAGE COMPARISON 2ND FLEXIBLE ROTOR (TIPS LINKED AND INCREASED WEIGHT)		
WIND SPEED [m/s]		5
REFERENCE ANGLE [°]		55.52
RPM	ANGLE [°]	DISPLACEMENT [°]
150	60.39	4.87
100	64.1	8.58
55	69.74	14.22

Table 5.10 - Second flexible rotor attempt blade displacement data with linked tips and increased weight at 5m/s wind speed
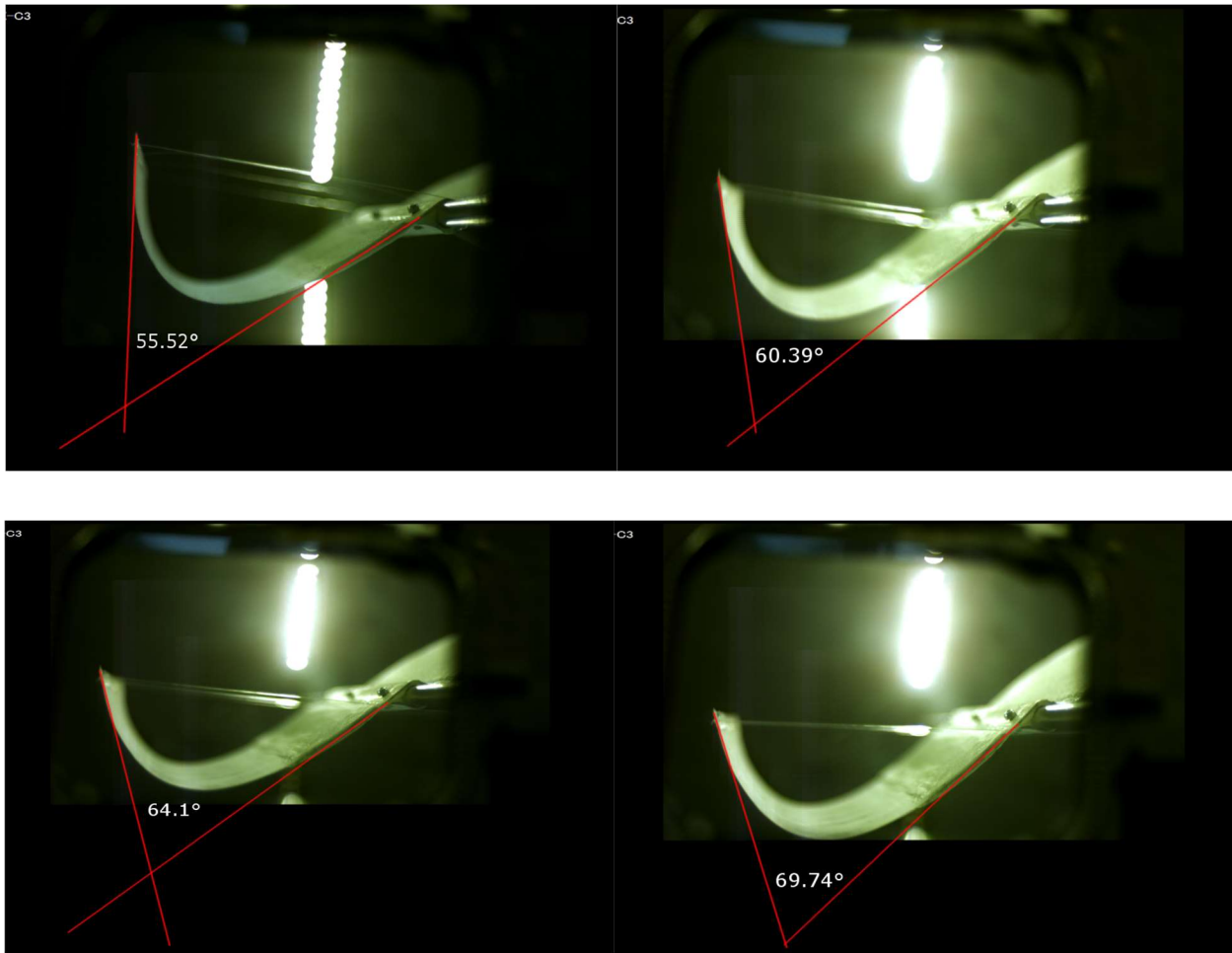
Figure 5.11 – Second flexible rotor attempt with linked tips and increased weight at 5m/s wind speed: standing blade image (upper-left), moving blade images at each rotational speed (other three)

IMAGE COMPARISON 2ND FLEXIBLE ROTOR (TIPS LINKED AND INCREASED WEIGHT)		
WIND SPEED [m/s]		3
REFERENCE ANGLE [°]		55.52
RPM	ANGLE [°]	DISPLACEMENT [°]
81	58.93	3.41
60	59.86	4.34
40	62.04	6.52

Table 5.11 - Second flexible rotor attempt blade displacement data with linked tips and increased weight at 3m/s wind speed
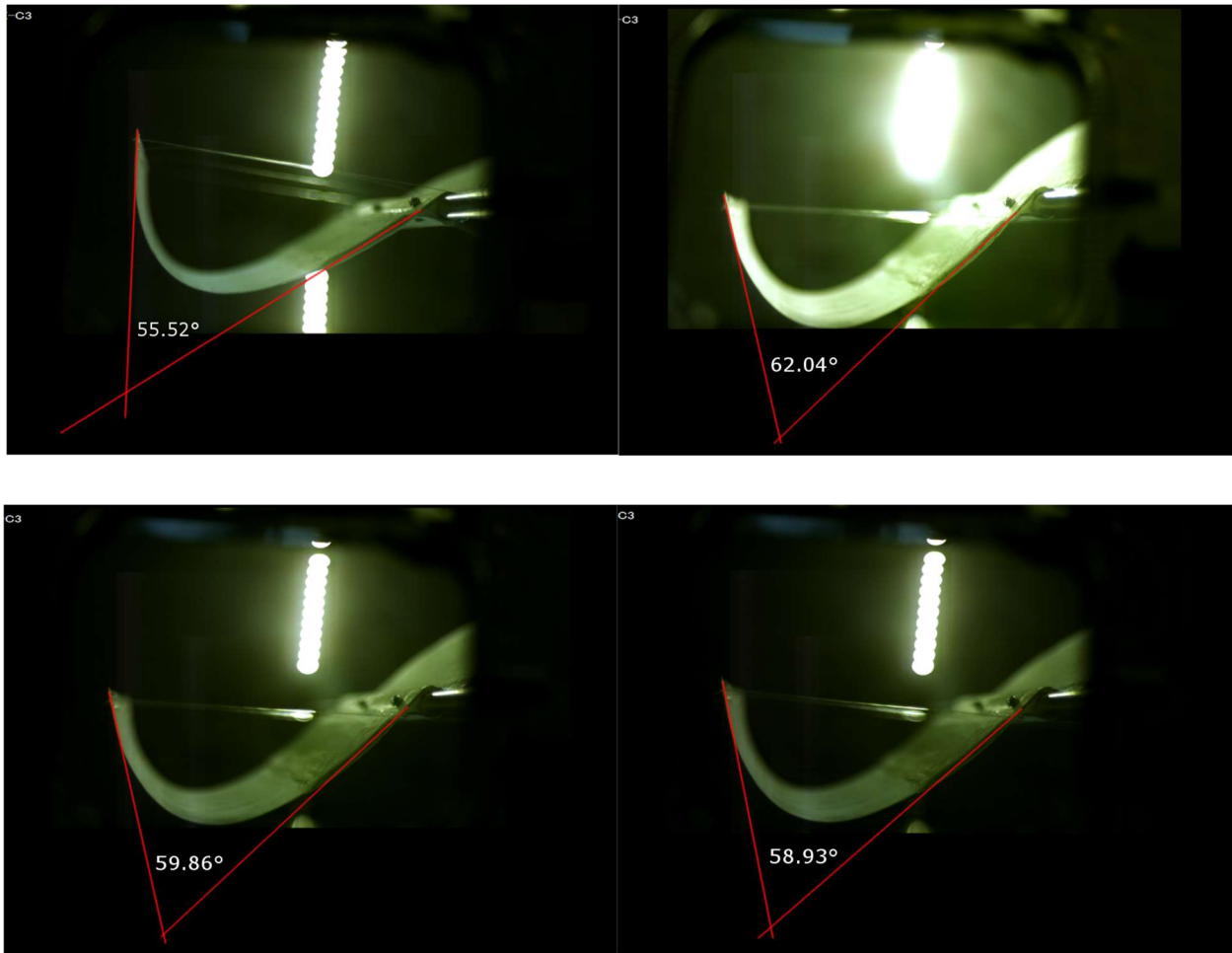
Figure 5.12 – Second flexible rotor attempt with linked tips and increased weight at 3m/s wind speed: standing blade image (upper-left), moving blade images at each rotational speed (other three)

The material addiction did not substantially affect the deformation features of the rotor, sure enough the same range of deformation was found for the 7m/s wind speed. It is noticeable that the images have a reference angle which is different for each experiment because the camera was removed and replaced several times so its position was slightly different each time. Moreover, the mirror position was changed starting with the third rotor experiments because of some issues with camera positioning.

6 TESTS, RESULTS AND COMPARISON

6.1 Tests

6.1.1 Collected data

Performance tests were conducted not only at the same wind speed considered in the previous thesis work (7m/s) but at six different wind speeds to obtain data suitable to evaluate the power productivity at low wind speed working conditions. As predicted, a Savonius configuration is more suitable for domestic application with low wind speeds because high wind speed produces an excessively high torque capable of breaking the gears connected to the rotor. The target of the tests was to plot two graphs to evaluate and compare the performances of the two rotors. Both the graphs had the TSR value on the horizontal axis but the torque coefficient (C_T) and power coefficient (C_P) were on the vertical axis of two separate graphs. The power coefficient is the most important parameter because it gives an efficiency value for the turbine. The test stand was able to collect information about the torque T, the wind speed, the air features and the rotational speed which were enough to calculate the coefficients. To collect wind speed and air features data a dynamometer was used while for the torque sensor provided information related to air features and rotational speed. The relation between the two coefficients and the TSR can then be found:

$$C_p = \frac{mechanical\ power}{available\ power} = \frac{P_m}{P_0} = \frac{T * \omega}{\frac{1}{2}\rho A v_1^3} \tag{6.1.1.1}$$

By multiplying and dividing the radius R and remembering the expression for the TSR:

$$TSR = \frac{\omega R}{v_1} \tag{6.1.1.2}$$

$$C_p = \frac{T * \omega}{\frac{1}{2}\rho A v_1^3} * \frac{R}{R} = \frac{T * TSR}{\frac{1}{2}\rho A v_1^2 * R} \tag{6.1.1.3}$$

The denominator is dimensionally a torque so the torque coefficient can be defined as follows:

$$C_t = \frac{T}{\frac{1}{2}\rho A v_1^2 * R} \tag{6.1.1.4}$$

$$C_t = \frac{T * \omega}{\frac{1}{2}\rho A v_1^3 * TSR} \tag{6.1.1.5}$$

6.1.2   Test Procedure

All the data were collected holding the wind speed constant and varying the rotational speed and therefore the torque produced by the hand brake. The rotational speed interval between every acquisition point was set between 15 and 30rpm in order to have data about every 0.1 units along the TSR scale for all the tested wind speeds. In fact, looking at the TSR definition is clear that for a high wind speed the rpm interval to have a 0.1 TSR step is bigger than for a lower wind speed. The tests were conducted in three main phases:

1. Regulation of the fan frequency to reach the right wind speed. An anemometer was used to check the wind speed in the wind tunnel. Information about temperature, humidity and pressure of the air were recorded to evaluate the available power from the wind flow more precisely.
2. Lubrication of every bearing on the supporting structure.
3. Wind speed increased until the starting point of the rotor and then decreased until the test speed. Data were recorded for each rpm.

74

6.1.3 Torque correction

The torque corresponding to each rotational speed value was recorded but the bearings and gears used for the test rig produced friction and therefore a correction to the measured torque had to be done and then added to the recorded data.

$$T = T_{sensor} + T_{friction}(\omega) \qquad (6.1.3.1)$$

The method used to calculate the friction of each bearing consisted in the recording of the torque without the use of the brake. In fact, as the following scheme of the rig shows (**Figure6.1**), there are two bearings on the brake side of the sensor and the torque measured without the brake corresponds to the friction produced by the two bearings on that side.
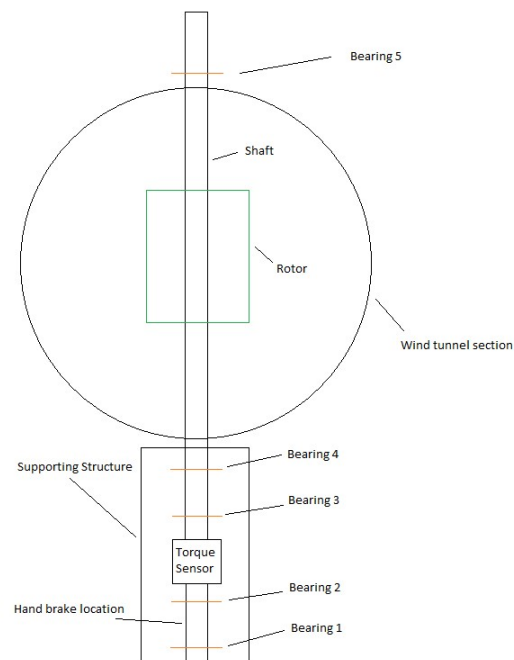
Figure 6.1 – Rig's scheme

Since there are three bearings on the shaft side, the resulting torque was subsequently multiplied by 5/2 in order to take them all into consideration. The tests were conducted for five different

wind speeds and therefore three different angular speeds and the results are shown on the next **Table6.1**:

BEARING LOSSES			
	ANGULAR SPEED	TORQUE	TOTAL TORQUE
RPM	[rad/s]	[N/m]	[N/m]
295	30.89232776	0.004	0.01
260	27.22713633	0.005	0.0125
230	24.08554368	0.004	0.01
150	15.70796327	0.0045	0.01125
90	9.424777961	0.0035	0.00875

Table 6.1 – Bearings torque losses

The calculated torque was almost constant for the tested angular speed so it was decided to add a constant value of 0.01 N/m to each recorded value.

6.1.4   Wind speed correction

Because of the use of a wind tunnel, another correction was necessary. When an object is placed into a wind tunnel, an increased value of the wind velocity on the test section appears and it is caused by the "tunnel blockage". To take this effect into consideration a blockage factor is calculated by the following equation suggested by Pope et al. [54] :

$$\varepsilon = \frac{1}{4} * \frac{Rotor\ front\ area}{Test\ section\ area} \qquad (6.1.4.1)$$

The blockage factor for a Savonius rotor is usually high because of the wide frontal area, in fact the calculation showed a blockage percentage of 3.4% which cannot be considered negligible. Therefore, a correction on the wind speed was done with the following equation:

76

$$v_{corrected} = v_{sensor} * (1 + \varepsilon) \qquad (6.1.4.2)$$

The wind speed used for the performance calculations are then listed in the following **Table6.2**:

BLOCKAGE FACTOR CORRECTION	
PERCENTAGE [%]	3.4
BLOCKAGE FACTOR CORRECTION	0.034
WIND SPEED FROM SENSOR [m/s]	CORRECTED WIND SPEED [m/s]
3	3.102
5	5.17
7	7.238
8	8.272
9	9.306
9.5	9.823

Table 6.2 – Wind speed corrections due to the blockage factor

6.2 Results

The results of the tests are shown in the next graphs (**Figure6.2**, **Figure6.3**, **Figure6.4**, **Figure6.5**, **Figure6.6**, **Figure6.7**, **Figure6.8**, **Figure6.9**, **Figure6.10**, **Figure6.11**, **Figure6.12**, **Figure6.13**). In each graph two series of data are shown to provide a visual comparison between the performances of the rotors for the same wind speed value.
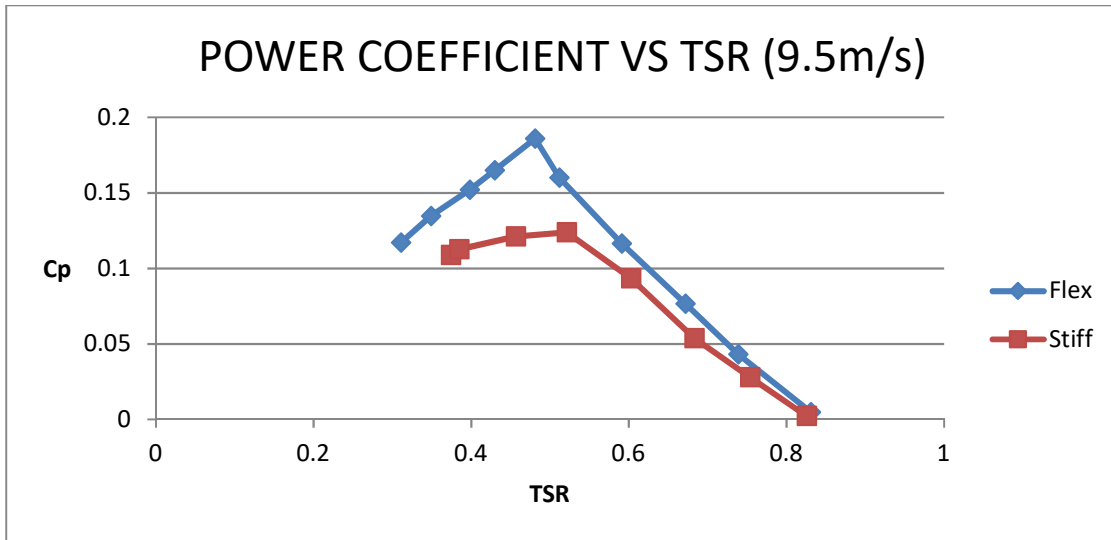
Figure 6.2 – Power coefficient vs TSR comparison between flexible and stiff rotor at 9.5m/s wind speed
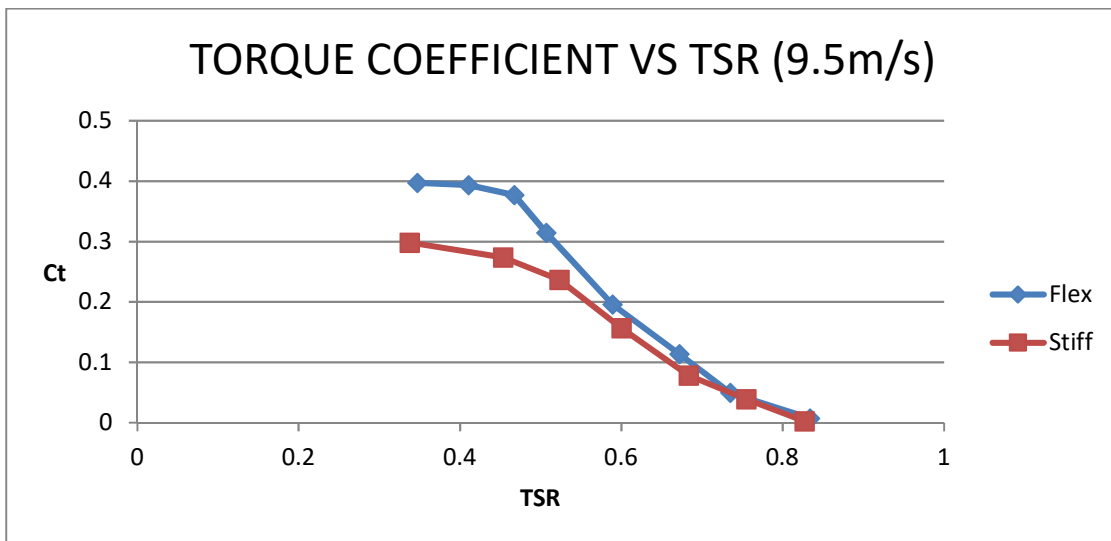
Figure 6.3 – Torque coefficient vs TSR comparison between flexible and stiff rotor at 9.5m/s wind speed
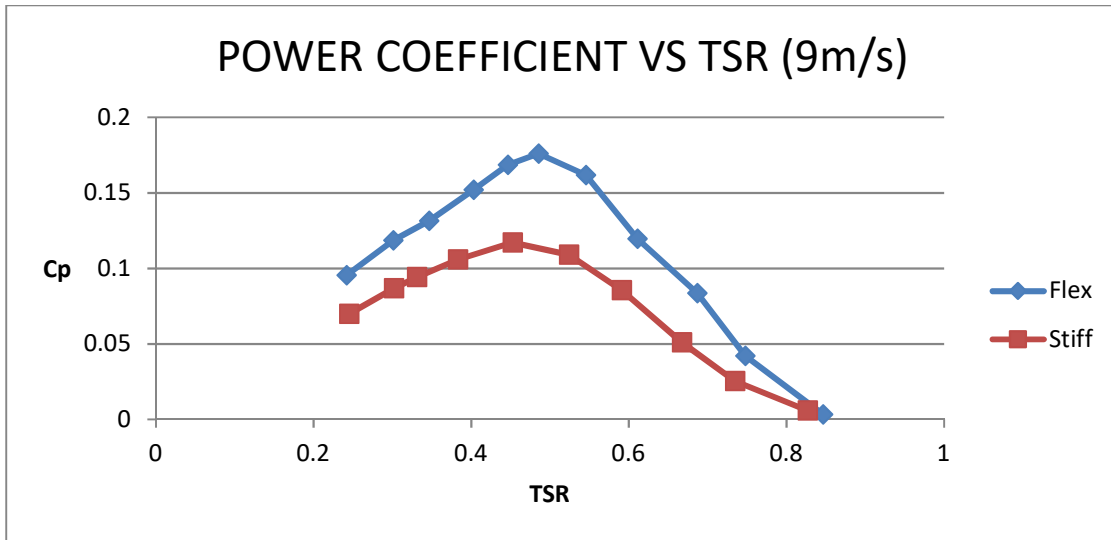
Figure 6.4 – Power coefficient vs TSR comparison between flexible and stiff rotor at 9m/s wind speed
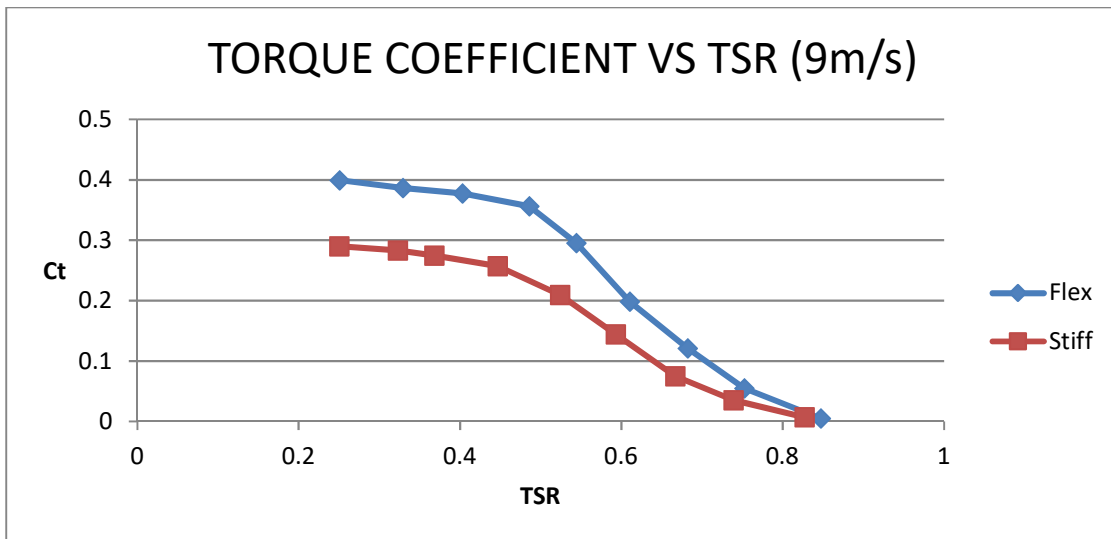
Figure 6.5 – Torque coefficient vs TSR comparison between flexible and stiff rotor at 9m/s wind speed
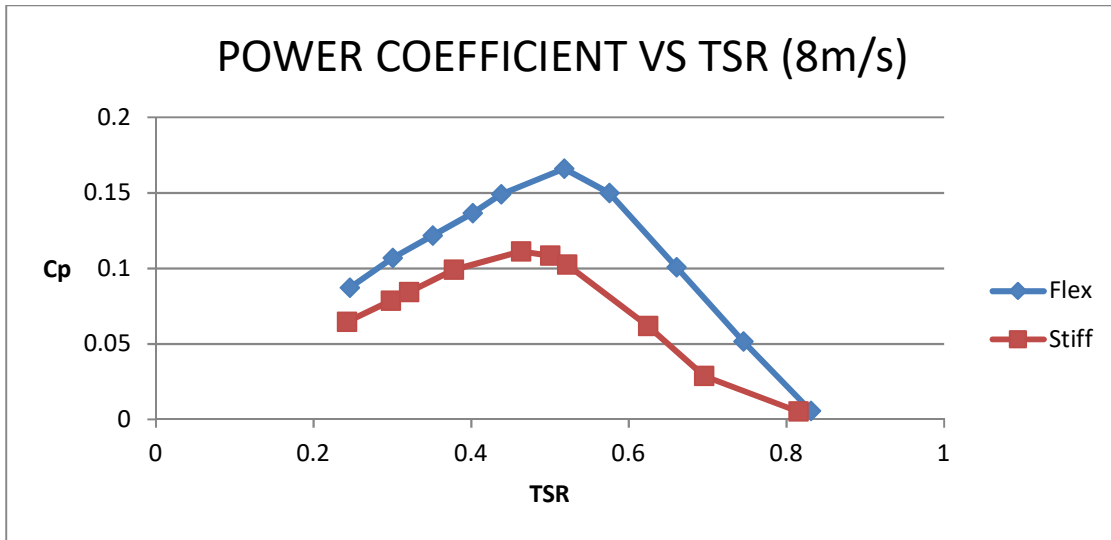
Figure 6.6 – Power coefficient vs TSR comparison between flexible and stiff rotor at 8m/s wind speed
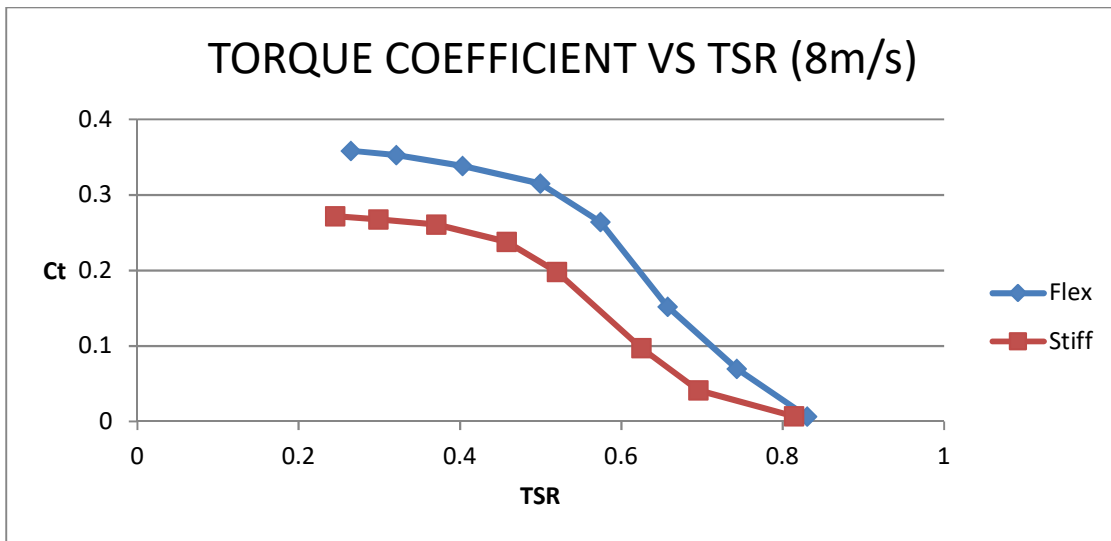
Figure 6.7 – Torque coefficient vs TSR comparison between flexible and stiff rotor at 8m/s wind speed

80
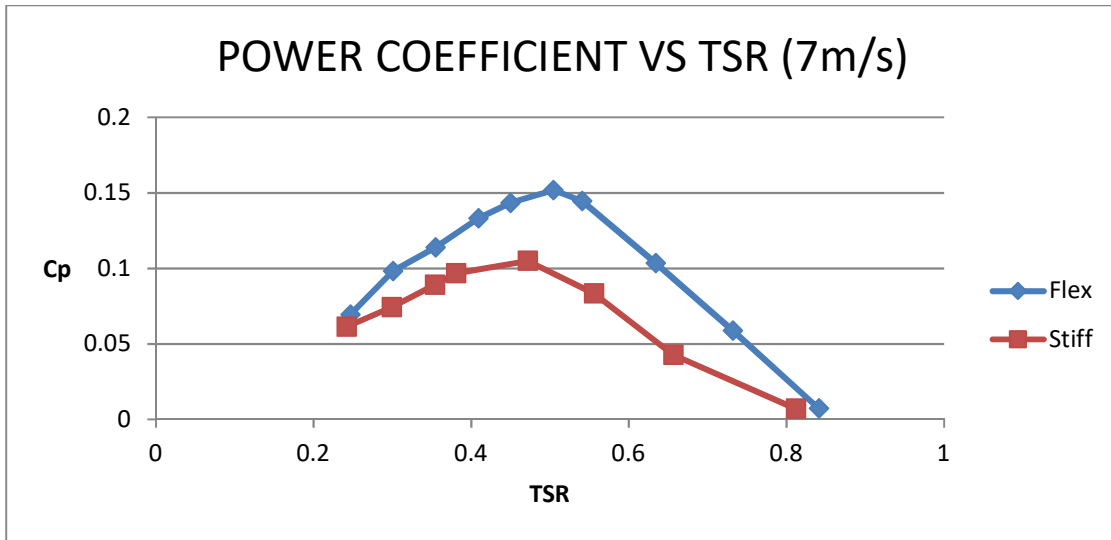
Figure 6.8 – Power coefficient vs TSR comparison between flexible and stiff rotor at 7m/s wind speed
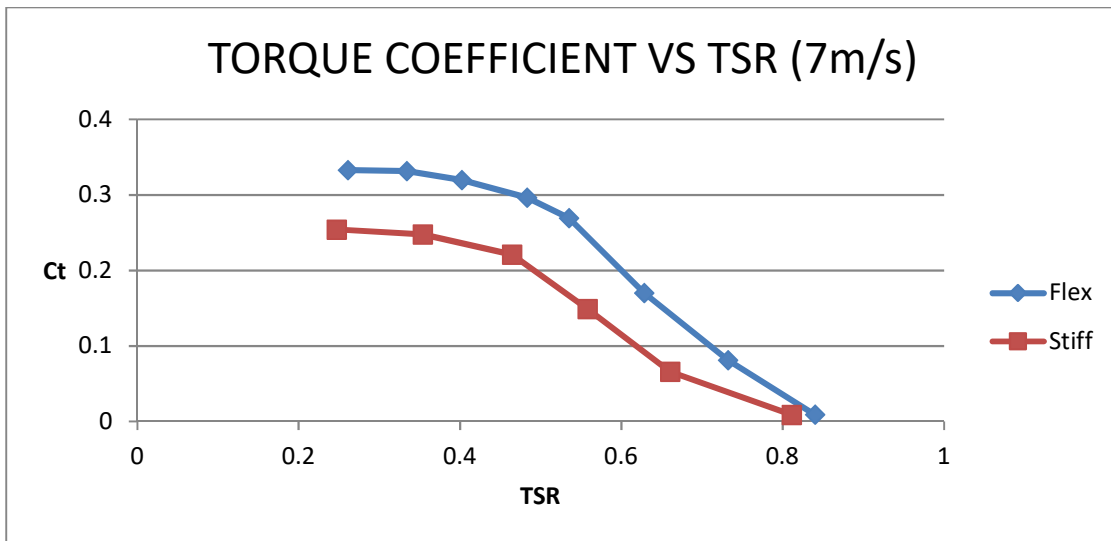
Figure 6.9 – Torque coefficient vs TSR comparison between flexible and stiff rotor at 7m/s wind speed
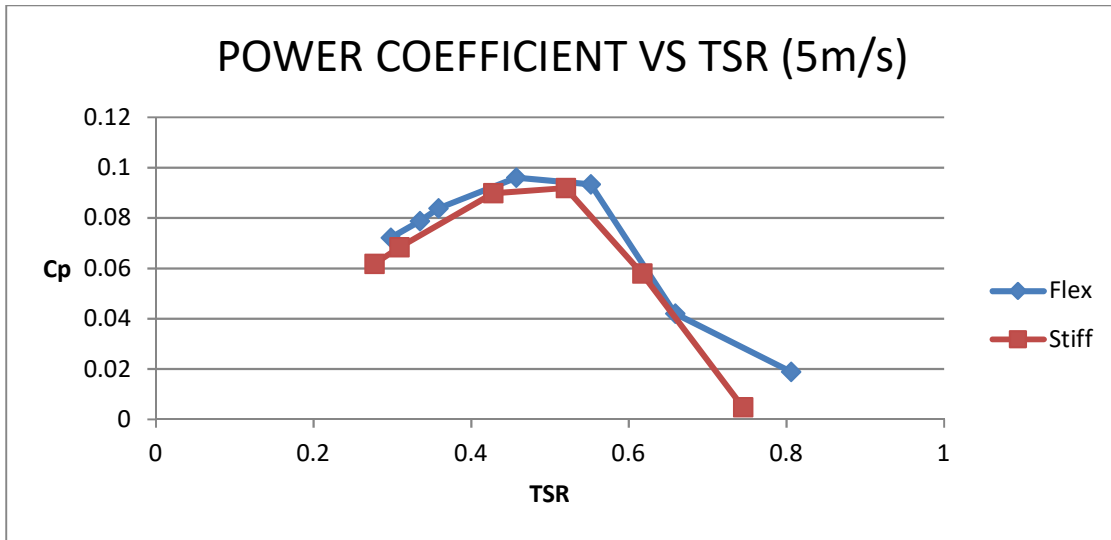
Figure 6.10 – Power coefficient vs TSR comparison between flexible and stiff rotor at 5m/s wind speed
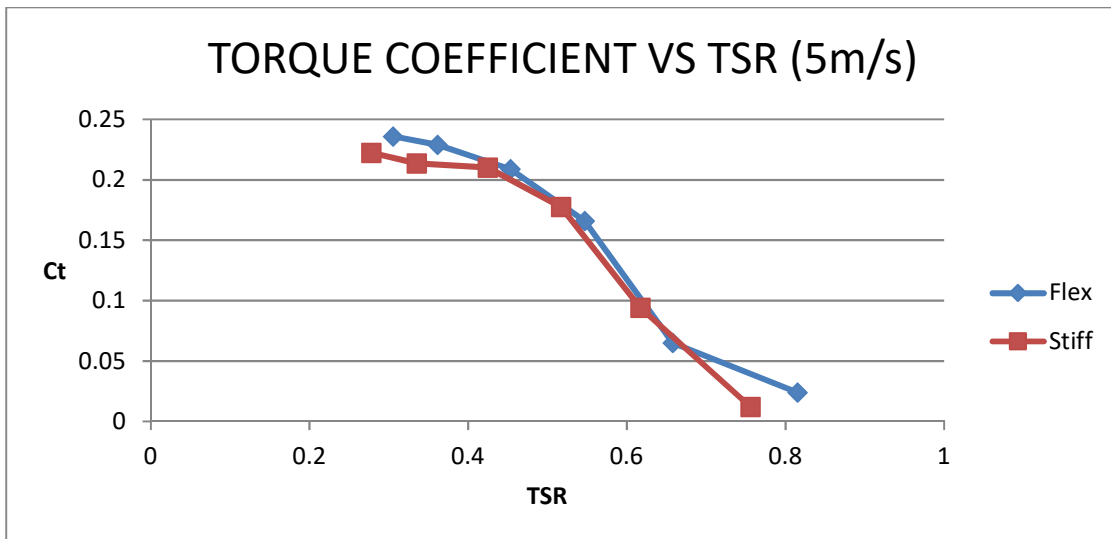
Figure 6.11 – Torque coefficient vs TSR comparison between flexible and stiff rotor at 5m/s wind speed
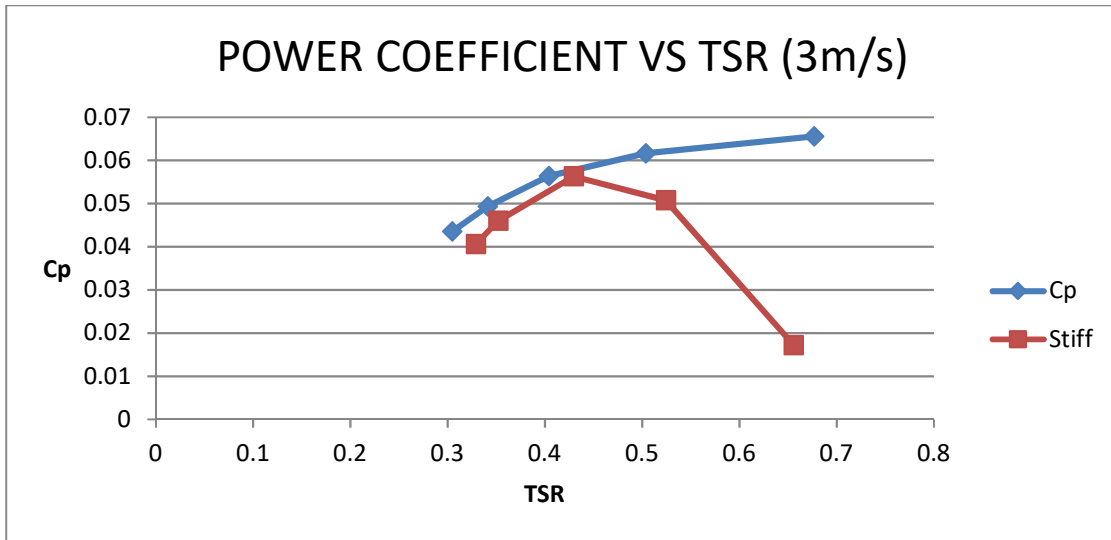
Figure 6.12 – Power coefficient vs TSR comparison between flexible and stiff rotor at 3m/s wind speed
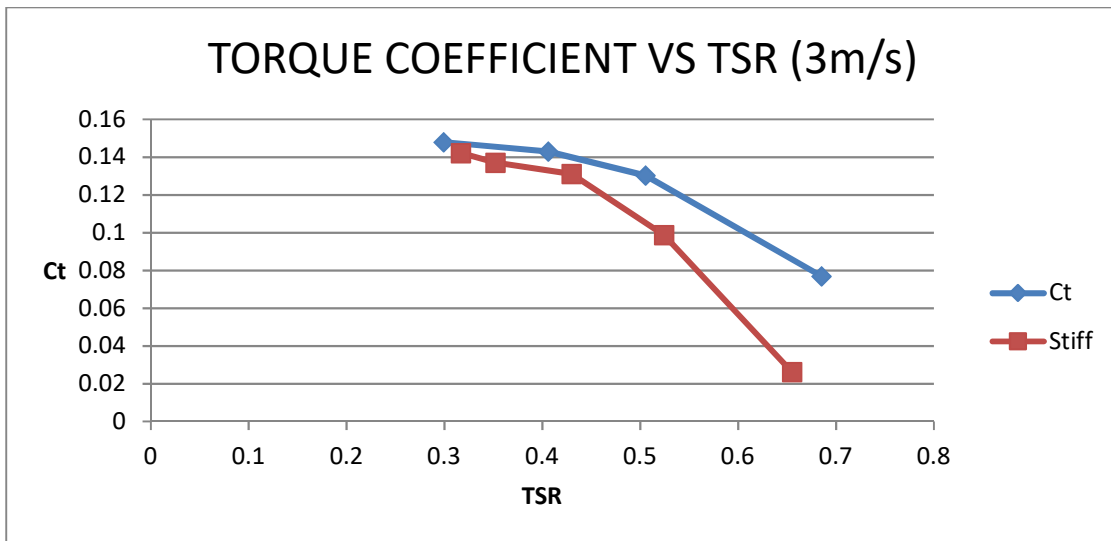
Figure 6.13 – Torque coefficient vs TSR comparison between flexible and stiff rotor at 3m/s wind speed

It is easy to notice that in every working condition the flexible rotor has higher efficiency and torque. The power coefficient for each rotor, at each wind speed, shows a maximum value around 0.5 TSR with the only exception at 3m/s for the flexible rotor. This different curve shape can be attributed to the fact that the torque of the flexible rotor, for this low wind speed, remains

at a pretty high value also for high value of the tip speed ratio. The improvement percentages of the maximum value of the efficiency and torque are shown in the next **Table6.3** and **Table6.4**:

BEST PERFORMANCE COEFFICIENT COMPARISON			
WIND SPEED [m/s]	STIFF	FLEX	INCREASE [%]
3	0.0563	0.0656	16.51865009
5	0.0919	0.096	4.461371055
7	0.105	0.152	44.76190476
8	0.111	0.166	49.54954955
9	0.117	0.176	50.42735043
9.5	0.124	0.186	50

Table 6.3 – Highest power coefficient comparison. Increase percentage of the flexible rotor

BEST TORQUE COEFFICIENT COMPARISON			
WIND SPEED [m/s]	STIFF	FLEX	INCREASE [%]
3	0.142	0.148	4.225352113
5	0.222	0.236	6.306306306
7	0.254	0.333	31.1023622
8	0.272	0.358	31.61764706
9	0.29	0.39	34.48275862
9.5	0.298	0.3974	33.3557047

Table 6.4 – Highest torque coefficient comparison. Increase percentage of the flexible rotor

Another aspect that is noticeable is that the improvement of the flexible rotor compared to the stiff is that it reaches the maximum value at 9m/s and then it starts to decrease slightly. That trend was expected because as the wind speed is increased the deformation reaches excessively high values, until a point where it has an almost constant deformation until the rotor experiences permanent damage. Passed 9m/s the deformation is expected to have marginal returns on the efficiency of the rotor. So, the difference between the two rotors is supposed to start to decrease at 9.5m/s. Since the wind tunnel used for the experiments is not suitable for high wind speed tests a complete trend is impossible to confirm. Similar results were achieved in a previous comparison between flexible and rigid VAWT conducted at San Diego State University by David Mc Phee [55]. Since a Savonius rotor has efficiency values which drop quickly as soon as

the TSR moves from the highest efficiency point, precise control systems are used in a real application to keep the rotational speed close to the best efficiency range. As a result, a graph showing the comparison between the two rotors at the maximum efficiency for each wind speed is provided in **Figure6.14** and the main difference is then found between 5 and 9m/s. At lower wind speed the difference starts to decrease because of the lower deformation of the blades for such low wind speed values.
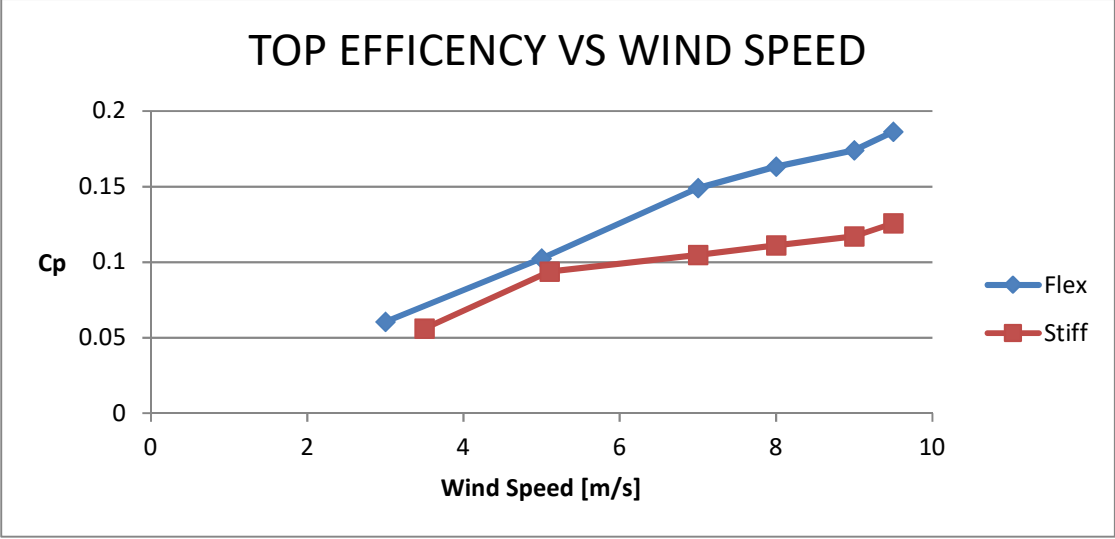
Figure 6.14 - Maximum efficiency comparison between the two rotors at each wind speed

Furthermore, a comparison between the performances of the flexible rotor for all the wind speeds tested is provided in **Figure6.15**. It is interesting to notice that the maximum efficiency rises as the wind speed increases and the same trend is visible for low value of TSR.
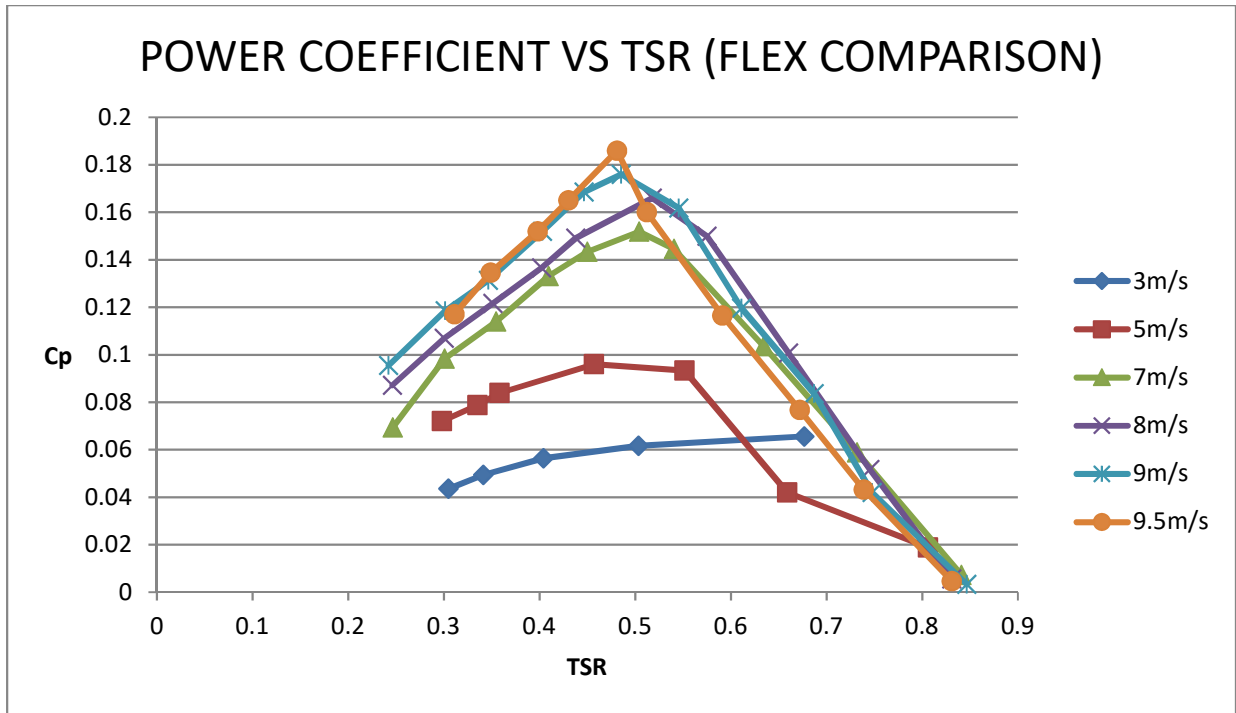
Figure 6.15 – Power coefficient vs TSR comparison of flexible rotor at all tested wind speeds

In order to find at which wind speed the flexible rotor has the overall maximum productivity it is sufficient to interpolate the experimental points to obtain a function which can be integrated. The integral will be calculated over the interval of 0.4-0.6 TSR considering that an rpm control system works to keep the TSR close to the maximum efficiency point. The interpolation was done only at 7, 8, 9, 9.5m/s because at 5 and 3m/s the productivity is much lower than the other cases (**Figure6.16**).
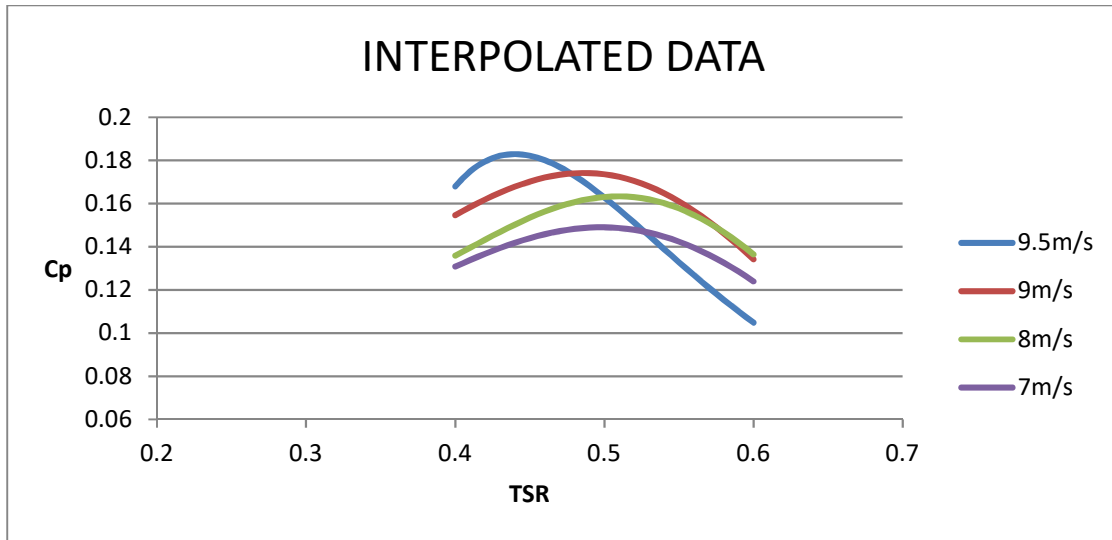
INTERPOLATED DATA

Figure 6.16 – Interpolated power coefficient vs TSR comparison of flexible rotor at 9.5, 9, 8, 7m/s wind speeds

As a result, the most productive wind speed for the flexible rotor is 9m/s. Therefore, an interesting conclusion can be achieved about the deformation of the rotor. By combining the deformation data and the performance data it was possible to find the best deformation for each wind speed and since the highest productivity was found at 9m/s the corresponding deformation can be set as the best for a Savonius rotor. Consequently, a deformation included in the interval 22°-32° has to be considered between 0.4-0.6 TSR to obtain the maximum productivity. Depending on the average wind speed available in a suitable urban spot the flexible rotor should be designed to have that deformation range for the most frequent wind speed. Eventually a trend of the top performance deformation vs wind speed is provided in **Figure6.17**.
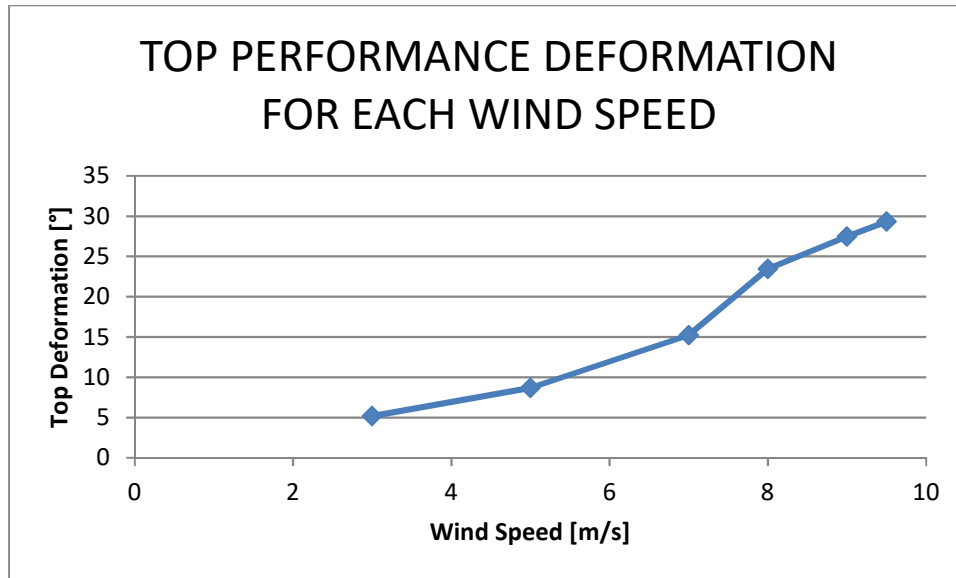
Figure 6.17 - Top performance deformation vs wind speed of flexible rotor

6.3   Comparison with The Previous Work

The first aim of this thesis was to provide the validation of the previous numerical work conducted by Michele Mari from Ferrara University who also worked on his Master's thesis at SDSU [52]. The first big difference that can be seen on the TSR is that the rotors in the simulations, thanks to the new shape and therefore to the increased lift force acting on the blades, were supposed to reach values over 1. In the experiments a maximum TSR value of only 0.85 was recorded. The reason for this fact is found in the dimensions of the rotor. The test standing has an elevated inertia and because of the small size of the rotor, the rotational speed didn't reach the same values as the simulations. By using a larger rotor and therefore a larger wind tunnel, higher values of the TSR might be reached. For that concern a direct comparison between the power coefficients cannot be done because of the different sizes, the simplified assumptions, the simulations and the test stand utilized. But, a comparison based on the improvements achieved by the flexible rotor can be made. As the simulations showed the flexible rotor had a remarkably higher efficiency than the rigid one, mainly around the maximum efficiency but it remains fairly high also at a low tip speed ratio. The experimental data shows the same high difference around the maximum efficiency point but then the efficiency results are higher either at higher and lower values of the tip speed ratio. At high TSR in both cases the efficiency values come closer to the

simulations; the rigid rotor even overcomes the flexible one while in the experiments for each tested TSR the performances of the flexible rotor are better than the rigid one. The torque coefficient follows the same trend in both the cases. In light of the last comparison, the improvement of a flexible rotor upon a rigid can be considered proven even if a real installation without the use of a wind tunnel should be investigated as further work.

6.4   Criticism

Although good results were achieved a critical look should be given. Firstly, the use of a wind tunnel certainly gives more realistic information than a CFD simulation however it can never generate absolute results. Therefore, the results obtained can partially confirm the simulation data but keeping in mind that only with a real application, absolute results can be achieved. Furthermore, a criticism can be made of the material used for the rotors for two reasons. One reason is that the manufacturing process is excessively slow for the numerous phases which were needed to build the rotors. That aspect makes the manufacturing process utilized not suitable for industrial production. Another reason is precise control of the flexibility is hard to obtain because it can be done only by a different position of the layers of fiber or by using a different resin with different elastic features. Another issue is that the position of the layers utilized in this to build the flexible rotor cannot be copied to obtain the same flexibility on a bigger scale rotor and as a result it would be necessary to proceed through successive attempts. Thus, a more suitable resin and manufacturing process has to be found.

7 ECONOMIC ANALYSIS

7.1 Introduction

The economic analysis presented in this section has the aim to provide a comparison between the flexible and stiff rotor in terms of energy savings and therefore money and pollutant savings. All studies have been done considering only part-load working conditions for wind speeds lower than 8 [m/s]. Sure enough the experimental work showed in this thesis was conducted on a low speed wind tunnel with a maximum wind speed of 9.5 [m/s] so the available data only covered this limited range. Furthermore, it is essential to take into consideration that the average wind speed in most cities throughout the world is around 3.5-4 [m/s] and wind speed values over 8 [m/s] are rare. Finally, the most important aspect is that a Savonius rotor is more suitable for low wind speeds because the high torque generated at high wind speed is capable of breaking the gears connected to the rotor and because of its structure, large scale applications are not possible. For those reasons a small-scale application such as a domestic installation in an urban site is the most appropriate. A more complete analysis covering a wider speed range might be done but the recorded data doesn't allow predictable values for wind speeds higher than 9.5 [m/s]. Values beyond 9.5m/s are unpredictable and an interpolation based on the experimental values could prove to be entirely incorrect. Next shown a **Table7.1** with the average wind speed in some cities:

AVERAGE WIND SPEEDS	
CITY	AVERAGE WIND SPEED [m/s]
San Diego	3.129272222
Portland	3.531607222
Cincinnati	4.02335
Miami	4.112757778
Berlin	4.02335
London	4.470388889
Stockholm	4.470388889
Madrid	3.129272222
Padua	2.011675
Paris	4.470388889

Table 7.1 – Average annual wind speed in some cities

7.2 Weibull Distribution and Productivity Evaluation

For the wind industry, it is fundamental to know the wind distribution in terms of speed of a certain site because the wind rotor designers need these statistical descriptions to minimize the generation costs. The Weibull distribution is the most used statistical distribution for wind power and the density probability function is its descripting function:

$$D\langle v \rangle = \frac{k}{s} \left(\frac{v}{s}\right)^{k-1} exp\left[-\left(\frac{v}{s}\right)^{k}\right] \qquad (7.2.1)$$

The parameter s *(scale factor [m/s])* and k *(shape factor [non-dimensional])* modify the general shape of the curve and they are chosen specifically for each site. The meaning of the function can be described as the probability that the wind speed v is included in the infinitesimal interval $v \leftrightarrow v + \delta v$ considering the expression $D\langle v \rangle \delta v$. An example of the descripted function and how the two parameters affect the function's shape is provided as follows (**Figure7.1**, **Figure7.2** and **Figure7.3**):
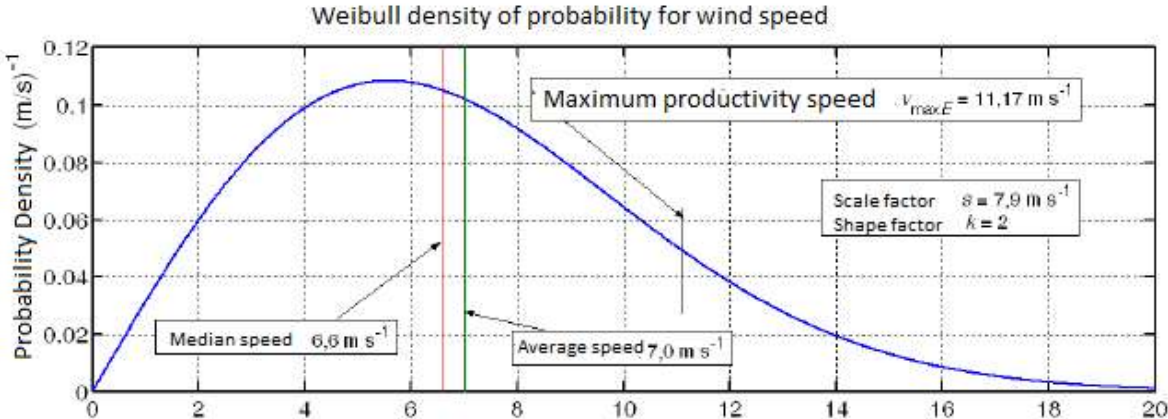
Figure 7.1 – Weibull distribution's function example (Source: [51])
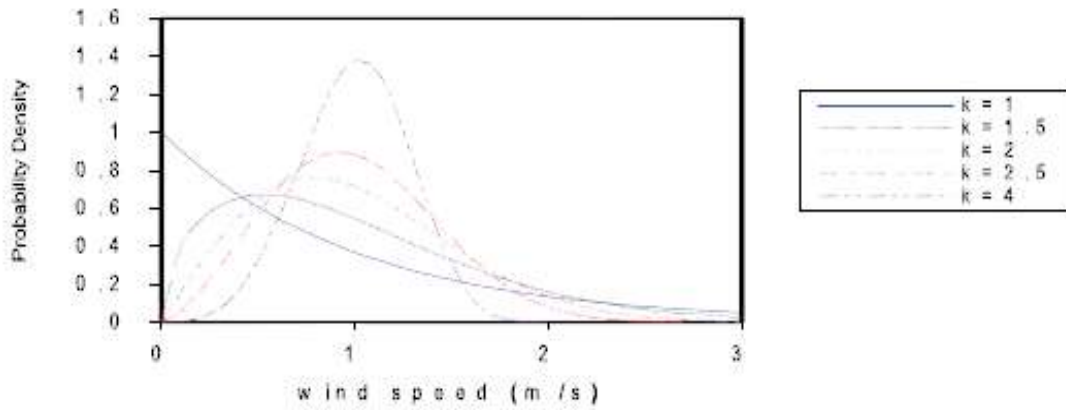
Figure 7.2 – *k* parameter influence on Weibull function's shape (Source: [56])
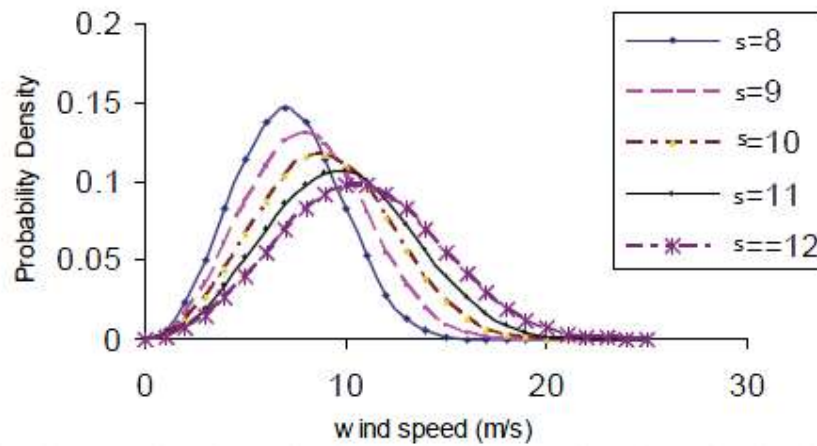
Figure 7.3 – *s* parameter influence on Weibull function's shape (Source: [56])

To calculate the total energy production during one year (kWh/year) the following expression has to be utilized:

$$E = \Delta\tau \int_{v_{cut-in}}^{v_{cut-out}} P\langle v \rangle D\langle v \rangle \, \delta v \qquad (7.2.2)$$

Where $\Delta\tau$ is the time period taken in consideration and $P\langle v \rangle$ is the power output function describing the power produced at each wind speed.

93

7.2.1 Parameter evaluation

The chosen site for this comparison was the city of San Diego so the parameters to define the Weibull distribution have to be chosen. The shape parameter is usually chosen as 2 as a default value for all the energy production estimations but since an urban application was investigated, a k=1.5 is chosen considering the more turbulent conditions of an urban site. The scale factor s is defined and calculated by the following expression:

$$s = \frac{\bar{v}}{\Gamma \langle 1 + \frac{1}{k} \rangle} \tag{7.2.1.1}$$

Where $\bar{v}$ is the average wind speed of the site and the function Γ is the "Eulero function" and it can be calculated by the following integral:

$$\Gamma \langle x \rangle = \int_0^\infty y^{x-1} \exp(-y) \delta y \tag{7.2.1.2}$$

$$x = (1 + \frac{1}{k}) \tag{7.2.1.3}$$

Where y, is the integrating variable. The value for that function is calculated and along with the scale factor. The average wind speed in San Diego is $\bar{v} = 3.13 \, [\frac{m}{s}]$ so after the calculation $\Gamma \langle 1 + \frac{1}{1.5} \rangle = 0.9027$ and the scale factor $s = 3.467 \, [\frac{m}{s}]$ were found. The Weibull distribution function is now defined.

7.2.2 Annual energy production

To calculate the total energy production of the two rotors a power output function $P \langle v \rangle$ has to be found. Firstly, is it important to remember that a Savonius rotor needs a precise rotational speed control system in order to maintain the working conditions around the point of maximum efficiency. A simplification was adopted for this study and the control system was considered to keep the speed of the rotor perfectly at the maximum efficiency point at every wind speed.

94

Therefore, the maximum efficiency which corresponded to each wind speed tested in the wind tunnel was plotted on a Cp vs Wind speed graph. Remembering the power output expression for each of the tested wind speeds was possible to find the power output, subsequently plotted:

$$P = \frac{1}{2}A\rho v_1^3 C_p \qquad (7.2.2.1)$$

Eventually, in order to solve the integral necessary for the energy calculation, the power output values were interpolated to obtain a function for both of the rotors as shown in **Figure7.6**. The two charts on which were based interpolations are shown in **Figure7.4** and **Figure7.5**.
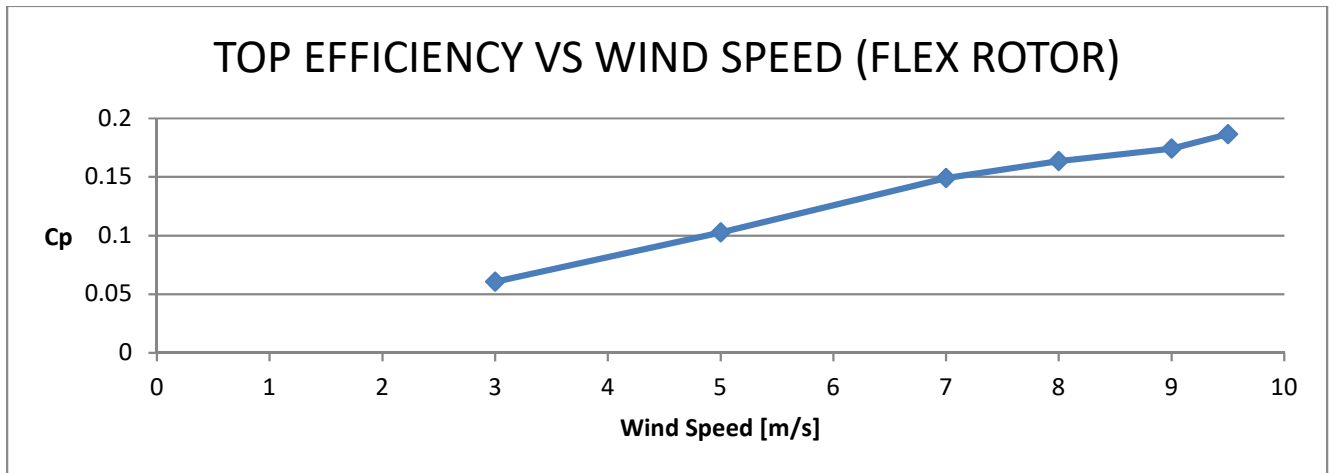
Figure 7.4 – Maximum efficiency vs wind speed for flexible rotor
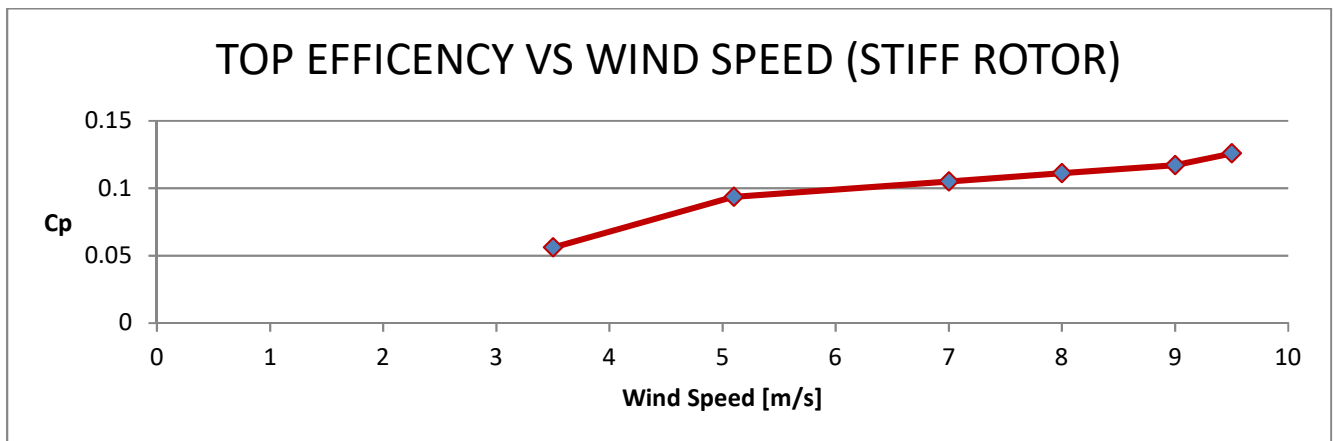
Figure 7.5 – Maximum efficiency vs wind speed for stiff rotor
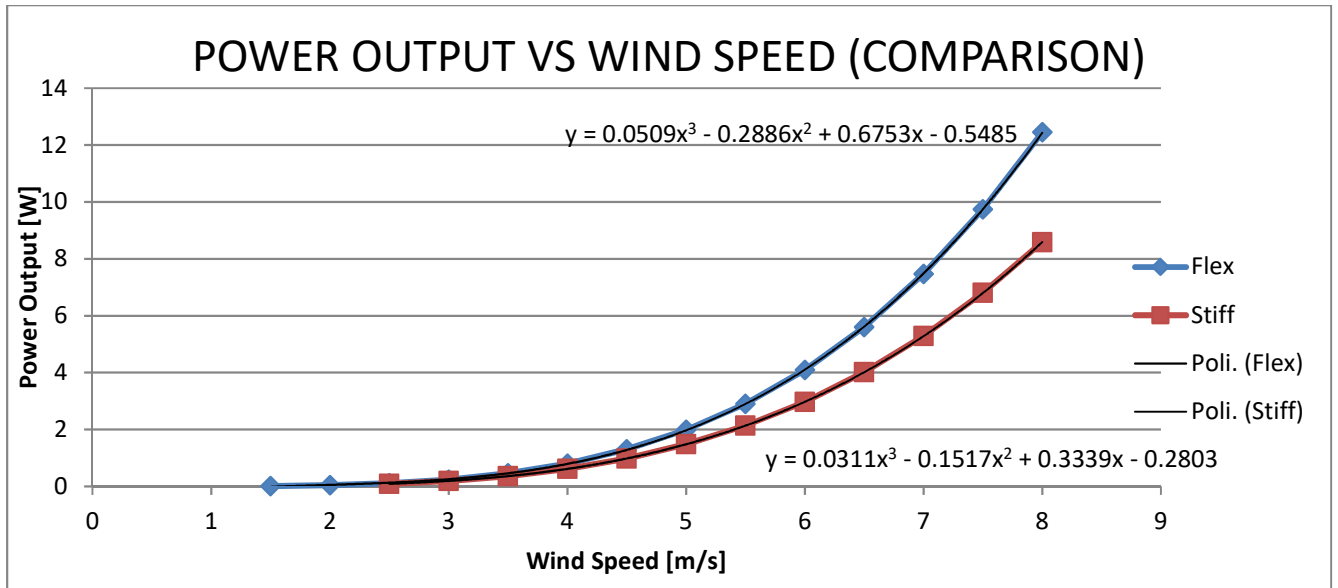
Figure 7.6 – Interpolated power output vs TSR comparison between stiff and flexible rotor

As shown in the last graph the interpolated functions for the power output have two different minimum values and the reason is that the minimum wind speed needed for the rotors to spin was calculated with a test where the wind speed was decreased until the rotor stopped. A minimum value of 1.5[m/s] was found for the flexible and 2.5[m/s] for the stiff rotor. The two values were considered as the cut-in speed for the respective rotor while 8[m/s] as cut-out speed and finally the annual energy production integral was calculated. The results are shown in the following **Table7.2**.

ANNUAL ENERGY PRODUCTION [kWh/year]	
FLEXIBLE ROTOR	STIFF ROTOR
8.5093	6.0128

Table 7.2 – Annual energy production in the city of San Diego

7.2.3 Starting speed correction

One of the main issues of a Savonius rotor is that it needs a certain amount of wind speed to start which is higher than the minimum wind speed at which the rotor can spin. The previous results were achieved without considering the starting speed of the rotors but only the cut-in and cut-out speed so actually the energy production would be lower because on some days the wind speed is enough to spin the rotors but not enough to start them. A correction has to be applied. Firstly, a test in the wind tunnel was conducted to find the minimum starting speed of the two rotors and it was found a value of $v_{start-flex} = 4.3 \left[\frac{m}{s}\right]$ and $v_{start-stif} = 5.6 \left[\frac{m}{s}\right]$. Then the climate data of San Diego was investigated and the energy produced during the days with a wind gust average below the starting speed was subtracted from the values previously found.

ANNUAL ENERGY PRODUCTION CORRECTED [kWh/year]	
FLEXIBLE ROTOR	STIFF ROTOR
8.503151224	5.927422831

Table 7.3 – Annual energy production in the city of San Diego with starting speed correction

The new values have only a really small difference compared to the uncorrected ones and the reason is that the most of the days with a gust average speed below the starting value, have an average wind speed that is lower than the cut-in speed, so they were not taken into consideration on the first calculation anyway.

7.3 Conclusion and Real Application Example

It is easy now to calculate the additional percentage of power output that the flexible rotor can produce over the stiff one.

$$100 * \left(1 - \frac{P_{out-stiff}}{P_{out-sflex}}\right) = Additional\ power\ output\ \% \qquad (7.3.1)$$

The result is 30.3% of additional power for the flexible rotor. The average cost of electrical energy for residential usage in California is 16.35¢/kWh [57] so by the use of a flexible wind rotor for a domestic installation instead of a standard one, is possible to save 4.954¢/kWh more.

In order to provide a quantitative realistic comparison based on the energy saving, a numerical simplified example will be shown. A real scaled application of the tested rotors is ignored because it was unknown if the rotors have the same behavior as in the wind tunnel, in a real application. An analysis done in that way might have produced results really far from the reality. Moreover, seeing as how the tunnel has limited size and dimensions, the tested rotors were much smaller than the size suitable for a domestic application so a prediction about the efficiency of a bigger rotor would have been hard to do. For that reasons a simplified comparison is provided. A comparison over a period of 20 years on the electric cost saving and CO_2 saving is going to be done and since the two rotors have similar manufacturing and maintaining costs they will not be considered in the analysis. The average electricity consumption per capita in the city of San Diego during the 2015 is about 6000kWh/year [58] and a Savonius wind power installation, with rigid blades, designed to cover the 20% of the consumption is considered. The projections show that the consumption is raising so the 20% of productivity is valid only for the first year and then it will decrease but it will not affect the results of the comparison. The increasing cost of the kWh and the inflation factor are taken into consideration by using an increasing factor of 1% per year [59]. The CO_2 emissions are evaluated considering an emission of 0.555 [kg/kWh] for residential consumption in U.S. [59]. However, the rising presence of renewable energy source involves a reduction in the emissions of CO_2 so a 1.1% reducing factor is utilized to take this aspect into account [60].

YEAR	kWh PRODUCED	ESTIMATED ENERGY COST [$/kWh]	CO2 SAVING [kg]	COST SAVING (ELECTRIC) [$]
SAVONIUS STIFF ROTOR CO2 AND COST SAVING (20 YEARS)				
1	1200	0.1635	666.00	196.20
2	1200	0.1651	658.67	198.16
3	1200	0.1668	651.43	200.14
4	1200	0.1685	644.26	202.15
5	1200	0.1701	637.18	204.17
6	1200	0.1718	630.17	206.21
7	1200	0.1736	623.24	208.27
8	1200	0.1753	616.38	210.35
9	1200	0.1770	609.60	212.46
10	1200	0.1788	602.89	214.58
11	1200	0.1806	596.26	216.73
12	1200	0.1824	589.70	218.89
13	1200	0.1842	583.22	221.08
14	1200	0.1861	576.80	223.29
15	1200	0.1879	570.46	225.53
16	1200	0.1898	564.18	227.78
17	1200	0.1917	557.98	230.06
18	1200	0.1936	551.84	232.36
19	1200	0.1956	545.77	234.68
20	1200	0.1975	539.76	237.03
	TOTAL		12015.78	4320.13

Table 7.4 – Stiff rotor cost and CO2 saving over a 20-year working period

YEAR	kWh PRODUCED	ESTIMATED ENERGY COST [$/kWh]	CO2 SAVING [kg]	COST SAVING (ELECTRIC) [$]
		SAVONIUS FLEX ROTOR CO2 AND COST SAVING (20 YEARS)		
1	1563.6	0.1635	867.80	255.65
2	1563.6	0.1651	858.25	258.21
3	1563.6	0.1668	848.81	260.79
4	1563.6	0.1685	839.47	263.40
5	1563.6	0.1701	830.24	266.03
6	1563.6	0.1718	821.11	268.69
7	1563.6	0.1736	812.08	271.38
8	1563.6	0.1753	803.14	274.09
9	1563.6	0.1770	794.31	276.83
10	1563.6	0.1788	785.57	279.60
11	1563.6	0.1806	776.93	282.40
12	1563.6	0.1824	768.38	285.22
13	1563.6	0.1842	759.93	288.07
14	1563.6	0.1861	751.57	290.95
15	1563.6	0.1879	743.30	293.86
16	1563.6	0.1898	735.13	296.80
17	1563.6	0.1917	727.04	299.77
18	1563.6	0.1936	719.04	302.77
19	1563.6	0.1956	711.13	305.79
20	1563.6	0.1975	703.31	308.85
	TOTAL		15656.56	5629.13

Table 7.5 – Flexible rotor cost and CO2 saving over a 20-year working period

As shown in **Table7.4** and **Table7.5**, the use of a flexible rotor can produce a cost and CO2 savings 23% higher than the standard rigid rotor.

8 FURTHER DEVELOPMENTS

The positive results obtained in this work, leave the way clear for a real application test. As underlined before the use of a wind tunnel doesn't allow to provide absolute information about productivity and efficiency. Keeping this in mind, a larger rotor should be built and tested for a domestic application, in an urban background for a period of one year. Only in this way it would be possible to have a confirmation about the feasibility for a convenient industrial development of this new technology.

Since a composite material is not the most appropriate for an industrial production, further studies on the type of material should be done once the improvement of this technology are proved by a real application test.

Finally, a new Savonius design solution proposed by Dr. Beyene similarly using the flexible blades to improve the performance has to be simulated, built, tested and eventually compared with the results in this work and in the previous one [52]. The biggest mechanical disadvantage of the Savonius rotor is the drag on the returning blade. While the concave shape allows it to create enough drag to rotate the rotor on the retreating side, it also creates a low-pressure vacuum on the opposite side. Studies have shown that a center overlap gap can reduce the magnitude of the vacuum. However, this also limits the surface area available to catch the wind as the blades are now slightly overlapped. In the **Figure7.7** is a proposed idea to add flexible section to the middle of each blade while the rest of the rotor is rigid.
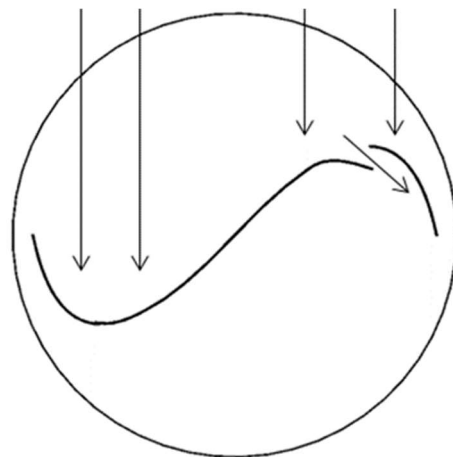
Figure 7.7 – New improvement idea of Savonius rotor with flexible section in the middle of the blades

This flexible part of the blade will be able to adapt to the flow. When rotating against the wind, it can flex backwards to allow air to pass through, which will hopefully decrease the magnitude of the low-pressure vacuum and the drag on that side of the rotor. When rotating with the wind, it can flex closed onto the rigid outer section of the blade and maintain its max surface area. By using a morphing blade, the rotor can self-adapt to the wind to either increase or decrease drag depending on its angle relative to the flow.

9 CONCLUSIONS

A comparison between two novel spline based Savonius rotors was investigated in this thesis. Starting from the positive results obtained in a previous numerical work two spine Savonius rotors were built, one with flexible and one with rigid blades. Fiber glass was found as a suitable material for the manufacture but further studies should be done. By managing the Young's modulus of the materials is possible to obtain a rotor with the same flexibility features achieved in this work but with no need of a tips link system. Numerous tests to check the flexibility were conducted through the use of a high-speed camera having a target as an optimal deformation range found on previous work but on different types of rotors. Once a good deformation range was achieved performance tests were conducted on the two rotors and finally a comparison was performed.

A power coefficient improvement included between 16 and 50% was found for the flexible rotor over the rigid. Moreover, in every working condition the flexible rotor showed better performances.

The most productive wind speed for the flexible rotor was found at 9m/s so the deformation obtained at that value (22°-32°) was considered as the best deformation for this kind of rotor. As a result, for any application of this type of rotor, it should be built using this specific deformation range around the rotational speed of maximum efficiency at the most frequent wind speed found in the chosen spot. In other words, for an urban application in a city such as San Diego (3.2m/s average speed) the most suitable flexible rotor would have a deformation range of 22°-32° at 3.2m/s wind speed.

A power output comparison was eventually analyzed at low wind speeds in the city of San Diego. The energy output of the rotors during an entire year was calculated and an improvement of 30% was found in the morphing blade compared to the rigid one.

10 REFERENCES

[1] G. Comini, S. Savino, "La captazione dell'energia solare". Udine: CISM, 2013.

[2] "World energy Outlook", IEA 2010. From www.theoildrum.com.

[3] "Wind Power Leads All New Power Generation", 2015 from www.gwec.net.

[4] Paul Denholm, Maureen Hand, Maddalena Jackson, and Sean Ong, "Land-Use Requirements of Modern Wind Power Plants in the United States", Technical Report NREL/TP-6A2-45834, August 2009.

[5] Wang, C., Prinn, R.G., 2010, "Potential climatic impacts and reliability of very large-scale wind farms", Atmospheric Chemistry and Physics, 10 (4), pp. 2053-2061.

[6] Keith, D. W., DeCarolis, J. F., Denkenberger, D. C., Lenschow, D. H., Malyshev, S. L., Pacala, S., et al., 2004, "The Influence of Large-Scale Wind Power on Global Climate", PNAS, 101(46), pp. 16115-16120.

[7] Fiedler, B.H., Bukovsky, M.S., 2011, "The effect of a giant wind farm on precipitation in a regional climate model", Environmental Research Letters, 6 (4), art. no. 045101.

[8] Tummala, A., Velamati, R.K., Sinha, D.K., Indraja, V., Krishna, V.H., 2016, "A review on small scale wind turbines", Renewable and Sustainable Energy Reviews, 56, pp. 1351-1371.

[9] Paraschivoiu, I., 2002, Wind Turbine Design with Emphasis on Darrieus Concept, Polytechnic International press, Canada, Chap. 2.2.

[10] Eriksson, S., Bernhoff, H., Leijon, M., 2008, "Evaluation of Different Turbine Concepts for Wind Power", Renewable and Sustainable Energy Reviews, 12, pp. 1419–1434.

[11] Lance Turner, "Micro wind power with a Savonius rotor", The Jan March 2000 issue of the Renew Magazine.

[12] Jeon, K.S., Jeong, J.I., Pan, J.-K., Ryu, K.-W., 2015, "Effects of end plates with various shapes and sizes on helical Savonius wind turbines", Renewable Energy, 79 (1), pp. 167-176.

[13] Kamoji, M.A., Kedare, S.B., Prabhu, S.V., 2009, "Experimental investigations on single stage modified Savonius rotor", Applied Energy, 86 (7-8), pp. 1064-1073.

[14] Mahmoud, N.H., El-Haroun, A.A., Wahba, E., Nasef, M.H., 2012, "An experimental study on improvement of Savonius rotor performance", Alexandria Engineering Journal, 51 (1), pp. 19-25.

[15]   Wenehenubun, F., Saputra, A., Sutanto, H., 2015, "An experimental study on the performance of Savonius wind turbines related with the number of blades", Energy Procedia, 68, pp. 297-304.

[16]   Kamoji, M.A., Kedare, S.B., Prabhu, S.V., 2009, "Performance tests on helical Savonius rotors", Renewable Energy, 34 (3), pp. 521-529.

[17]   Altan, B.D., Atilgan, M., Özdamar, A., 2008, "An experimental study on improvement of a Savonius rotor performance with curtaining", Experimental Thermal and Fluid Science, 32 (8), pp. 1673-1678.

[18]   Tartuferi, M., D'Alessandro, V., Montelpare, S., Ricci, R., 2015, "Enhancement of savonius wind rotor aerodynamic performance: A computational study of new blade shapes and curtain systems", Energy, 79 (C), pp. 371-384.

[19]   Yang, B., Lawn, C., 2011, "Fluid dynamic performance of a vertical axis turbine for tidal currents", Renewable Energy, 36 (12), pp. 3355-3366.

[20]   Kacprzak, K., Sobczak, K., 2015, "Computational assessment of the influence of the overlap ratio", Symkom 2014, Open Eng. 2015; 5:314–322.

[21]   Tian, W., Song, B., Van Zwieten, J.H., Pyakurel, P., 2015, "Computational fluid dynamics prediction of a modified savonius wind turbine with novel blade shapes", energies, 8 (8), pp. 7915-7929.

[22]   Alaimo, A., Esposito, A., Milazzo, A., Orlando, C., Trentacosti, F., 2013, "Slotted Blades Savonius Wind Turbine Analysis by CFD", Energies, 6(12), pp. 6335-6351.

[23]   Hoogedoorn, E., Jacobs, G.B., Beyene, A., 2010, "Aero-elastic Behavior of a Flexible Blade for Wind Turbine Application: a 2D Computational Study", Energy, 35, pp. 778-785.

[24]   Krawczyk, P., Beyene, A., Macphee, D., 2013, "Fluid structure interaction of a morphed wind turbine blade", International Journal of Energy Research, 37 (14), pp. 1784-1793.

[25]   Macphee, D., Beyene, A., 2015, "Aeroelastic Behavior of a Morphing Wind Turbine Rotor in Varying Wind", Proceedings of ECOS 2015 – the 28TH International Conference on Efficiency, Cost, Optimization, Simulation and Environmental Impact of Energy Systems, Pau, France.

[26]   Macphee, D., Beyene, A., 2015, "Experimental and Fluid Structure Interaction analysis of a morphing wind turbine rotor", International Journal of Energy Research, 90 (1), pp. 1055-1065.

[27]   Butbul, J., MacPhee, D., Beyene, A., 2015, "The impact of inertial forces on morphing wind turbine blade in vertical axis configuration", Energy Conversion and Management, 91, pp. 54-62.

[28]   "History of Wind Energy", U.S. Department of Energy, form www.energy.gov.

[29]   TelosNet Web Development and Darrell Dodge, "Early History Through 1875" [Figure1.1], Part 1, 2015, from www.telosnet.com.

[30]   Ackerman, T., Soder, L. (2000), "Wind Energy Technology and Current Status: A Review", Renewable and Sustainable Energy Reviews.

[31]   Mathew Sathyajith (2006), "Wind Energy: Fundamentals, Resource Analysis and Economics", [Figure1.2].

[32]   [Figure1.3], 2015, Wincharger.com.

[33]   Beauchamp E. Smith Smith-Putnam Wind Turbine Experiment in Joseph M. Savino (ed), "Wind energy conversion systems: workshop proceedings" [Figure1.3], Washington, D. C., June 11–13, 1973, National Science Foundation (U.S.)/ National Aeronautics and Space Administration, 1973 page 6.

[34]   Danish Wind Industry Association, "The Wind Energy Pioneers: The Gedser Wind Turbine" [Figure1.3], 2003, from http://www.windpower.org/en/pictures/juul.htm.

[35]   S. Brusca, R. Lanzafame, M. Messina. "Design of a vertical-axis wind turbine: how the aspect ratio affects the turbine's performance". 2014.

[36]   Felix van König (1978). "Windenergie in praktischer Nutzung". Pfriemer. ISBN 3-7906-0077-6.

[37]   Paul Gipe, "Wind Energy Comes of Age", 1995, pp. 78.

[38]   Wei Tong, "Wind Power Generation and Wind Turbine Design", [Figure1.4], 2010, pp. 15/16.

[39]   "Development of Renewable Energy Trainer for Education", [Figure1.5], 2015 from http://muhammaddahrulikmal.blogspot.it/

[40]   Ben Franske, "An active water pumping windmill in Iowa", [Figure1.5], 2008, from Wikipedia.com

[41]   "About the Tower: First-to-Market Hybrid Solar-Wind Energy Technology.", [Figure1.6], Solar Wind Energy, Ltd. Accessed March 21, 2015.

[42]   Verma, Preeti, "Multi Rotor Wind Turbine Design and Cost Scaling", [Figure1.7], Masters Theses 1896 -February 2014. Paper 1158.

[43]   A. Cherubini, A. Papini, R. Vertechy, M. Fontana, "Airborne Wind Energy Systems: A review of the technologies", Renewable and Sustainable Energy Reviews, 51, 2015, pp. 1461–1476.

[44]   James Provost, "Helium or hydrogen inflated airborne wind generator. Unit is 17 m by 9 m.", [Figure1.8], 2008.

[45]   Al-Bahadly, I. H., and A. F. T. Petersen, "A Ducted Horizontal Wind Turbine for Efficient Generation", INTECH Open Access Publisher, 2011.

[46]   No, T.S., J.E. Kim, J.H. Moon, and S.J. Kim. "Modeling, Control, and Simulation of Dual Rotor Wind Turbine Generator System." Renewable Energy 34, no. 10 (2009): 2124-2132.

[47]   Jifeng Wang, Janusz Piechna and Norbert Müller, "Computational Fluid Dynamics Investigation of a Novel Multiblade Wind Turbine in a Duct" [Figure1.9], J. Sol. Energy Eng 135(1), 011008 (Sep 08, 2012) (6 pages) Paper No: SOL-11-1128; doi: 10.1115/1.4007089.

[48]   "VAWT Vertical Axis Wind Turbine", 2015, review from http://www.reuk.co.uk.

[49]   [Figure1.10] from http://en.wind-turbine-models.com/foto/565/dornier-darrieus-55-vertikalachser.

[50]   "Pinson Cycloturbine at New Mexico State University Las Cruces", New Mexico circa 1979, from http://www.wind-works.org/cms/index.php?id=500.

[51]   A. Cavallini, "Energia eolica: appunti per il corso di Energie Rinnovabili", 2011, from R. Pallabazzer, "Sistemi eolici", Rubbettino Editore, Soneria Mannelli 2004.

[52]   M. Mari, "Performance Evaluation of Novel Vertical Axis Wind Turbine Blades Based on the Savonius Concept", 2015, Master's thesis, Ferrara University.

[53]   Butbul, Jonathan Amichai. "The Impact of Inertia Forces on a Morphing Wind Turbine Blade in A Vertical Axis Configuration: A Wind Tunnel Test." Master's Thesis, San Diego State University, 2014.

[54]   Ben F. Blackwell, Robert E. Sheldahl, Louis V. Feltz. "Wind Tunnel Performance Data for Two- and Three-Bucket Savonius Rotors", 1977, Sandia Laboratories, Albuquerque, New Mexico.

[55]   MacPhee, David William. "Flexible Blade Design for Wind Energy Conversion Devices", PhD dissertation, University of California: San Diego, San Diego State University, 2014.

[56]   Paritosh Bhattacharya. "Weibull Distribution for Estimating the Parameters", Department of Mathematics, College of Engineering & Management, Kolaghat, India, 2011.

[57]   "Local Electricity Rates & Statistics", from www.electricitylocal.com.

[58]   "California Energy Consumption Database", from www.ecdms.energy.ca.gov.

[59]   "Short-term Energy Outlook", U.S. Energy Information Administration, from www.eia.gov, 2016.

[60]   "U.S. Energy-Related Carbon Dioxide Emissions", U.S. Energy Information Administration, from www.eia.gov, 2014.